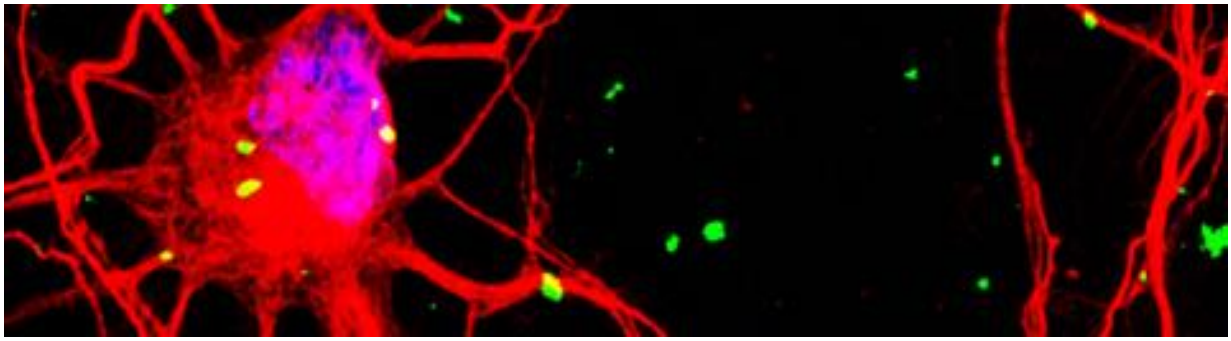

Corso di Dottorato in Neuroscienze,
Curriculum Neuroscienze e Neurotecnologie

Ciclo XXX

Titolo:

"Two-photon bidirectional control and imaging of neuronal excitability with cellular resolution in vivo"

Autore: Angelo Forli

Supervisor: Tommaso Fellin

ISTITUTO ITALIANO DI TECNOLOGIA

UNIVERSITÀ DEGLI STUDI DI GENOVA

The ineffectiveness of natural thinking comes from being overwhelmed by an infinity of possibilities and facts. In order to go on, you have to know what to leave out; this is the essence of effective thinking.

Kurt Gödel

CONTENTS

1. Introduction and state of the art 1

1.1. Neuronal activity patterns underlying brain function 1

1.2. Population measures and two-photon functional imaging *in vivo* 4

1.3. Causal manipulations: optogenetics 12

1.4. Two-photon optogenetics 18

1.5. Patterned two-photon illumination through phase modulation 22

1.6. Simultaneous two-photon monitoring and manipulation of neural activity with high spatial resolution 27

1.7. Recent technical developments in two-photon optogenetics 30

2. Rationale and aims 36

3. Materials and methods 38

3.1. Animal strains, viral injections, and animal surgery 38

3.2. Optical set-up 40

3.3. Phase modulation for holographic illumination 42

3.4. *In vivo* electrophysiological recordings 43

3.5. *In vivo* two-photon imaging and photostimulation 44

3.6. Slice electrophysiology 45

3.7. Data analysis and statistics 46

4. Results 49

4.1. Cellular resolution two-photon holographic stimulation *in vivo* 49

4.2. Two-photon holographic stimulation across cortical cell types and layers 53

4.3. Cellular resolution two-photon holographic inhibition *in vivo* 57

4.4. Simultaneous two-photon imaging of red-shifted indicator and holographic stimulation of blue light-sensitive opsin **60**

5. Discussion **64**

6. Bibliography **70**

7. Acknowledgements **90**

1. Introduction and state of the art

1.1 Neuronal activity patterns underlying brain function

One major goal of neuroscience is to describe how behavior or cognitive states stem from brain activity. For example, much experimental and theoretical effort has been devoted to understanding how the perception of sensory stimuli, motor schemes, emotions and memories are generated by the coordinated activity of the network of neurons. Addressing these questions, however, poses remarkable challenges. Even in the rudimentary nervous system of the nematode *C. elegans*, one of the simplest model organisms used in biology [1], as well as inside the complex mammalian brain, neurons are highly interconnected and constitute intricate three-dimensional circuits. Moreover, many different neuronal subtypes (classifiable by transcription profiles, morphology, connectivity and function) are organized in specialized activity-dependent sub-networks. This intricate circuitry is believed to be at the basis of the computations that allow animals to perceive, act, learn, and remember [2]–[4]. In this framework, one central issue concerns how patterns of neuronal activation control brain function and behavior [5]–[9]. For example, population recordings in primary sensory areas of the rodent cortex have shown that following the presentation of an external stimulus (e.g., a moving object in the visual field or the deflection of a single whisker), complex spatial and temporal patterns of neuronal activation are generated (Fig. 1) [9]–[13].

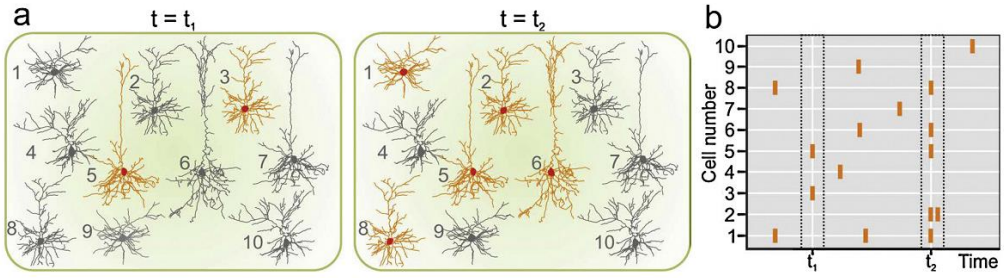

Figure 1. Neuronal circuits display complex spatial and temporal patterns of activity. A. A simplified network model composed of ten neurons is shown. Complex patterns of electrical signals that display diverse degrees of synchrony among different cells are generated over time. For example, at $t = t_1$ (left panel), two cells (orange) are concurrently active while most other neurons (gray) remain in an inactive state. At $t = t_2$ (right panel), electrical activity is synchronously generated in a larger number of cells (neurons nos. 1, 2, 5, 6, 8). **B.** A raster plot showing electrical activity (vertical orange bar) in the different cells over time. The times corresponding to $t = t_1$ and $t = t_2$ are highlighted (dotted gray line). Adapted from [9].

Similar studies in the rodent motor cortex have shown that motor learning coincides with a refinement of the activity of movement-related neurons toward a smaller population, exhibiting reproducible spatiotemporal sequences of activity (Fig. 2) [14]. Analogous stereotyped patterns of activity were found in the brain of songbirds during song production (Fig 3) [15] and in the mouse CA1 hippocampal region during spatial navigation [16], to list just a few examples. How do these patterns of neuronal activity contribute to producing the perception of a sensory stimulus, the execution of a motor scheme, or the generation of a certain behavior? How are different behavioral features encoded in neural circuits, in particular in the spatial and temporal structure of network activation? These unanswered questions are of fundamental importance for our understanding of brain function and are in line with a recent proposal indicating that neural circuits rather than individual neurons should be considered the functional building blocks of the brain [17]. Based on fundamental scientific results achieved in many field of research in the past, it is likely that answering the aforementioned questions will rely on the development of novel methods that enable the systematic *recording* and *manipulation* of neural activity patterns with high spatial and temporal resolution [18]. Such a tool would provide the possibility to identify activity patterns generated by a sensory stimulus, bias and modify them, or replicate them in

the absence of the stimulus. All these manipulations could thus be used to causally test the role of specific activity patterns in a given behavior.

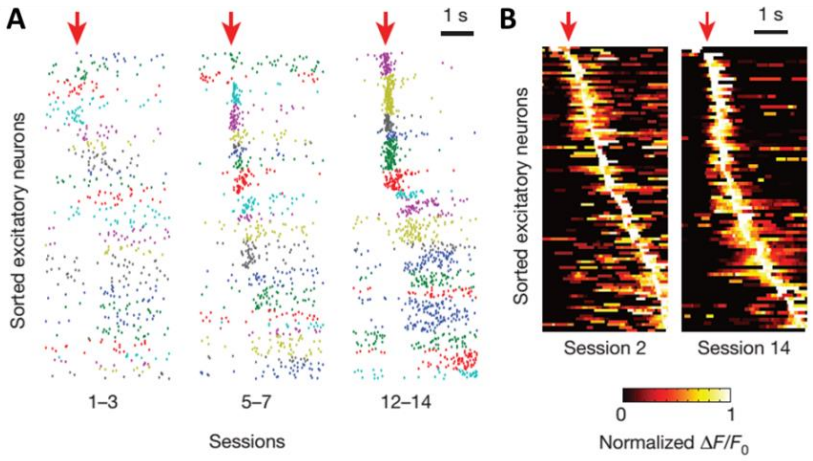

Figure 2. Neural activity patterns associated with motor behaviors. A. Activity onsets of excitatory neurons from one mouse that are movement-related and active in at least 10% of trials in the indicated sessions. Arrow, movement onsets; colors, individual neurons sorted according to their preferred timing. Note that the same colors across sessions are not necessarily the same neurons. **B.** Maximum-normalized average activity from all movement-related neurons from all animals in session 2 (left, 106 neurons) and session 14 (right, 84 neurons) aligned to movement onset (arrow). Activity timing is refined over time, shown by narrower peaks and lower background in session 14, and shifts toward movement onset. All error bars are s.e.m. Adapted from [14].

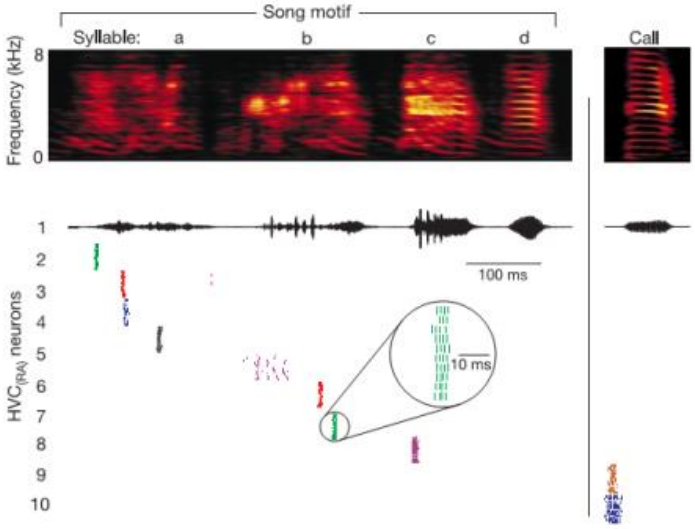

Figure 3. Activity patterns during vocalization. Spike raster plot of ten HVC (RA) neurons recorded in one bird during singing (left) and call vocalizations (right). Each row of tick marks shows spikes generated during one rendition of the song or call; roughly ten renditions are shown for each neuron. Neural activity is aligned by the acoustic onset of the nearest syllable. HVC (RA) neurons burst reliably at a single precise time in the song or call. Adapted from [15].

1.2 Population measures and two-photon functional imaging *in vivo*

Efficient recording of the activity of several neurons with high spatial and temporal resolution is the first step toward the identification of basic mechanisms underlying brain function at the circuit level. Moreover, to *correlate* neural activity patterns with specific brain functions, such as sensory perception or motor action, it is evident that recordings should be accomplished in living organisms (*in vivo*), where the connectivity between cells, spontaneous network activities and the cellular environment are preserved. However, measuring *in vivo* how neuronal populations process and integrate information about the external world or internal states is a challenging task. Consider, for example, the adult mouse neocortex (120 - 130 mm^2 in area, on average 112 mm^3 in volume, approximately 14 million neurons) [19]–[21] and focus on a single barrel column, which constitutes the basic functional unit in the rodent whisker primary sensory cortex (each whisker is mostly represented by its own so-called barrel column, Figure 4).

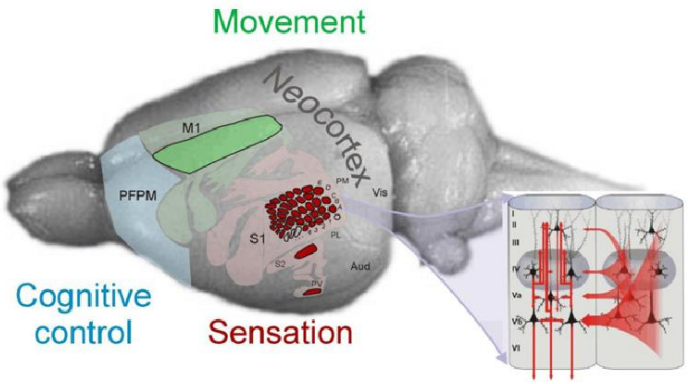

Figure 4. Microscopic and macroscopic scales of brain organization: the rodent barrel cortex as a model system. The blow up of the barrel cortex circuit diagram on the right shows the richness of intra- and trans-columnar cortical connections, which by far outnumber the topographically-ordered, layer-specific thalamic inputs. The microscopic structure of the barrel column is very well studied. The macroscopic level is less well characterized and can be studied as sensorimotor integration needed to guide and optimize active discrimination. The neuronal correlate is highly accessible and is provided by the embedding of whisker-related touch representations in the unimodal primary and secondary somatosensory cortex (S1, S2), as well as the association somatosensory cortices PV, PL, and PM. Whisker movement is processed by association of the primary motor cortex, and cognitive processes affecting whisker-related active touch can be studied in the prefrontal/premotor cortical areas (PFPM). Whisker representations are highlighted. Adapted from [22].

This basic cortical module, which processes sensory information related to vibrissal touch, consists of approximately 10,000 neurons belonging to distinct functional and genetic classes and located in a six-layered three-dimensional structure spanning around 300 x 300 x 900 µm [22].

Neurons in a whisker-related column generate very fast electrical signals on the ms time scale (action potentials, APs) in response to a whisker stimulus. These signals propagate along neural processes and transfer information to many postsynaptic cells. Thus, even the smallest sensory stimulus elicits responses in hundreds to thousands of neural cells. Thus, an ideal technique for monitoring circuit activation should be minimally invasive and have high spatial and temporal resolution over large fields of view. Such a recording technique, even if only *correlative* in nature, could provide evidence about *where* and *when* signals associated with specific behaviors are generated, as well as suggest *what* information is conveyed by these activity patterns (to demonstrate their *necessity* or *sufficiency* for information coding, see the next sections).

Because of its exceptional temporal resolution and ability to integrate neuronal signals over wide scales (from individual APs to network oscillations, [23]), electrophysiology has long been the preferred technique for studying the brain. For decades, intracellular [24] and extracellular electrical recordings have been the prevailing recording method in systems neuroscience [25]. Huge progress in micro- and nano-fabrication techniques for multielectrode arrays [26]–[29] ensure improvements in sampling density and biocompatibility, while modern analytical methods suggest that several types of information can be extracted from this kind of recording [30], [31]. Despite these tremendous improvements, electrophysiological approaches suffer from several limitations, such as invasiveness [32], difficulty obtaining genetically selected neuronal populations, limited structure-function correlation [33], and a general bias towards sorting high-frequency spiking cells in unit recordings. Alternative experimental methods as macro-scale imaging techniques, such as fMRI, have had a

remarkable impact in neuroscience, allowing us to investigate the involvement of spatially distributed neuronal circuits in response to external stimuli or in certain behavioral states during normal and under pathological conditions [34]–[36]. However, fMRI and other approaches related to the hemodynamic response have limited temporal resolution and cannot provide a movie of brain dynamics at cellular or subcellular resolution. During the last 30 years, the development of optical imaging methods and fluorescent activity reporters have provided an additional efficient tool to study the function of neural networks that overcomes some of the limitations of the above-described methods [11], [37]–[40]. In particular, two technical advances, namely the synthesis of *fluorescent calcium indicators* and the development of *non-linear microscopy*, have made it possible to record in intact tissue the activity of large ensembles of neurons with subcellular spatial resolution and adequate temporal resolution [39]–[41].

The use of calcium indicators as reporters of neuronal activity dates back to the discovery that certain ester forms of synthetic calcium indicators, such as fura-2, can be used to load the fluorescence moiety inside the cell and thus label neurons in brain tissue [42]. AP firing (as well as synaptic inputs) lead to opening of voltage-gated calcium channels and thus to a transient elevation in cytoplasmic Ca^{2+} concentration, which is typically between 50–100 nM to 5–10 µM and can be detected by the fluorescence calcium indicator. Neurons stained with these compounds thus show changes in somatic fluorescence concurrently with AP firing [43]. Localized calcium transients decay over 100–500 ms through diffusion, the activity of calcium extrusion mechanisms, and internal buffering molecules [38]. Calcium excitability is not a prerequisite for electrically excitable cells, i.e., cells that generate AP firing. For example, glial cell astrocytes, which play an important modulatory role in many brain functions [44]–[46], display variations in intracellular calcium levels that correlate with neuronal activity. Therefore, imaging calcium in both neural and non-neural cells could be used as an effective

technique to monitor their activity. Synthetic calcium indicators such as the one mentioned above [42], [47] were among the first to be introduced [38], [48]. Since their initial synthesis, several different calcium dyes were developed with various affinities for calcium, different dynamic ranges, and kinetic properties [49]. These dyes were widely used in neuroscience research due to their ease of implementation and large signal-to-noise ratios [10], [38], [50], [51]. Main limitations of synthetic calcium indicators include difficulty in labeling genetically specified cell populations and their limited lifetime in cells, which precludes chronic measurements. To overcome these limitations, an important breakthrough come from the laboratory of the Nobel Prize awardee Roger Tsien [52]: the introduction of protein-based *genetically encoded calcium indicators* (GECIs). These fluorescent calcium binding proteins, when combined with the use of cell-type promoters, subcellular targeting sequences and transgenic technology, can be stably expressed in specific cell subpopulations (Figure 5) over long periods of time [38], [49], [53]–[55]. Initially, GECIs had relatively restricted applications due to their slow response kinetics and small signal-to-noise ratios [56]–[58]. During the last 15 years, there had been incredible progress in the development and refinement of brighter and more sensitive variants, in some cases reaching performances comparable to those of synthetic calcium indicators [59]–[61]. At present, ultrasensitive genetically encoded calcium indicators of the GCaMP6 family [55] and RCaMP family [62]–[64] are sufficiently sensitive to report, under optimized experimental conditions, the calcium transients associated with the discharge of single AP *in vivo*. The development of fluorescent activity indicators demonstrated that neural activity could be monitored indirectly by examining changes in the intracellular concentration of specific ions. However, fundamental advances in optical imaging were necessary to apply them to monitor the activity of neural circuits (and glial cells) in the intact central nervous system with high spatiotemporal resolution [38]–[40]. Standard wide-field fluorescence microscopy was initially used in combination with fluorescence indicators, and it is

optimally suited to address several experimental questions due to its minimal invasiveness, high spatial (μm) and temporal resolution (ms-μs), and large field of view.

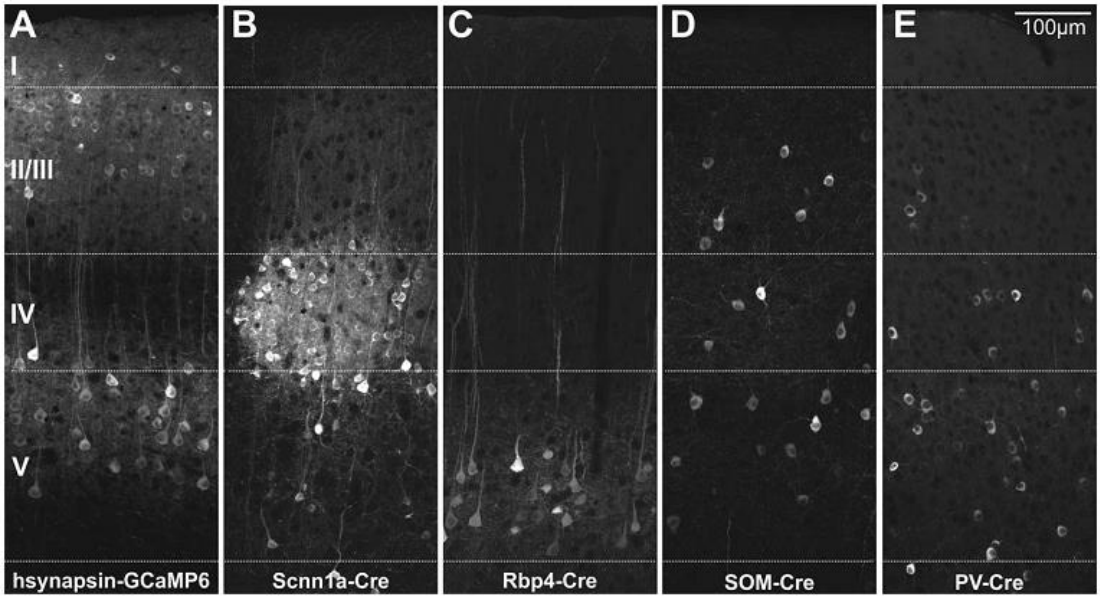

Figure 5. Cell type-specific expression of genetically encoded calcium indicators. A. Confocal image showing GCaMP6 expression in cortical neurons of the mouse somatosensory cortex. Indicator expression was achieved through viral infection in wild-type mice using an adenoassociated virus carrying the GCaMP6 sequence under the human synapsin promoter. **B–E.** Confocal images showing GCaMP6 expression confined primarily to layer 4 excitatory neurons (B), layer V pyramidal cells (C), somatostatin-(D), and parvalbumin-(E)-positive interneurons. Cell type-specific expression of the fluorescence indicator is achieved using Cre-lox technology and injecting Scnn1a-Cre (B), Rbp4-Cre (C), SOM-Cre (D), and PV-Cre (E) mouse lines with adeno-associated viruses carrying a double floxed GCaMP6 sequence. Image courtesy of S. Bovetti and C. Moretti. Adapted from [39].

However, the contrast and resolution rapidly degrade when imaging densely labeled samples in the highly scattering mammalian brain tissue [65]. In this case, the wide-field fluorescence image quality worsens with the tissue depth. Confocal microscopy overcomes some of these limitations, but is intrinsically accompanied by signal loss (the pinhole rejects scattered photons coming from the focus), phototoxicity and photobleaching in out-of-focus planes [66]. Moreover, confocal microscopy usually employs visible wavelengths for excitation, which are largely sensitive to scattering. For these reasons, standard wide-field and confocal fluorescence microscopy are best applied to thin samples, such as neurons in culture or superficial structures in biological tissue.

Since its first experimental validation more than 20 years ago, multiphoton microscopy – in particular *two-photon laser-scanning microscopy* (2PLSM) - has revolutionized biological imaging by providing high-resolution and high-contrast fluorescence images hundreds of microns deep inside intact tissue [67], [68]. In practice, 2PLSM is a laser-scanning method that exploits localized 'nonlinear' excitation to stimulate fluorophores only within a thin raster-scanned plane [69]. In standard wide-field fluorescence, fluorophore excitation is caused by the absorption of a single photon and therefore depends *linearly* on the intensity of the incident light. Nonlinear techniques rely on 'higher-order' light-matter interactions, involving the absorption of multiple photons. In this latter case, fluorophore excitation depends *non-linearly* on the incident light intensity [41], [68]. In two-photon (2P) excitation - which was first postulated by Marie Goeppert-Mayer [70] – the energy of two photons that arrive 'quasi-simultaneously' (within fractions of a fs) at the fluorophore is absorbed to promote the transition of one electron from the ground state to the excited state. The electron in the excited state then decays following the normal fluorescence-emission (or photochemical reaction) pathway as in single photon fluorescence excitation (figure 6a, [66]).

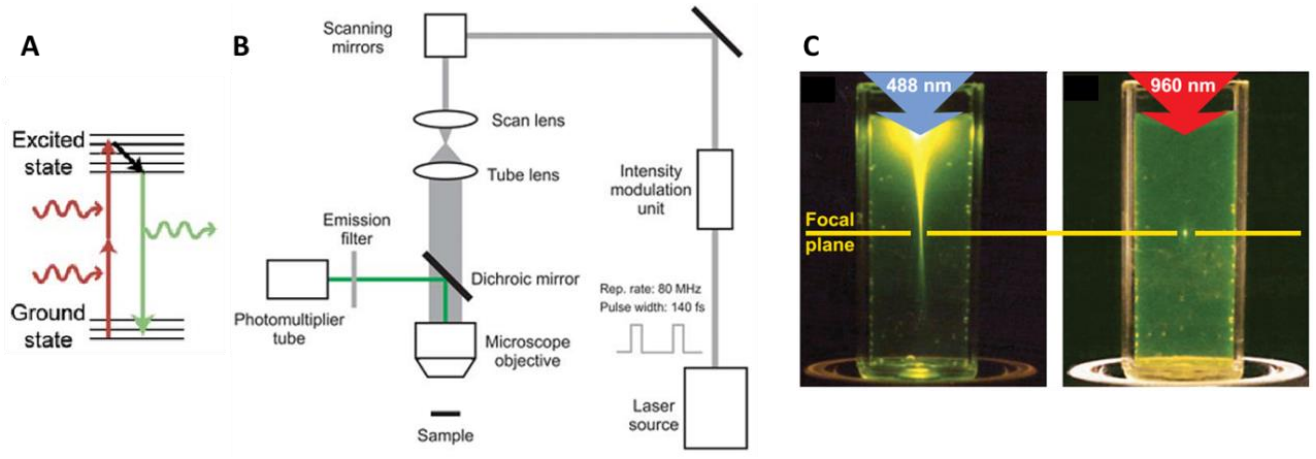

Figure 6. **Two-photon excitation of fluorescent molecules. A.** Simplified Jablonski diagram of the 2PE process. Adapted from [41]. **B.** Basic design of 2P microscopes. Adapted from [39]. **C.** Localization of excitation by 2P excitation. (left) Single-photon excitation of fluorescein by focused 488-nm light (0.16 NA). (right) Two-photon excitation using focused (0.16 NA) fs pulses of 960-nm light. Adapted from [69].

At higher photon densities, three (or more) absorption events can occur [71].

The yield of multiphoton absorption depends on the *multiphoton absorption cross-section* of the molecule (σ_{mP}) at a given wavelength (λ) and on the spatiotemporal distribution of the excitation photons, which must be considerable. High spatial densities are usually obtained by focusing coherent light from a laser source through a high numerical aperture (NA) objective. The concentration of photons in time requires the use of pulsed lasers that emit 'ultrashort' ($\tau \approx 140$ fs) light pulses with high peak intensities and a fast repetition rate ($f \approx 80$M Hz). In general, the number of molecules *dn per* unit of time *dt* excited by a pulsed laser focused in a diffraction limited volume (neglecting photo-bleaching and saturation of the transition) is given by (1) [72]:

$$\frac{dn}{dt} = \frac{6.9}{(\pi hc)^2} \frac{C\sigma_{2P}\lambda}{\tau f} P_{ave}^2$$

where C is the molecule concentration, P_{ave} is the average laser power, h is Planck's constant and c is the speed of light. The above relationship illustrates the well-known proportionality between the excitation rate and the square of the incident power and the independence of the excitation rate on objective NA, or on how tightly the beam is focused. Following the Goeppert-Mayer theoretical demonstration, 2P excitation waited almost 30 years to be proven experimentally due to the introduction of the first high-power pulsed lasers [73], [74]. The 2P excitation was first applied for fluorescence microscopy in 1990 [75]. The standard optical set up for 2PLSM for in vivo applications is shown in Figure 6b. The intensity of the laser beam is modulated and directed onto a fast scanning system based on the scanning mirrors (galvanometric or resonant) [75], [76]. The scan and tube lenses form an afocal telescope, which expands the laser beam to fill the objective pupil and conjugate the rotation plane of the scanning mirrors with the back focal plane of the objective. The focused spot is scanned across the sample, and the excited fluorescence is collected by the objective and directed onto one or more detectors (photomultiplier tubes, PMTs) by a dichroic mirror placed between the tube lens

and the objective (non-descanned configuration, [39], [77]). Three major advantages make 2P microscopy an extremely powerful technique for imaging thick samples *in vivo* [68]:

1. For commonly used fluorophores, 2P absorption occurs in the near-infrared wavelength range (700–1100 nm). Near-infrared light penetrates deeper into scattering tissue and is generally less phototoxic than visible light.
2. The fluorescence signal (S) depends on the square ($S \propto I^2$) of the light intensity (I, see also previous paragraphs). Thus, when focusing the laser beam through a high NA objective, 2P absorption in non-saturating conditions is limited to the perifocal region (Fig. 6c) [78].
3. In 2PLSM, the sample is sequentially excited, and the signals are collected in a point-by-point manner. This strategy overcomes the pixel cross-talk observed when wide-field imaging is performed in scattering tissues. In 2PLSM, all fluorescence photons are assumed to originate from the perifocal region (see previous point), and the most efficient detection strategy is to collect as many fluorescence photons as possible (for example, by using a low-magnification high-NA objectives, large dichroic mirrors, and detectors positioned close to the microscope objective in the non-descanned configuration).

For the reasons explained in the previous paragraphs, it is thus clear that the combination of 2PLSM with fluorescent activity reporters constitute one of the most powerful approaches to investigate the intact central nervous system at cellular resolution, enabling a wide range of neuroscience studies in model organisms, such as functional connectivity measures *in vivo*, mapping the encoding of sensory information, structure-function correlation, neurovascular coupling, anatomical and functional plasticity studies [11], [41], [68], [79]–[82]. Since the first validation of 2PLSM, several lines of progress have been achieved in the optical design of multiphoton microscopes, in computational microscopy, and in probe engineering, leading to an increased signal-to-noise ratio, temporal

resolution, field-of-view dimensions, penetration depth, and accessible volume for *in vivo* imaging (reviewed in [40]). Because of these developments, the visualization of neuronal activity in circuits of thousands of cells with single neuron resolution in the intact brain of behaving mammals has become a reality.

1.3 Causal manipulations: optogenetics

The correlative readout of neuronal activity during behavior with 2P microscopy provides fundamental insights into how brain functions relate to cellular activity, demonstrating the involvement and the refinement of specific networks of neurons in different behavioral tasks. However, using statistical analysis and correlative evidence *alone* to test, for example, how precise sensory features or motor schemes are generated by the activity of specific neural circuits may be difficult and, ultimately, provide inconclusive evidence[83]. To causally test whether a neural activity pattern truly carries information that drives behavior, we need to *perturb* the circuit while measuring the behavioral or network effects of this *causal intervention* [83]–[85]. Among all the interventional approaches that have been employed in neuroscience (e.g., pharmacological manipulation or electrical stimulation) to demonstrate the role of a certain neuronal network in specific behaviors, *optogenetics* has a unique set of features that currently make it a preferred choice under many experimental conditions. Optogenetics combines genetic and optical methods to stimulate or inhibit defined subpopulations of cells in living tissue or behaving animals [86] with extraordinary high cell-type specificity and high temporal resolution.

The first efficient tool for manipulating neurons with light was developed in 2005 in Stanford by Deisseroth, Boyden, Nagel and colleagues. Using a modified light-sensitive cation channel named Channelrhodopsin-2, it was possible to control neuronal firing with millisecond temporal precision

shining light [87]. More than 10 years later, optogenetics has become one of the most powerful techniques in Circuit and System Neuroscience. Three main features have been critical for the development of this method: i) microbial rhodopsins, which are integral membrane proteins from ancient organisms (algae or archaebacteria) that efficiently transport specific ions across the membrane upon light stimulation, with fast kinetics and great light sensitivity; ii) advanced bioengineering techniques for specific, stable and strong expression of light-sensitive proteins in mammalian neurons; iii) optical methods to control and delivery precisely timed illumination to specific brain areas, cells or subcellular compartments [88]. During the last years, a large number of studies led to significant improvements in the optogenetic toolbox available to the community [89]–[99], providing an expansive variety of depolarizing and hyperpolarizing tools, with various light sensitivity and different spectral properties, which allow versatile control over neural activity under many experimental conditions.

The microbial rhodopsins commonly used in optogenetics are integral membrane proteins constituting a family of molecules that are distinct from the rhodopsins that mediate photo-transduction in the vertebrate eye. Photoexcitation of these proteins leads to retinal isomerization that triggers a cycle of protein conformational changes. Unlike rhodopsins in the vertebrate eye, in which the chromophore is cleaved from the protein after a photo-cycle, in microbial rhodopsins it is not (and this is fundamental for their efficient function, for details see [100], [101]). In practice, microbial rhodopsins are light-gated ion channels or light-driven ion pumps, which enable the optical activation or inhibition of defined neuronal types. Three major branches of microbial type I rhodopsins have been effectively applied in optogenetics: channelrhodopsins, halorhodopsins and bacteriorhodopsins (Figure 7).

- *Channelrhodopsins* (ChRs) are light-gated ion channels that are principally permeable to H^+, Na^+ and, to a lesser extent, K^+ and Ca^{++} [102]. Of the two different isoforms that have been identified in the

unicellular green alga *Chlamydomonas reinhardtii*, ChR2 was selected in pioneer studies due to its superior expression levels in host cells [87], [103], [104]. The mutated version, $ChR2_{H134R}$, has improved Na^+ conductivity [105].

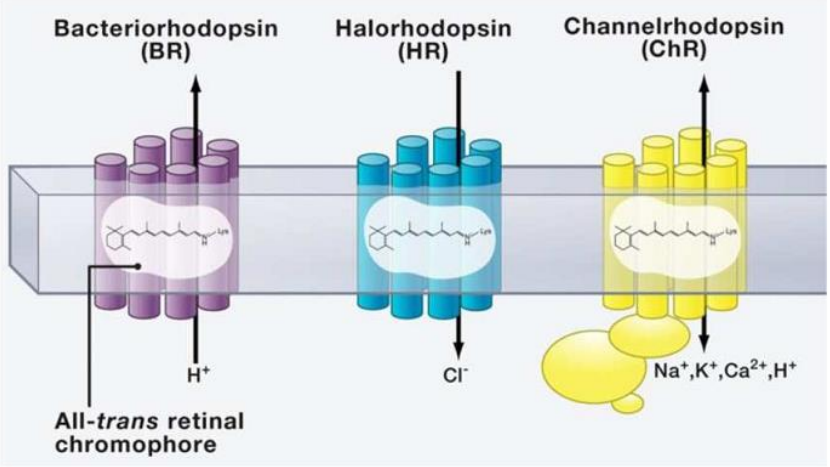

Figure 7. Microbial opsins for optogenetic manipulation of neuronal circuits. Representation of the three most widely used microbial opsins in optogenetic experiments. Bacteriorhodopsin and Halorhodopsin inhibit neurons by pumping protons outside or chloride inside the cell, respectively. Channelrhodopsins are commonly used to excite neurons because of their permeability to cations. Adapted from [106].

ChR2 remains one of the most commonly used opsins to induce neuronal activation. Illumination with blue light pulses of ChR2-expressing neurons evokes AP firing with millisecond precision and mediates currents in the nA range [105]. In recent years, many ChR variants have been identified from other algal species, engineered by point mutations, or generated as chimeras by combining different ChRs. Because of these studies, a large set of genetically encoded depolarizing tools is now available that differ in photo-current magnitude, wavelength selectivity, light sensitivity, ion permeability, and photocycle kinetics [92], [98], [100], [107]. For example, by performing targeted mutagenesis of the permeability pore, Cl^--permeable channelrhodopsins were recently developed [96], [108] and concurrently identified in nature [99], [109].

- *Halorhodopsins* are electrogenic pumps originating from the archaea *Natronomonas pharaonis* (Halo/NpHR), which are typically inhibitory when expressed in neural cells. They are chloride pumps that transport one Cl^- ion into the cytoplasm *per* photocycle triggered by yellow light illumination [110], [111]. The expression of these opsins in neurons hyperpolarizes the membrane potential and decreases the AP firing probability. Limited membrane trafficking of these proteins in mammalian cells make photocurrents carried by the first generation of halorhodopsins (and more generally by microbial ion pumps) extremely variable and dependent on expression levels [90]. Newer generations of halorhodopsins have undergone extensive optimization, leading to enhanced versions with optimized membrane targeting. One such example is the halorhodopsin eNpHR3.0, which represents a very effective inhibitory tool used by the neuroscience community [90], [112].

- *Bacteriorhodopsins* were the first discovered microbial opsins [88], [113], [114] and, similar to halorhodopsins, are largely used to silence neuronal activity. Among these proteins, archaerhodopsin (Arch) is the most commonly used. Arch was discovered in the archaea *Halorubrum sodomense* and is a proton pump that generates H^+ outward transport upon yellow light illumination. When Arch is expressed in neurons, activation of Arch causes membrane potential hyperpolarization and efficiently decreases AP firing [115]. In recent years, two additional proteins of the bacteriorhodopsins family have emerged as efficient silencers: i) ArchT [91], which was derived from the TP009 strain of the *Halorubrum* family and shows higher light sensitivity; ii) eArch3.0 [92], a trafficking-enhanced version of Arch that is characterized by greater photocurrents.

The range of scientific breakthroughs that benefited from optogenetics is remarkable and continues to grow [88], [115]–[121]. To be an effective tool for neuroscience applications, optogenetics does not only require functional opsins and effective illumination methods, but also efficient strategies to drive

the robust expression of these proteins in selected brain tissue. The delivery of transgenes encoding microbial rhodopsins has been successfully applied to various species, including mice, rats, turtles, marmosets, and primates, mostly using lentiviruses and adeno-associated (AAV) viral vectors [122], [123]. In general, viral approaches (Figure 8) achieve selectivity of neuronal subtypes by fusing the opsin gene to a required and cell type-selective promoter.

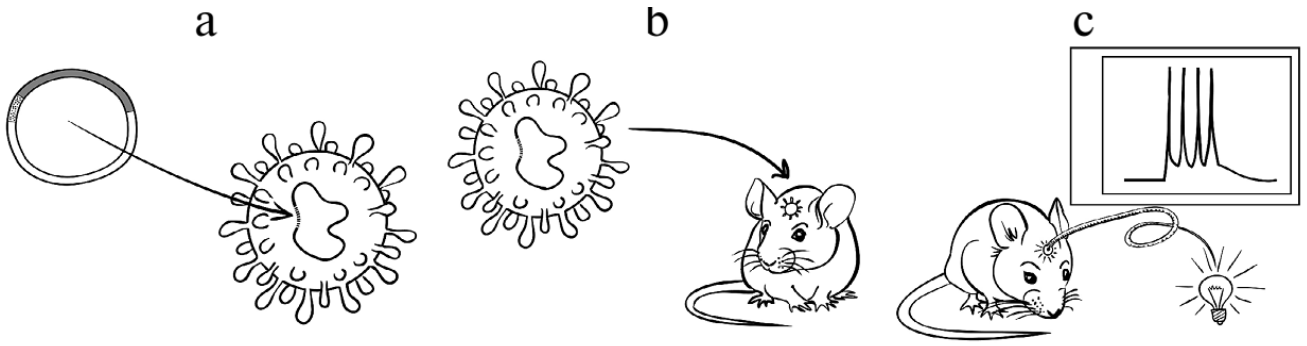

Figure 8. Schematic of the basic steps in a prototypical optogenetic experiment in vivo. A. preparation of virus particles transducing an opsin construct; **B.** incorporation of the opsin gene in the genome of a recipient animal; **C.** synthesis of the encoded protein that mediates photoregulation of neuronal activity and study of the functional implications of the optical manipulation. Adapted from [101].

Despite their extensive use, viral vectors do have limitations. Some of the disadvantages of commonly used viral vectors include the following: i) potential inflammatory responses that could affect neuronal and glial physiology; ii)limited size of the coding sequence that can be inserted in the cargo plasmid; iii) unexpected viral tropism for particular neuronal types or brain regions; iv) an unwanted tendency to retrograde/anterograde infection. In recent years, the use of transgenic or knockin animals in optogenetics (see for example [124] and the selection of particular AAV serotypes [125] overcame some of the abovementioned limitations. For example, when the target neuronal population is individuated by a weak cell-specific promoter, intersectional genetic switches are usually adopted to achieve selective and high-level opsin expression [126]. In mice, the Cre/lox recombination system is the most common approach to achieve high yet specific transgene expression levels in specific cell types [94], [127]–[130]. Alternatively, in utero electroporation (IUE) of plasmids can be used to target

opsin expression in precise brain areas or specific cortical layers [131]–[134]. Recent developments in the fabrication and geometry of electrodes for IUE now allow the targeting of previously inaccessible brain areas [135], [136].

Most optogenetic studies are currently performed by illuminating opsin-expressing neurons in wide-field mode, providing visible light with extended illumination sources [87], [104], [137]–[140], optical fibers, or miniaturized LEDs [117], [141]–[143]. Comprehensive reviews of the impressive results derived from the use of wide-field optogenetics in neuroscience are available [88], [118], [144], [145]. However, in all the studies using the wide-field illumination approach, the possibility of stimulation or inhibition with high spatial resolution neurons that belong to the same genetic class is prevented due to difficulties in the precise confinement of single-photon illumination within the brain tissue. By simultaneously stimulating multiple neurons expressing the opsins, the wide-field stimulation mode can thus generate oversynchronous responses. Thus, under most experimental conditions, the wide-field optogenetic approach largely probes neural networks with non-physiological stimuli. Given that many neural computations and behaviors likely depend on complex activity patterns that are distributed across neural network in both space and time, the wide-field optogenetic approach may lead to a biased and incomplete understanding of brain function [8], [11], [146], [147].

To reach the fine-scale dimensions that are required to address questions about the role of neuronal activity patterns driving behavior (see paragraph 1.1), the spatial resolution of optogenetics must reach the dimension of individual neurons (Figure 9). This is certainly a non-trivial goal and it requires overcoming the limitations imposed by the low penetration depth of visible light in brain tissue and the lack of optical sectioning of the wide-field illumination approach. Importantly, improvement of the spatial resolution of light delivery may be fundamental to solve another issue of primary importance, i.e., the unwanted activation of opsins expressed in neuronal fibers and presynaptic terminals.

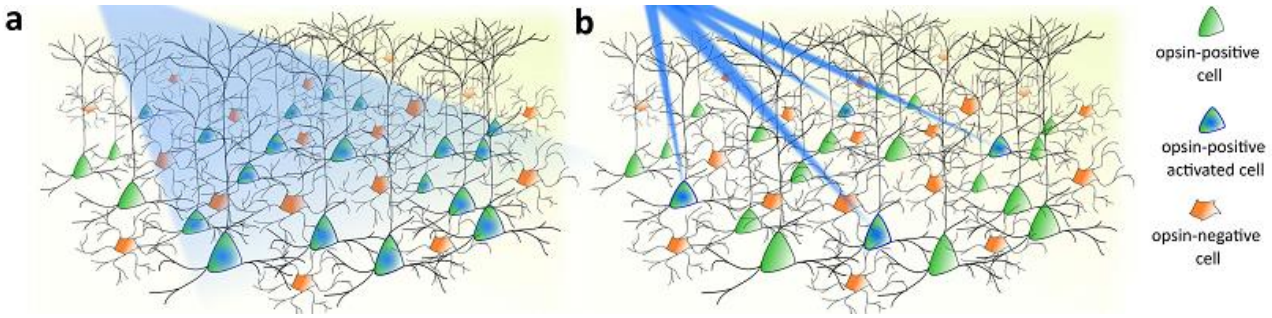

Figure 9. Wide-field and patterned illumination approaches for optogenetic stimulation. A. Cell-type genetically targeted investigations enabled by all opsin-expressing neuron activation via wide-field illumination. **B.** Spatially-targeted investigations enabled by selective activation of a specific pool of neurons via light-targeting strategies. Adapted from [148].

This issue is often overlooked and not fully characterized in many studies, but it is of primary importance and may lead to potential misinterpretations of experimental results. Indeed, some evidence demonstrates that activation of inhibitory opsins expressed on presynaptic termini leads to counterintuitive and non-physiological excitatory effects [149]. A restricted illumination technique or subcellular targeting of opsin expression [150] may provide an efficient solution to these problems.

1.4 Two-photon optogenetics

As detailed in the previous paragraph, optogenetics is an extremely powerful tool to causally test the role of neuronal populations in specific behaviors. However, to address questions about the causal role of activity patterns in driving behavior, we need the ability to precisely manipulate the activity of neurons with high spatial and temporal resolution, overcoming limitations inherent in standard wide-field optogenetics. Early attempts to solve the lack of spatial precision of optogenetics involved the use of digital micromirror devices (DMDs; [151]) or computer-generated holography (CGH, [152], [153]) to restrict one-photon illumination to specific regions of interest [148]. These approaches are unlikely to provide single-cell resolution in the case of densely labeled neuronal populations due to the lack of optical sectioning intrinsic of one-photon excitation. This is especially true *in vivo*, where the

degradation of spatial resolution occurs due to tissue scattering [154]. A solution to improve spatial resolution in optogenetic studies comes from 2P excitation. In agreement with the advantages offered by non-linear microscopy for functional imaging studies (see Paragraph 1.2), 2P excitation of opsins provides confines excitation in small volumes and improves the penetration depth within the biological tissue.

Early efforts to validate 2P excitation of opsins started in 2008 in the laboratory of Michael W. Berns with the first demonstration that ChR2 could be activated by a 2P process when illuminated with near-infrared light (λ≈920 nm) from an ultrafast pulsed laser [155]. A more extensive examination of the phenomenon was provided the subsequent year [156], showing that ChR2 has a relatively high 2P cross-section and that 2P excitation of ChR2 at modest intensity levels can be used to elicit APs in neurons *in vitro* by fast scanning of a low-NA Gaussian beam across the cell soma (Figure 10).

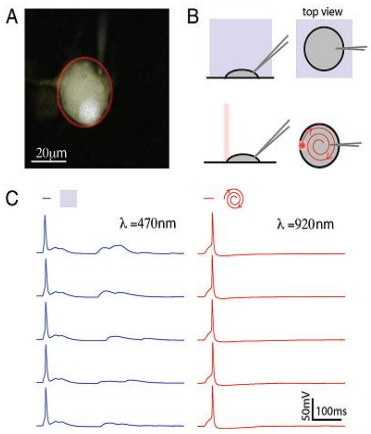

Figure 10. Stimulation of APs using 2P optogenetics. A. The 2P fluorescence image of a patch-clamped neuron in culture (ChR2-EYFP, yellow; volume- filling Alexa 594, gray). The red outline indicates the outer boundary used to designate a spiral-scan trajectory. **B.** Schematic of geometries of whole-cell blue-light excitation (upper panel) and scanning 2P stimulation (lower panel), shown in side view and from the top. **C.** Current-clamp recordings of membrane voltage changes, stimulated using wide-field blue-light illumination (left) or 32-ms-long spiral scans with 2P excitation (N.A. = 0.3, right). Overlying lines indicate stimulation times. Adapted from [156].

In Rickgauer et al., the basic idea was that if the scanning time is smaller than the decay time of the light-gated current, temporal integration of the photocurrents evoked in different scanned points on the cell surface will occur. However, the biophysical properties of ChR2 initially made it challenging to stimulate opsin-expressing neurons with standard laser scanning 2P excitation. Indeed, ChR2 has a low conductance (~ 80 femtoSiemens, [157]) and relatively fast closure kinetics [92], which largely limits photocurrent temporal integration. Due to the high 2P absorption cross-section of ChR2, no major advantage derives from increasing excitation intensity because saturation of excited ChR2 channels at the focal spot is rapidly reached. In this case, photocurrents excited away from the focus can easily exceed focally excited currents [156], leading to a degradation of spatial resolution. Since the first demonstrations of 2P excitation of ChR2, several methods have been developed to overcome some of the aforementioned limitations. Photocurrent integration during 2P laser scanning, for example, can be augmented by selecting and engineering opsins with slow closure kinetics and high conductance.

Following this idea, robust AP generation was demonstrated *in vitro* and *in vivo* with high spatial precision [158], [159] using the red-shifted channelrhodopsin variant C1V1 [92], [160] in combination with raster scanning (Figure 11). Nevertheless, using opsins with slow off kinetics in combination with scanning approaches limits the temporal precision of photostimulation, which is constrained by the minimum time needed to scan the cell [9], [148], [153], [154]. In this context, 2P illumination approaches encompassing extended shapes may overcome this constraint by simultaneously exciting a large number of opsins over the neuron membrane. Illumination with an extended circular shape of the dimensions of a neuron soma can be realized, for example, by underfilling the objective back aperture, which results in an increase in the focal spot size [68].

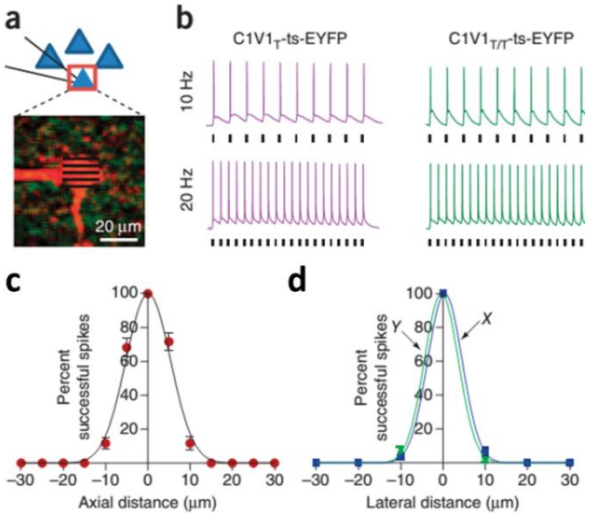

Figure 11. 2P control of neural spiking with C1V1 variants in acute brain slices. A. Top, targeted neurons during TPLSM excitation (red box, ROI). Bottom, 2P image of patched/Alexa 594–filled neurons expressing C1V1T-EYFP; lines schematize the TPLSM pattern. **B.** TPLSM spike generation under 1,040-nm illumination in neurons expressing C1V1T-ts-EYFP or C1V1T/T-ts-EYFP. Resting membrane potential (Rm), −65 to −70 mV; black ticks, scan onset. **C.** Percent successful spikes versus axial position in C1V1T-ts-EYFP–expressing cortical neurons. Rm, −65 mV. **D.** Percent successful spikes versus lateral distance from the center of a representative cortical cell expressing C1V1T-ts-EYFP. Blue, X; green, Y; Rm, −65 mV. Adapted from [159].

Underfilling the pupil diameter worsens the axial confinement of the illumination profile. However, the z resolution can be restored by using the temporal focusing (TF, Figure 12) technique [161], [162]. In a TF optical setup, a diffraction grating conjugated with the sample *via* a dispersion-free telescope is used to spread in space the spectral components of the laser ultrashort excitation pulse. These components, each characterized by a narrow wavelength distribution but broad temporal duration (as a consequence of the indetermination principle applied to photons), propagate separately in the direction of the objective focal plane, resulting in a temporally spread pulse above and below the focal plane. The different components are then combined and temporally focused back in the focal plane to generate efficient 2P excitation only in this plane. This approach was successfully adopted for 2P stimulation of ChR2 expressing neurons *in vitro*, with higher temporal resolution [163] compared with 2P scanning methods of comparable duration [156]. However, these approaches required a much larger power density value. Combining TF 2P illumination with a standard galvanometer-based scanning

system resulted in the efficient *sequential* photostimulation of multiple cells with extended illumination both *in vitro* [164] and *in vivo* [165]. This approach, however, still does not permit truly synchronous activation of multiple neurons.

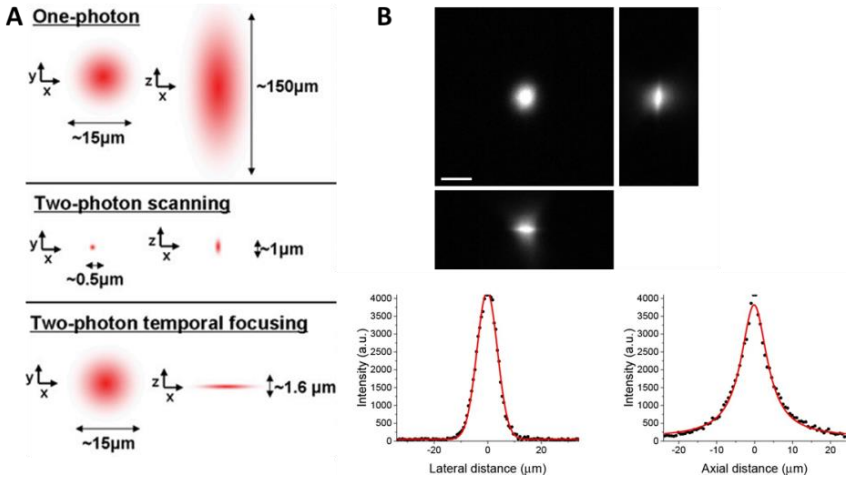

Figure 12. Excitation volume in 1P and 2P optogenetics. A. Illustrative comparison of typical one-photon, 2P scanning, and 2P temporal focusing (i.e., sculpted light) axial and lateral excitation profiles. Adapted from [163]. **B.** Orthogonal projections from a z-stack of a spin-coated layer of 200 nm fluorescent beads imaged with the temporal focusing beam and collected with a CCD camera. Scale bar = 20 µm. The full width at half maximum was 9.0 µm in the xy plane and 9.5 µm in the axial plane. Adapted from [164].

1.5 Patterned two-photon illumination through phase modulation

One attractive solution to the aforementioned problems is ideally a technique that allows the precise illumination of multiple neurons with extended shapes with an arbitrary geometry, which can be achieved with a class of modern optical techniques, termed patterned illumination [9] or parallel illumination methods [148], [153]. These methodologies generate specific spatial photoactivation configurations by projecting an illumination intensity pattern that is tailored on the morphology of the sample (Figure 9b). In patterned illumination, all the targets are simultaneously illuminated, thus potentially leading to higher temporal resolution during excitation. The increased temporal resolution comes at the cost of a larger laser power density needed for the sample [148], [153], [166]. Practical

implementations of patterned illumination can be based either on the modulation of light intensity with digital micromirror devices or on the modulation of light wave-front by means of spatial light modulators (SLMs, for review see [148]). The low efficiency inherent to intensity-modulation techniques largely precludes the use of intensity modulation with 2P excitation. In contrast, intensity modulation has been extensively used in combination with one-photon excitation, sharing the same issues with respect to axial resolution as other one-photon excitation techniques [148], [167], [168]. As explained in detail below, phase-modulation methods combined with 2P excitation are, at present, considered the optimal choice to generate precise illumination patterns in deep biological tissue.

The working principle behind patterned illumination through phase modulation is the modulation of the light intensity in the sample plane of the objective by modifying the phase of a coherent light beam at the back focal plane (i.e., the Fourier plane) of the same objective lens [9], [148]. According to the laws of diffractive optics, the electric field in the front focal plane of a lens is the Fourier transform of the electric field in the back focal plane of the lens, which can be used to analytically calculate the wave front modulation profile corresponding to a desired intensity pattern [169]. In practice, the phase-map in the Fourier plane (called diffractive optical element, DOE, [170]) corresponding to a desired intensity pattern in the sample (figure 13a) is usually calculated iteratively [171], [172] by specific algorithms (from which was derived the term *computer generated holography*, CGH, [173]. These algorithms iteratively search through different possible DOE for the one with an inverse Fourier transform that produces an intensity profile that better matches the desired illumination profile. Phase modulation is provided by pixelated liquid crystal SLMs (LC-SLMs, figure 13b). These devices were initially developed for correction of optical aberrations induced by the atmosphere during astronomy observations [174], [175]. Subsequently applied in the field of optical-tweezers [176], [177], LC-SLM-related techniques were adapted for neuroscience applications approximately ten years ago and used for

precise uncaging of neurotransmitters, direct optogenetic stimulation of neurons, and fast functional imaging [148], [178]–[185]. The core of these programmable devices consists of a matrix of active cells (or pixels), each enclosing nematic liquid crystals (LC). Within each pixel, re-orientation of liquid crystals through the application of an electric field results in modulation of the local refractive index and, therefore, in the phase of an incident wave (Figure 13b,c, [9], [186]).

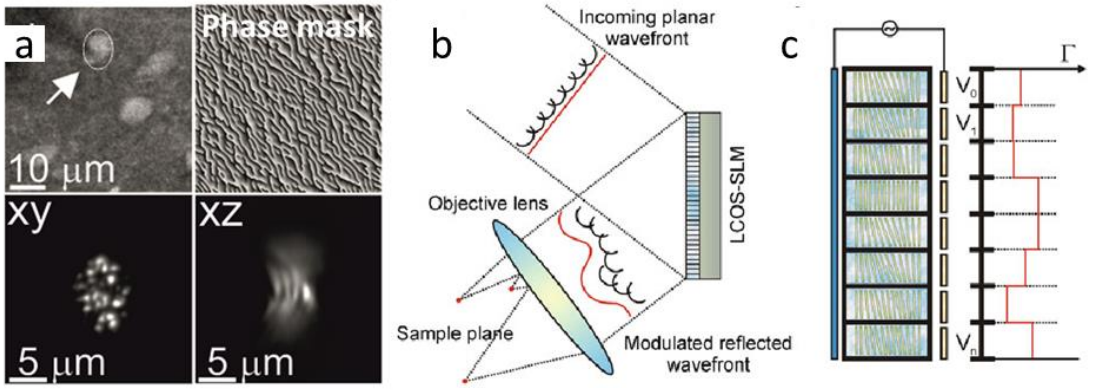

Figure 13. Phase modulation with LC-SLMs. A. Intensity modulation through phase modulation. Top-left: image representing neurons stained with a fluorescence reporter. The desired elliptical shape to be projected is indicated by the arrow. The corresponding calculated phase (DOE) in the Fourier plane is shown in the top-right panel. Bottom: intensity profiles in the focal plane (xy, left) and along the axial direction (xz, right) for the extended shape (top-left) generated with the holographic illumination system (Forli et al. Submitted). **B.** LCOS-SLM working principle: schematic view of the effect of LCOS-SLM in shaping an incident planar laser wave front (red straight line). By modulating the phase of the spherical components (black semicircles), the LCOS-SLM modifies the wave front of the reflected light beam (curved red line). This change in phase that is introduced in the Fourier space by the LCOS-SLM results in the generation of patterned illumination in the sample plane (behind the objective lens). **C.** Zoom-in showing the structure of the LCOS-SLM as a matrix of active cells. By controlling the liquid crystal orientation pixel-by-pixel through the voltage v_i, each cell (or pixel) can differentially modulate the phase of the light (Γ) impinging upon it. Adapted from [186].

To combine 2P patterned illumination with a LC-SLM, the SLM in usually placed in a plane that is optically conjugated to the objective back focal plane (Figure 14). Several modifications of this basic scheme are possible, each exploiting particular features or addressing some of the limitations of 2P-CGH-based techniques[148], [154]. A detailed protocol to insert a holographic module in a 2P scanning microscope can be found in [148], [186], [187]. One limitation of standard CGH is the presence of intensity inhomogeneity in the projected pattern, called “speckles” (Figure 13-14), which

arise because the iterative algorithms used in CGH optimize the phase map based on a desired amplitude distribution in the sample plane and leave the phase in the sample plane as a free parameter. Due to the high coherence of the laser illumination, however, pseudo-random phases of neighboring locations in the sample interfere either constructively or destructively, causing speckles [178], [188].

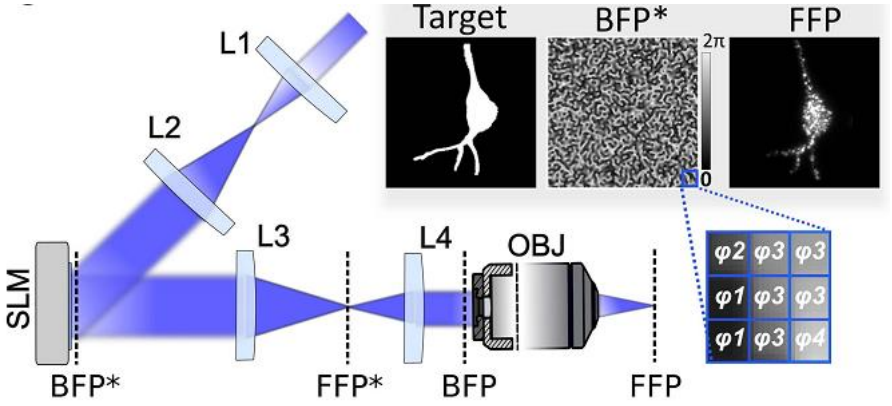

Figure 14. Typical set-up for CGH. Illumination intensity patterns in the frontal focal plane (FFP) are obtained by modulating the phase of the illumination beam in the back focal plane (BFP) of the objective by means of an LC-SLM placed in a conjugated plane (BFP*). Inset: CGH pattern generation process. A binary image is designated as the target illumination (here tailored after the shape of a neuron) (left), and a phase-only modulation is calculated via Gerchberg–Saxton (GS) algorithms, and addressed on the SLM in the form of a gray-scale image where each gray level is associated with a phase delay ji ranging from 0–2 π (middle). A speckled holographic-based intensity distribution is generated in the FFP (here visualized by exciting a thin fluorescent layer under the 2PE regime) (right). Adapted from [148].

Several hardware or software solutions have been suggested to minimize the spatial inhomogeneity in CGH (reviewed in [148]) and should be considered when the uniformity of the illumination pattern is essential. For example, generalized phase contrast (GPC) extends Zernike's phase contrast [189] to optically convert user-defined phase-variations, created by an SLM, in proportional amplitude variations in the sample plane. Through computationally simple SLM encoding and few additional optics, GPC allows speckle-free intensity patterns with steep edges [173], [188]. Due to poor axial confinement, however, 2P-GPC alone has limited applicability for neuronal stimulation and is intrinsically inadequate for 3D illumination [173]. However, GPC can be combined with temporal focusing to provide speckle-free 3D-confined patterned illumination. This approach was used to

provide the first demonstration of 2P optogenetic activation of neurons *in vitro* using spatially-shaped excitation with high spatial resolution [182].

In general, the deterioration of axial resolution is a concern for 2P-CGH, especially for large illumination patterns [180] and when projecting through scattering tissue. In recent years, the combination of 2P-CGH with TF has led to significant improvements in the axial confinement of the projected shapes and, additionally, has been shown to be robust in response to optical aberrations [190] and scattering [191]–[193] (Figure 15a). Moreover, very recent developments [154], [194] have demonstrated that 3D patterned illumination, although practically possible with standard 2P-CGH [195], [196], would particularly benefit from implementations including TF, especially in the case of extended 3D projection volumes inside scattering tissue (Figure 15b-c).

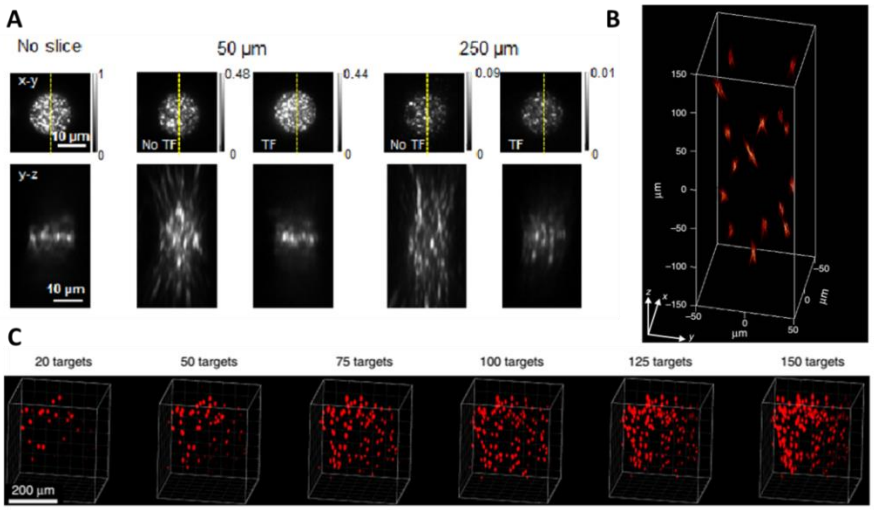

Figure 15. 3D holographic stimulation. A. Top: x-y cross sections of the holographic beam in the objective focal plane, without scattering tissue and after propagating through 50 and 250-µm fixed brain slices, with or without TF in the optical setup; bottom: corresponding y-z cross-sections along the yellow dashed lines. λ = 800 nm. Adapted from [191]. **B.** Volumetric reconstruction of the three-dimensional distribution of 5-mm-diameter holographic spots. Adapted from [194]. **C.** Example 3D renderings from tomographic images of 2P absorption from single-shot holograms targeting increasingly larger numbers of randomly distributed spots. Adapted from [154].

After the first proof-of-principle demonstrations of 2P activation of opsins [155] and 2P stimulation of neurons [156], [163], [182], several studies efficiently implemented methods for precise 2P optogenetic stimulation of neurons, both *in vitro* and *in vivo*, either with extended shapes or by multiplexing and scanning 2P spots [9], [148], [153]. This thesis work focuses on the use of patterned illumination for spatially-precise 2P optogenetics. However, it is important to mention that 2P patterned illumination has been fundamental for the development of scanless 2P imaging methods, which allowed a significant increase in acquisition speed and addressable volume for functional imaging studies [183]–[185], [197].

1.6 Simultaneous two-photon monitoring and manipulation of neural activity with high spatial resolution

As described in paragraph 1.1, determining which codes are used by the brain to drive behavior is a major unreached goal in circuit neuroscience. New techniques to optically record and manipulate the activity of neural circuits with high spatial precision would greatly facilitate the attainment of this goal. In particular, to causally link specific neuronal activation motifs – which may differ across individuals - to behavioral decisions, imaging and manipulation must be performed within the same experiment, preferably simultaneously, with high spatial and temporal resolution in the intact brain of a behaving animal [9], [18], [153]. Despite remarkable progress in the field of optogenetic actuators, genetically encoded activity sensors, and the optical techniques described above, all-optical interrogation of neural circuits remains a non-trivial challenge. Early implementations [166], [198]–[200] of simultaneous optical readout and manipulation, entirely or partially relying on one-photon microscopy, have encountered two main problems: (i) *cross-talk* between the imaging and manipulation channels, which includes artifacts in the recording channel during optogenetic illumination, or inadvertent optogenetic activation caused by the imaging light; (ii) *reduced spatial resolution*, which is inherent to the one-

photon excitation scheme. Spatial resolution, as extensively detailed in previous paragraphs, can be significantly improved by using 2P excitation, both for imaging and photostimulation. Indeed, methods relying on simultaneous 2P glutamate uncaging and 2P calcium imaging have been employed [180], [201], [202], but they lack genetic specificity and may be sub-optimal, especially *in vivo*. Minimization of cross-talk between the imaging and stimulation channels requires accurate selection of activity sensors and actuators, with well separated absorption spectra and/or precise kinetic parameters, combined with the use of appropriate filters, availability of laser sources, and careful calibration of power levels and, more generally, of illumination parameters [9], [148], [153]. In this regard, genetically encoded actuators and activity reporters with suitable features were only introduced in the last few years, paralleling progress in optical techniques. These advancements made it possible to obtain simultaneous two photon imaging and stimulation of neurons in awake mice co-expressing the red-shifted opsin C1V1 together with the calcium indicator GCaMP (figure 16), either through AAV-mediated C1V1 expression in the hippocampus of GCaMP3 transgenic mice [165] or AAV-mediated C1V1/GCaMP6 co-expression in cortical neurons [203]. More specifically, [203] applied SLM to generate multiple stimulation spots at 1064 nm, which were synchronously (spiral- or raster-) scanned over the soma of target neurons co-expressing the opsin and the calcium indicator. The optical setup for photo-stimulation was combined with a resonant scanning 2P microscope to simultaneously perform functional imaging of GCaMP6-expressing neurons. Efficient photocurrent integration during 2P scanning was facilitated by the use of the slow red-shifted opsin C1V1, as demonstrated in previous reports [158], [159]. This allowed the authors to simultaneously trigger and record activity transients in ten target neurons in layer 2/3 of the mouse somatosensory cortex, with near cellular resolution and high reliability (Figure 16a-b, [203]). [165] adopted a similar actuator/reporter combination (C1V1 and GCaMP3) but a slightly different optical setup to demonstrate simultaneous all-optical imaging and stimulation *in vivo*. Imaging was performed using a standard raster scanning 2P microscope combined

with a photostimulation system capable of projecting either a single temporally focused illumination disk (for extended illumination) or a spatially focused low-NA spot (to be scanned over the soma of opsin-expressing neurons) at a 1064-nm excitation wavelength.

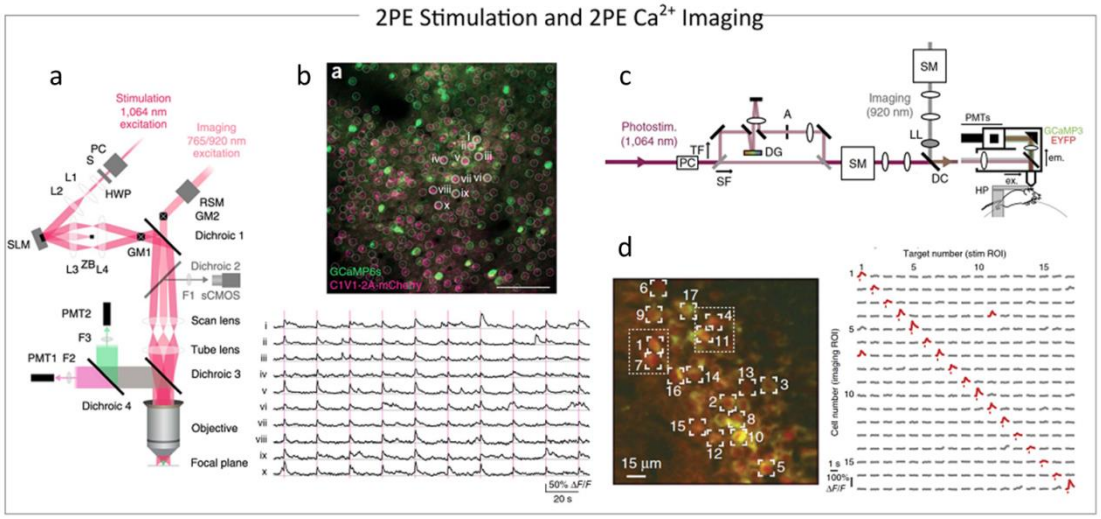

Figure 16. 2P stimulation and 2P calcium imaging. A. Optical setup coupling holographic-based 2PE scan multi-site photostimulation (dark pink path) and 2PE raster scanning imaging (light pink path). GM: galvo-mirrors, PC, Pockels cell; S, shutter; HWP, half-wave plate; L, lenses; SLM, spatial light modulator; ZB, zero-order block; GM, galvanometers; RSM, resonant scanning module; F, filters; PMT photomultiplier tubes. Adapted from [203].**B.** Simultaneous targeting of multiple cells. (Top) A 2PE fluorescence image of neurons in layer 2/3 of the somatosensory cortex co-expressing C1V1-2A-mCherry and GCaMP6s in an anesthetized mouse (scale bar, 100 μm); (bottom) ΔF/F calcium traces from ten photostimulated neurons (white circles in the top image). From [203].**C.** Optical setup coupling photostimulation via spatially-focused (SF) low-NA raster scanned beams or temporally focused disk-shaped beams (purple path) with 2PE raster scanning imaging (gray path). PC, Pockels cell; DG, diffraction grating; A, aperture; SM, scanning mirrors; LL, liquid lens; DC, dichroic mirror. From [165]. **D.** Serial targeting of multiple cells. (Left) A 2PE fluorescence image of CA1 hippocampal neurons expressing GCaMP3 and C1V1(E122T/E162T)-2A-EYFP in an awake mouse; (right) matrix of Ca2+ transients from 17 cellular targets (numbered in the left image), with significant responses shown in red. From [165]. Adapted from [148] .

Stimulation of multiple target neurons with high resolution was performed by sequentially moving the temporally focused 2P disk with galvanometric mirrors while simultaneously imaging their activity (Figure 16c-d, [165]. In both studies, the laser sources used for imaging and photostimulation were high-repetition rate ultrashort-pulsed lasers. Although spectral separation between the 2P absorption peaks of GCaMP and C1V1 plus accurate titration of power levels has allowed authors to minimize cross-talk, both reports showed increases in spontaneous neuronal firing during imaging sessions,

particularly in neurons with high opsin expression and/or during imaging at high magnification [165], [203]. In another recent paper [147], repetitive photostimulation of a field of view comprising 60–100 neurons in the visual cortex of awake mice by a scanned 2P spot was sufficient to recruit the stimulated cells into a neuronal ensemble (i.e., groups of coactive neurons). These induced ensembles reoccurred spontaneously and could be recalled via single-cell photoactivation, confirming early postulates of Hebbian plasticity [147]. Among other things, this remarkable result additionally indicated that cross-talk during all-optical experiments must be minimized. Additional studies have performed simultaneous 2P imaging and stimulation of the same cells using GCaMP6 and soma-targeted ChR2 [164], GCaMP6 and ChrimsonR [204], or GCaMP6 and ChR2 [196]. In all the diverse configurations, cross-talk between imaging and photostimulation remains a major issue. The work described in this thesis demonstrates a new experimental configuration to efficiently minimize cross-talk in simultaneous all-optical imaging and manipulation.

1.7 Recent technical developments in two-photon optogenetics

Photoinhibition

To causally link neuronal patterns of activation with behavior, it is fundamental to have the ability to both stimulate and inhibit neurons with high spatial precision. While several studies have addressed the problem of spatially shaped stimulation of neurons through 2P illumination of excitatory opsins (see previous paragraphs), photo-inhibition at the single-cell level remains a considerable challenge *in vivo*. Engineered halorhodopsins or bacteriorhorodpsins (see paragraph 1.3) are largely used to silence neuronal activity through one-photon wide-field illumination [115], [139]. However, to date, only the engineered archeorhodopsin eArch3.0 [92] has been validated for 2P inhibition of neuronal firing *in vitro* by sequential raster scanning (Figure 17) [159]. One issue with inhibitory light-driven ion pumps is linked to their limited photocurrents, given that they are light-sensitive transporters that translocate

only a single charge per absorbed photon. Moreover, light-driven pumps are usually characterized by fast closure kinetics [92], which requires an extended illumination approach for optimal stimulation. One solution to these limitations is represented by light-gated ion channels that are selective for K^+ or Cl^-. These channels conduct many charges *per* photocycle, leading to larger photocurrents. Light-gated ion fluxes through these channels depend on the membrane potential, are limited only by single channel conductance, and may provide shunting effects (something that cannot be achieved with light-sensitive transporters).

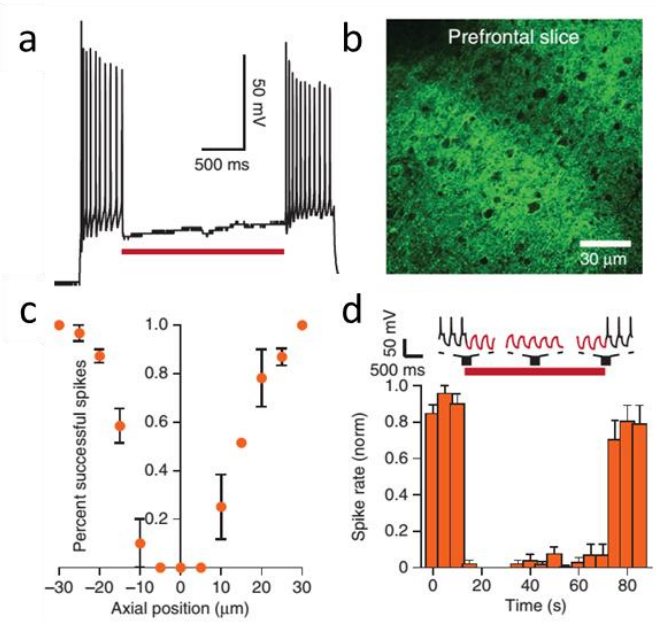

Figure 17. Two-photon optogenetic inhibition. A. Trace of 2PLSM-mediated spike inhibition in a cultured neuron expressing eArch3.0; spiking evoked by 300-pA current injection. **B.** 2P image of pyramidal prefrontal neurons expressing eArch3.0. **C.** 2PLSM activation of eArch3.0 showing spike-inhibition dependence on 2PLSM axial (z) position targeting. (k) Axial position versus successful spikes. n = 4. Values were normalized to the maximum number of spikes within the cell across all axial positions. **D.** 2PLSM inhibition over long timescales with eArch3.0. Top, traces showing key temporal windows. Bottom, spike rate over time. n = 5. 2PLSM scan initiated at 15 s and terminated at 75 s. Adapted from [159].

In recent years, several efforts have been made to engineer cation-permeable ChRs to conduct anions (in particular Cl^-) [95], [96], but many such optogenetic tools still show residual cationic conductance and are characterized by limited light sensitivity [109]. Artificial anion-conducting ChRs have been generated through targeted mutations [205], [206]. Moreover, natural light-gated anion channels with

higher performances have been discovered [109]. These channelrhodopsins (named GtACR1 and GtACR2) from the cryptophyte alga *Guillardia theta* are fast, anion-permeable, and yield very large photocurrents when expressed in mammalian cells [109], [207]. As mentioned above, in contrast to ion-pumping rhodopsins, chloride permeable ChRs, like $GABA_A$ receptors, can efficiently ‘‘shunt’’ the membrane potential to the reversal potential of Cl^- [149], [208]. The family of cryptophyte anion-conducting ChRs was recently extended to several additional members, with very promising features for applications in optogenetics [99]. In particular, the large conductance and high light sensitivity of these channels make them perfect candidates for efficient inhibition of neurons using 2P illumination, as demonstrated in this thesis work.

Somatic tagging of opsins

Illumination methods for neuronal stimulation still presents some limitations in precision, particularly in spatial resolution. Even if 2P stimulation techniques – especially when combined with temporal focusing – enable the control of spiking at nearly the single-cell level, subthreshold light-gated depolarizations frequently extend beyond the soma of the target neuron and in some cases even exceed focally induced depolarization [156], [159], [164]. In general, the spatial resolution of 2P photostimulation is the convolution of the illuminating volume with the volume where the opsin is expressed. Thus, the spatial resolution of 2P stimulation methods deteriorate during the activation of off-target cell bodies by sideline regions of the illumination shape and/or stimulation of opsin-expressing fibers belonging to on-target or off-target neurons (fibers of passage). The influence of both mechanisms depends on opsin expression levels and on the illumination quality; in the first case, the resolution would benefit from better confinement of the excitation shape (for example with TF), whereas in the second instance, confinement of opsin expression to the somatic compartment would help. It is well known that confined or enriched expression of transgenes in specific subcellular

compartments of neurons can be achieved by using *protein targeting motifs*, which are adopted by the cells for correct localization of certain endogenous proteins [150]. Using this strategy combined with an AAV-mediated targeting approach, it was possible to induce polarized opsin expression in the soma, dendritic field or axonal initial segment of retinal ganglion cells [150]. The $K_V2.1$ motif derived from the voltage-gated K^+ channel, in particular, was found to be highly efficient for targeting opsin expression to soma and proximal dendrites of neurons. Because of these findings, it was recently possible to demonstrate the high-resolution stimulation of single neurons *in vitro* by combining temporally focused 2P illumination and somatic targeting of ChR2 (Figure 18) [164]. Similar results have recently been achieved with a different motif (taken from the kainate receptor, [209]), providing significant improvement in spatial resolution of optical manipulations in intact brain.

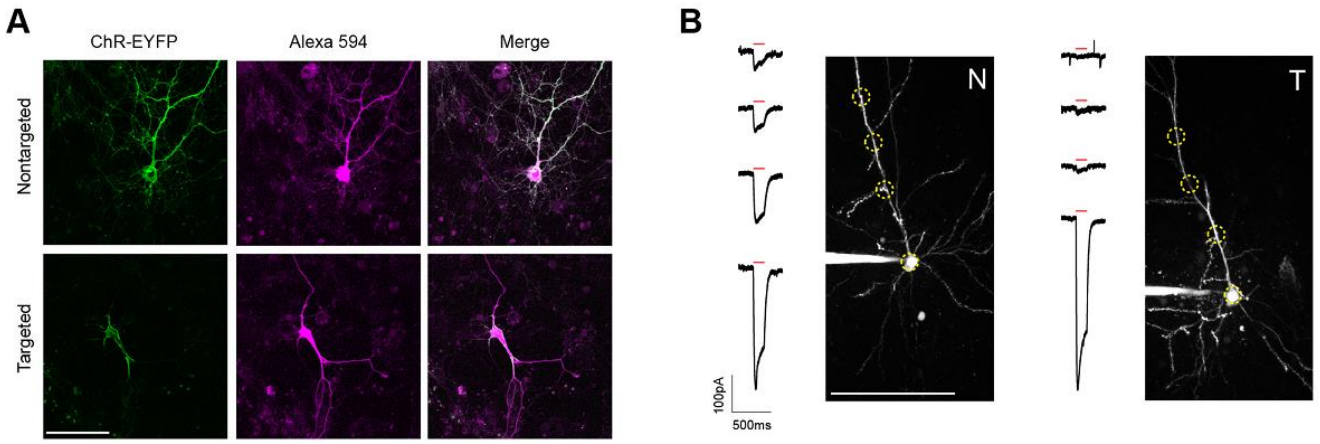

Figure 18. Characterization of soma-targeted channelrhodopsin (st-ChR2). A. Fluorescence of ChR2-EYFP (green) in live dissociated cortical neurons that had been patched and filled with Alexa 594 dye (magenta) as visualized by 2P microscopy. Scale bar = 100 mm. **B.** Representative two-photon maximum intensity projections of Alexa 594 fluorescence and current responses to a single 150 ms temporally focused 2P stimulation pulse (red bar) for patched and dye-filled pyramidal cells in acute slices expressing nontargeted (N) or targeted (T) ChR2. Scale bar = 100 mm. Adapted from [164].

Use of low-repetition rate lasers

As explained above, reaching the degree of precision – both in space and time – necessary to optogenetically probe the neural code, requires joint progress in bioengineering strategies and

illumination methods. Improving the efficiency of stimulation, which in turn is related to increasing the number of excited/inhibited neurons, extending the penetration depth inside the tissue, and achieving higher temporal precision and stimulation efficiency, constitute a current major effort in all-reading and manipulating approaches. In recent years, several methods have been developed to increase the efficiency of light stimulation of neurons [148]. These methods comprise the development of opsins with fast opening kinetics or high sensitivity and large conductance [93], [98] and the refinement of 2P illumination strategies that are either more resistant to scattering inside the tissue [191], [192] or aimed to increase the number of recruited opsins on the neuron membrane [159], [182]. An attractive idea is the use of low repetition rate lasers. Inspired by the field of multiphoton imaging, recent evidence has demonstrated the possibility of significantly reducing the average illumination power density needed for 2P stimulation and improving the temporal precision of neural responses using low repetition rate lasers (Figure19) [154], [209]–[212]. From the formula (1) in paragraph 1.2, it is simple to derive that the efficiency of multiphoton absorption at a given average power is inversely proportional to the repetition rate of the pulsed laser as a consequence of the energy conservation principle: at a constant average power, a decrease in the pulse frequency corresponds to an increase in the peak power, therefore increasing the density of photons during a laser pulse and, thus, the efficiency of multiphoton absorption (Figure19A) [71], [213], [214]. Based on this principle, recent studies have reported reliable stimulation of AP firing with high temporal precision and low temporal jitter in neurons *in vitro* by combining extended illumination approaches with a low repetition rate (500 kHz-1 MHz)-amplified lasers, at power densities lower than 0.02 mW/μm^2 (few mW *per* neuron). Due to the highly non-linear nature of photodamage in biological tissue [66], [215]–[218] and issues related to excitation saturation of opsins under 2P illumination [156], further studies are needed to elucidate the range of validity of these tools for neuroscience applications. For example, when opsins with high multiphoton cross section are stimulated, excitation saturation conditions may be easily reached. In that case, the use of

low-repetition rate lasers as illumination sources may lead to a decrease in spatial resolution and an increase in photo-damage, with no major advantage in terms of stimulation efficiency.

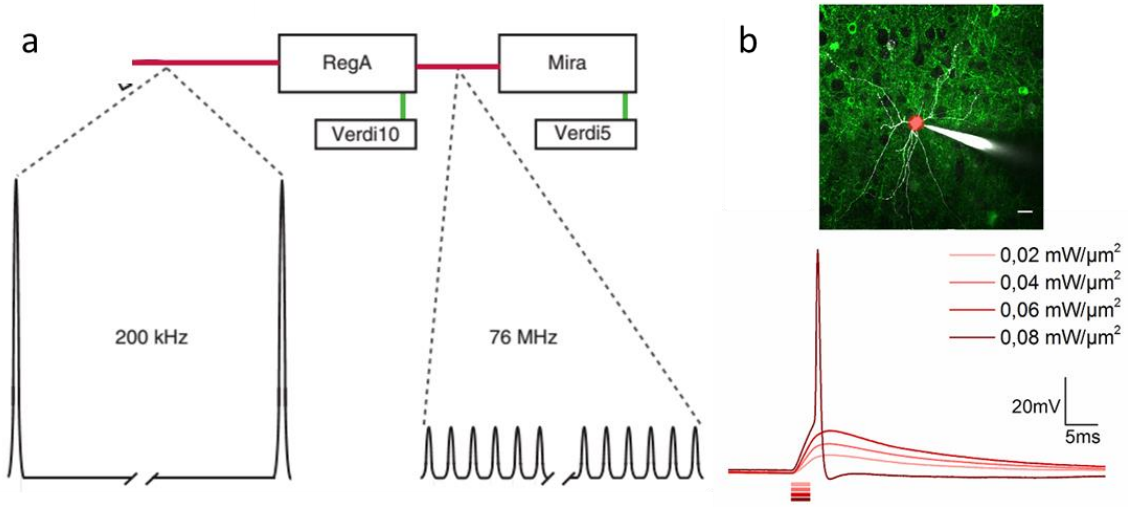

Figure 19. 2P otptogenetics with low repetition-rate lasers. A. Basic optical path for a regenerative amplifier (RegA) low repetition-rate laser seeded by a pulsed Ti:Al2O3 laser source (Mira). Pulses from the source laser were subsampled and amplified in the RegA (not to scale) and dispersion compensated (data not shown). The pulses entered the microscope at a frequency of <200 kHz, whereas the pulses entering the regenerative amplifier had a frequency of ~76 MHz. Adapted from [213]. **B.** Top, 2P image from acute cortical brain slice showing a patched/Alexa 594-filled (white) interneuron of layer 2/3 expressing Chronos-GFP (green). The neuron was photostimulated by a 10-µm holographic spot (red spot). Scale bar 20 µm. (b) Representative light-evoked membrane potential depolarization over different illumination powers in a Chronos-expressing interneuron. Illumination was provided by an amplified laser operated at 500kHz. Adapted from [212].

2. Rationale and aims

Within brain circuits, information about sensory stimuli is encoded in complex spatial and temporal patterns of activity distributed across cells [11], [219], [220]. For example, population recordings combined with statistical analysis have shown that specific features of sensory stimuli (e.g., the direction or the orientation of a moving bar in the visual field) elicit temporally-structured responses in specific ensembles of neurons [14], [147], [221]. However, using statistical analysis and correlative evidence to causally test which sensory features are encoded in neural circuits and how this information is used to drive behavior may be difficult [83]. To achieve this goal, we would ideally need a method to monitor and bidirectionally perturb the activity of multiple neurons while maintaining single-cell resolution. With such a technique, it would be possible to study precisely how the concerted activity of the identified neurons contributes to the network function by specifically activating or inactivating populations of functionally characterized neurons at cellular resolution.

The use of 2P microscopy in combination with wave front engineering and optogenetics holds great promise for achieving this goal (see Introduction). However, several limitations must be overcome to efficiently apply these approaches. First, cross-talk between imaging and photostimulation needs to be minimized. For instance, the red-shifted channelrhodopsin C1V1 is maximally activated using 540 nm light [160], but it is still half-maximally activated by 475 nm light. This shoulder towards shorter wavelengths [160], which is typical for red-shifted opsins [222], is reflected in their 2P absorption spectra [159], [211] and may lead to non-negligible neuronal depolarization during 2P GCaMP imaging [165], [203]. This undesirable effect worsens for opsins with slow off kinetics and high amplitude photocurrents, which are the preferred choice for 2P activation of neurons with the raster or spiral scanning approach [153], [159]. Second, while published data demonstrate cellular resolution 2P activation of neurons [165], [203], evidence for efficient patterned 2P inhibition *in vivo* remains to be

provided. Third, it is currently unclear whether single-cell 2P optogenetics can be efficiently applied across the various cell types that are engaged during sensory stimulation and that differ in morphology, biophysical properties, and cortical depth. Finally, simultaneous stimulation of multiple neurons with extended shapes, which maximizes instantaneous membrane currents [182], [209] (but see the recent [154]), awaits validation in the highly scattering mammalian brain *in vivo*.

This thesis work aimed to develop a unique experimental approach to address all of these challenges in the mouse neocortex *in vivo*. Building on previous studies [180], [183], [184], [186], I developed the hardware for combined 2P-imaging and stimulation, I optimized the expression of the multiple transgenes used in this thesis work, and I performed all the electrophysiological and imaging experiments included here, thus validating the applicability of patterned illumination for functional studies in living rodents.

3. Materials and methods

3.1 Animal strains, viral injections, and animal surgery

All experiments were carried out according to the guidelines of the European Communities Council Directive and approved by the IIT Animal Health Regulatory Committee and by the National Council on Animal Care of the Italian Ministry of Health (authorization # 34/2015-PR).

Animals were housed in individually ventilated cages under a 12-hour light:dark cycle. A maximum of 5 animals *per* cage was allowed. Access to food and water was *ad libitum*. Experiments were performed on young-adult animals (5-12 weeks old for *in vivo* experiments, 4-7 weeks old for *in vitro* experiments, either sex). C57BL/6J mice (Charles River, Calco, Italy), B6;129S6-*Gt(ROSA)26Sor*$^{tm14(CAG-TdTomato)Hze}$/J (JAX #007908 referred here as tdTomato line), B6;129P2-*Pvalb*$^{tm1(cre)Arbr}$/J (JAX #008069, called PV-cre line), STOCK*Sst*$^{tm2.1(cre)Zjh}$/J (JAX #013044, called SST-cre line), B6;C3-Tg(Scnn1a-cre)3Aibs/J (JAX #009613,called Scnn-cre line) were purchased from the Jackson Laboratory (Bar Harbor, USA) and used in this study.

The adeno-associated viruses (AAVs) AAV1-EF1a-dFlox-hChR2(H134R)-mCherry-WPRE-hGH, AAV1-EF1a-DIO-hChR2(H134R)-EYFP-WPRE-hGH, AAV9-EF1a-DIO-hChR2(H134R)-EYFP-WPRE-hGH, AAV1-CAG-flex-tdTomato-WPRE-hGH, AAV9-EF1a-DIO-C1V1(E122T/E162T)-TS-EYFP-hGH, AAV1-CamKII0.4-Cre-SV40, AAV2.1syn.NES.jRCaMP1a, AAV2.1syn.flex.NES.jRCaMP1a were purchased from the University of Pennsylvania Viral Vector Core. AAV carrying GtACR2 (AAV2/1.hSyn.GtACR2.EGFP) was produced as previously described in [149]. AAVs carrying ChR2 targeted to the soma (AAV1.hSyn.hChR2(H134R).EYFP.Kv2.1) was produced as in [164]. Viral injections were performed on postnatal days 1 - 2 (P1 - P2; the day of birth was designated as P0) or in young adults (> P30) similarly to [134], [168]. For the experiments in Figures 23, 25-31 in which injections were performed at P1 - P2, pups were deeply anaesthetized by placing them in ice for 4 minutes and then immobilized in a refrigerated custom stereotaxic apparatus.

The skull above one brain hemisphere was exposed with a small incision to the skin and ~ 250 nl of viral suspension was slowly injected with a glass micropipette (stereotaxic coordinates: 1 mm posterior from bregma, 1.5 mm lateral of the sagittal sinus and at 0.25 mm depth). After the removal of the pipette, the skin was sutured and the pup was revitalized under an infrared heating lamp. Four-ten weeks after injection, mice were used for experiments. For the experiments displayed in Figure 21, 24 and 26, 4 - 7 weeks old animals were anesthetized with 2% isoflurane/0.8% oxygen, placed into a stereotaxic apparatus (Stoelting Co, Wood Dale, IL), and maintained on a warm platform at 37 °C for the whole duration of the anesthesia. After scalp incision, a small hole was drilled on the skull above the neocortex to lower the micropipette into the tissue (pipette depth: 0.25 - 0.3 mm from the pia). 1 µl of virus was injected at 30 - 50 nL/min by means of a hydraulic injection apparatus driven by a syringe pump (UltraMicroPump, WPI, Sarasota, FL). The scalp incision was then sutured and covered with antibiotic cream, and the animals were monitored until recovery. 3 - 5 weeks after injection, mice were used for experiments. For combined imaging and photo-stimulation experiments (Figure 30-31), injection of the AAV transducing the opsin was done at P1-P2, while the AAV carrying the jRCaMP1a construct was injected 4 - 5 weeks later with procedures similar to those described previously with the exception that the injection was performed in 2 sites, 200 nl injected solution in each site. Three-four weeks after this latter injection, mice were used for experiments.

For *in vivo* experiments mice were first deeply anesthetized with intraperitoneal urethane (16.5 %, 1.65 g/kg). The scalp was removed while infiltrating all incisions with lidocaine. A custom-made chamber with a central hole (hole diameter: 4 mm) was attached with dental cement to the animal's skull for head-fixation under the microscope. A craniotomy (~ 700 x 700 μm^2) was opened over the somatosensory (or visual cortex in the case of experiments in Scnn mice) cortex and the dura was carefully removed (unless otherwise stated). The location of the craniotomy was decided based on the

intensity of the fluorescence signal of the expressed transgene which was observed under an epifluorescence stereoscope (sites with middle/high fluorescence intensity were targeted for craniotomy). The surface of the brain was kept moist with normal HEPES-buffered artificial cerebrospinal fluid (ACSF, composed of 127 mM NaCl, 3.2 mM KCl, 2 mM $CaCl_2$, 10 mM HEPES, pH 7.4). Body temperature was maintained at 37 °C with a heating pad. Respiration rate, heartbeat, eyelid reflex, vibrissae movements, reactions to tail and toe pinching were typically monitored to control the depth of anesthesia throughout the surgery and the experiment.

3.2 Optical set-up

The optical set-up for 2P holographic illumination was composed of two pulsed laser sources (S in Figure 20A and S_1 in Figure 30A, Chameleon Ultra II, tuned at 920 nm, and S_2 in Figure 30A Chameleon Discovery tuned at 1100 nm, Coherent, Milan, IT), a customized scanhead (Bruker Corporation, former Prairie Technologies, Milan, IT), an upright epifluorescence microscope (BX61 Olympus, Milan, IT), and a liquid crystal spatial light modulator (SLM, X10468-07 SLM, Hamamatsu, Milan, IT). The laser beam intensity was modulated by a Pockels cell (P in Figure 1A and P_{1-2} in Figure 30A, Conoptics Inc, Danbury, CT) and then directed to the SLM by a sequence of mirrors (BB1-E03 Thorlabs, Newton, NJ). A half-wave plate ($\lambda/2$ in Figure 20A, RAC 5.2.10 achromatic $\lambda/2$ retarder - B. Halle Nachfl GMBH, Berlin, DE) was placed before the SLM in order to obtain the optimal polarization for phase-only modulation. A first telescope (L_1 and L_2 in Figure 20A, IR doublets 30 mm and 75 mm, Thorlabs, Newton, NJ) expanded the laser beam to fill the active window of the SLM. A second telescope (L_3 and L_4 in Figure 20A, IR doublets 300 mm and 150 mm, Thorlabs, Newton, NJ) was used to resize the laser beam to fit the dimensions of the scanning mirrors inside the scanhead (G in Figure 20A and G_1 in Figure 30A) and to optically conjugate the plane of the SLM with the back aperture of the objective. For alignment purposes, the SLM was mounted on a lab jack (L200/M,

Thorlabs, Newton, NJ), a translator (PT1/M, Thorlabs, Newton, NJ), and a rotation platform (RP01/M, Thorlabs, Newton, NJ). Two multi-alkali photomultipliers tubes (PMTs, Hamamatsu, Milan, IT) were used as detectors for raster scanning imaging. Dual emission filters in front of the two PMTs were 525/70 nm and 607/45 nm, respectively. D_1 in Figure 20A and Figure 30A was a 660 nm long-pass dichroic mirror, D_2 a 575 nm long-pass dichroic mirror. The Olympus LUMPlanFl40X/IR objective (0.8 NA) was used for most experiments, except those in Figure 30 and Figure 31, in which an Olympus XLPLN25XWMP2 (1.05 NA) was used. A mechanical shutter (Uniblitz, VCM-D1 Shutter Driver, Vincent Associates, Rochester, NY) controlled by a TTL signal was used to control holographic illumination duration. For the simultaneous two-photon imaging and stimulation experiments in Figure 30 and Figure 30, the telescope downstream the SLM was replaced by two IR doublets (400 mm and 125 mm, Thorlabs, Newton, NJ) and the stimulation beam was relayed onto a second set of galvanometric mirrors inside the scanhead (G_1 in Figure 30A). Imaging and stimulation beams were combined by a dichroic (D_3 in Figure 30A, zt980rdc, Chroma Technology Corporation, Bellows Falls, VT) positioned between the two sets of galvanometric mirrors and the scan lens. Calibration of the SLM projection plane at the sample and the imaging field of view (FOV) was performed by imaging the sample plane with a CCD camera (ORCA R2, Hamamatsu, Milan, Italy) *via* the objective and the tube lens. A short-pass dichroic mirror (FF670-SDi01, Semrock Inc, Rochester, NY) reflected 2P excitation light onto the sample and allowed the detection of emitted fluorescence by the camera.

Single-photon stimulation of opsins was performed at 488 nm or 491 nm with a laser (MLD or Calypso respectively, COBOLT, Solna, SE) and a multimode fiber (core diameter 200 µm, 0.22 NA, QMMJ-3X-UVVIS-200/240-0.4-6, OZ Optics Ldt, Ottawa, CA). The laser was coupled to the fiber via a 10X objective (MPLN10X, Olympus, Milan, IT). On-off control of illumination was performed directly

with a TTL input to the laser driver or *via* an acousto-optic modulator (R23080-3-LDT, Gooch & Housego PLC, Liminster, UK). Light intensity was 0.2 - 6 mW at the fiber tip. During all the experiments, the optical fiber was positioned ~ 500 µm above the craniotomy, at an angle of ~ 30°. Images in Figure 20B were acquired with a CCD camera (ORCA R2, Hamamatsu, Milan, Italy) imaging a subresolved ultrathin fluorescent layer [223] *via* the objective and the tube lens under 920 nm 2P holographic illumination.

3.3 Phase modulation for holographic illumination

The SLM was controlled by custom software in Labview (National Instruments Corp, Austin, TX). Phase masks corresponding to desired illumination patterns were generated with a Gerchberg-Saxton (GS) Iterative Fourier Transform Algorithm [172]. Before each experiment, a calibration routine was performed to match with sub-micrometric precision the FOV acquired in raster scanning with the holographic projection plane at the sample. This process relied on a customized ImageJ plugin (modified from StackReg) [224] and through a TCP/IP communication protocol between the proprietary PrairieView software and the custom software. Extended shapes of arbitrary geometry were drawn on reference images acquired in raster scanning before each photostimulation session. Shapes were then transformed into binary masks and used as input for the GS algorithm to obtain the desired illumination patterns at the sample. For 2P holographic illumination experiments, individual neurons were illuminated with an elliptical shape covering the cell body. Wavelength for 2P holographic illumination was 920 nm. The non-modulated component of light (zero order) was shifted into an out-of-focus plane (below the objective focal plane) by moving the position of L_2 while keeping the modulated component in focus by imposing appropriate phase modulation on the SLM. The same phase modulation applied to the SLM was also used in the laser-scanning configuration to acquire reference images. Under the experimental conditions used in this study, the power of the zero order

component was in the range 3-10% of the total power illuminating the sample. We did not block the zero order component along the optical path because this solution prevented stimulation of neurons located in a small region in the center of the FOV. Illumination power used for *in vivo* experiments was in the range 10-92 mW *per* cell, corresponding to an intensity range of 0.11-0.97 mW/μm^2 *per* cell (calculated on an average illuminated area of 95 μm^2).

3.4 In vivo electrophysiological recordings

2P targeted juxtasomal electrophysiological recordings were performed as described in [225]. In brief, borosilicate glass pipettes were pulled with resistance 4 - 9 MΩ and were filled with ACSF solution mixed with Alexa Fluor 488 (20 μM). Neurons were targeted by imaging the fluorescent reporter with the 2P microscope while monitoring the pipette electrical resistance by applying brief voltage pulses. When the pipette tip and the target cell were in close contact one to the other, a negative pressure was imposed to the pipette in order to achieve the juxtasomal configuration (resistance > 20 MΩ). For whole-cell shadow-patch recordings [226], pipettes were filled with intracellular solution containing 140 mM K-gluconate, 8 mM NaCl, 1 mM $MgCl_2$, 10 mM HEPES,10 mM Tris-phosphocreatine, 2 mM Na_2ATP, 0.5 mM NaGTP, pH 7.2 with KOH, mixed with Alexa Fluor 488 (20 μM). The fluorescent dye was injected into the extracellular space via pressure injection while imaging with the 2P microscope. Target neurons were visualized and identified as dark 'shadows' in the 2P image. For both shadow-patch (Figure 22) and 2P targeted patch (Figure 28) recordings, experiments were performed in whole-cell current-clamp mode. To assess expression of functional excitatory opsins in each recorded neuron, we recorded the cell response to a brief single-photon stimulus (stimulus duration: 50 ms; power at fiber tip: 0.2 - 6 mW) in the cell attached configuration. Only neurons that showed spiking responses with brief latency (2 - 3 milliseconds) and low jitter were kept for successive 2P stimulation. GtACR2 functionality *in vivo* was assessed at the beginning of the experiment using single-photon

illumination (stimulus duration: 500 ms; power at fiber tip: 0.2 - 6 mW) and observing efficient silencing of the spontaneous firing or of the firing evoked by current injection (50 - 400 pA) in whole-cell configuration. Access resistance and resting potential were monitored during the experiment. Series resistance was not compensated and data were not corrected for the liquid junction potential. Cells with average resting potential more depolarized than -55 mV were excluded from analysis. Electrical signals were amplified by a Multiclamp 700B, low-pass filtered at 2.6 kHz, digitized at 50 kHz with a Digidata 1440 and acquired with pClamp 10 (Axon instruments, Union City, CA). Electrophysiological traces were analyzed using Clampfit 10.4 software (Molecular Device, Sunnyvale, CA) and IgorPro (WaveMetrics, Portland, OR).

3.5 In vivo two-photon imaging and photostimulation

Initially, 2P imaging (λ_{exc} = 1050 nm) was performed in layer 2/3 to assess the expression pattern of the opsin (ChR2-eYFP or ChR2-eYFP soma-targeted) and the calcium indicator (jRCaMP1a) at the same time. A reference image of the selected FOV was then acquired and shapes covering the soma of target neurons were generated by the SLM (λ_{exc} = 920 nm) and projected at the sample. Temporal series were simultaneously acquired in raster scanning configuration with the imaging beam (100 x 100 pixels; frame rate, 11 Hz; pixel dwell time, 4 µs; λ_{exc} = 1100 nm). Holographic photostimulation duration was 500 ms and was repeated at 0.08 Hz for 7 - 9 repetitions. For analysis, temporal series acquired *in vivo* were imported into the open source ImageJ/Fiji software in order to identify regions of interest (ROIs) defined by jRCaMP1a labeled neurons. For each ROI, the change in fluorescence relative to the baseline ($\Delta F/F_0$) was computed as a function of time with the fluorescence baseline (F_0) calculated in ten frames at the beginning of the recorded session. A stimulus artefact was recorded in the red PMT during holographic illumination. This artefact was in some cases removed by background subtraction

(Figure 31). When this procedure was not efficient, a blanking region corresponding to the stimulation period was used (Figure 30).

3.6 Slice electrophysiology

Acute cortical coronal slices were prepared from the neocortex of P26 - P49 animals. After inducing deep anesthesia with urethane (16.5 %, 1.65 g/kg), brain was quickly dissected and placed in an ice-cold cutting solution containing: 130 mM K-gluconate, 15 mM KCl, 0.2 mM EGTA, 20 mM HEPES, and 25 mM glucose, with pH adjusted to 7.4 with NaOH and oxygenated with O_2 100%. Slices (slice thickness: 300 μm) were cut with a vibratome (VT1000S, Leica Microsystems, GmbH, Wetzlar, Germany) and immersed for 1 min in solution at room temperature (RT) containing: 225 mM D-mannitol, 25 mM glucose, 2.5 KCl, 1.25 NaH_2PO_4, 26 $NaHCO_3$, 0.8 mM $CaCl_2$, 8 mM $MgCl_2$, pH 7.4 with 95% O_2/5% CO_2. Slices were then incubated for 30 min at 35°C in standard ACSF (sACSF) composed of: 125 mM NaCl, 2.5 mM KCl, 25 mM $NaHCO_3$, 1.25 mM NaH_2PO_4, 2 mM $MgCl_2$, 1 mM $CaCl_2$, 25 mM glucose, pH 7.4 with 95% O_2/ 5% CO_2. After incubations slices were maintained in sACSF at RT until use. During photostimulation experiments, slices were positioned in submerged recording chamber (RC#, Warner Instruments, Hamden, CT, USA) and continuously perfused with fresh bathing solution (125 mM NaCl, 2.5 mM KCl, 25 mM NaHCO3, 1.25 mM NaH_2PO_4, 2 mM $MgCl_2$, 2 mM $CaCl_2$, 25 mM glucose, pH 7.4 with 95 %O_2/5 % CO_2) maintained at 30 - 32 °C by an inline solution heater (TC-344B, Warner Instruments, Hamden, CT, USA). The same objective (Olympus 40x, 0.8 NA) was used for *in vivo* electrophysiology and slice experiments. Pipettes (pipette resistance: 3 - 4 MΩ) were filled with intracellular solution containing: 140 mM K-gluconate, 8 mM NaCl, 1 mM $MgCl_2$, 2 mM Na_2ATP, 0.5 mM NaGTP, 10 mM HEPES, 10 mM Tris-phosphocreatine to pH 7.2 with KOH. Alexa Fluor 488 (20 μM) was added to the intracellular solution to allow identification of patched neurons under 2P illumination. Pipette guidance during patch-clamp

recordings was performed using infrared differential interference contrast. After the establishment of the whole-cell configuration, functional expression of GtACR2 was first verified using brief single-photon light pulses (pulse duration, 500 ms; power at the fiber tip, 0.2 - 6 mW). For holographic 2P illumination, a high resolution image of the recorded neuron filled with Alexa Fluor 488 was acquired with the 2P microscope in raster scanning and an extended elliptical shape was projected to the cell body of the recorded neuron (stimulus duration: 500 ms). Currents evoked by holographic illumination were recorded in voltage-clamp at -50 mV. Access resistance, resting potential and injected current necessary to maintain the recorded neuron at -50 mV were monitored during the experiment. Series resistance was not compensated and data were not corrected for the liquid junction potential. Cells with average resting potential more depolarized than -55 mV were excluded from analysis. Voltage-clamp recorded currents were low-pass filtered at 2 kHz, digitized at 10 kHz with the same instrumentation used for *in vivo* recordings.

3.7 Data analysis and statistics

For juxtasomal recordings, traces were high-pass filtered (cutoff frequency: 10 Hz) and spikes were detected with a threshold criterion. The threshold value was optimally adjusted for each recorded sweep and always set > 3 times the standard deviation of the trace. AP firing frequency was calculated in a time window before (Pre; window duration, 1 s), during (Stim; window duration, 0.5 s) and after (Post; window duration 1.5 s) holographic stimulation over 15 - 20 stimulation trials. The response to stimulation, quantified as Δ_{AP}Freq, was calculated as the difference between the firing frequencies of the Stim and Pre time windows. Opsin-positive cells (defined based on their response to single-photon stimulation see *In vivo electrophysiological recordings*) were considered as responsive to holographic 2P stimulation when Δ_{AP}Freq was at least > 1 times the firing frequency in the Pre period at stimulation power ≥ 80 mW *per* shape. The fraction of opsin-positive neurons that were responsive to holographic

illumination was: 14/16 for CaMKII$^+$ neurons expressing ChR2 (Figure 21), 10/10 for CaMKII$^+$ neurons expressing ChR2 + C1V1 (Figure 24), 31/33 for SST$^+$ interneurons expressing ChR2 (Figure 25), 25/26 for PV$^+$ interneurons expressing ChR2 (Figure 25), 19/20 for Scnn$^+$ neurons expressing ChR2 (Figure 25), and 21/21 for neurons expressing the soma-targeted ChR2 (Figure 23). For the calculation of the spatial resolution in holographic illumination, neuronal responses (quantified as Δ_{AP}Freq) were recorded first with the 2P illumination shape centered on the cell body of the recorded neuron and then during successive shifts of the excitation volume in the radial direction (20 µm steps) and in the axial direction (± 25 µm steps). Δ_{AP}Freq as a function of the spatial shift (x) was then plotted for every recorded neuron in the three conditions (radial, $axial_{up}$ and $axial_{down}$) and fitted with a mono-exponential function ($\Delta_{AP}Freq(x) = A*exp(-l*x)$) [203]. Fitting curves with $l < 0$ or with values of A that were different by more than 25% compared to Δ_{AP}Freq at position $x = 0$ were not considered. The spatial resolution, $l_{1/2}$, was defined as the distance at which the evoked response (calculated from fit) was equal to A/2.

For the analysis of *in vivo* whole-cell recordings from GtACR2$^+$ cells, AP firing frequency was calculated during injection of positive current steps (current amplitude: 50-100 pA) in a time window before (Pre; window duration, 0.4 s), during (Stim; window duration, 0.5 s) and after (Post; window duration, 0.4 s) holographic stimulation over 15 - 120 stimulation trials. Δ_{AP}Freq and the spatial resolution were calculated as for juxtasomal electrophysiological recordings. A cell was considered responsive to 2P holographic illumination if Δ_{AP}Freq was < -0.1 of the average firing frequency in Pre and Post periods at power values ≥ 80 mW *per* shape and current injection of 50-100 pA. 14 out of 15 GtACR2-positive cells were considered as 2P responsive. In slice experiments, the amplitude of GtACR2 photocurrents was calculated as the peak current in the first 100 ms after light onset on a current trace obtained by averaging 3 - 7 stimulation trials.

All values are expressed as mean ± s.e.m, unless otherwise stated. All recordings with no technical issues were included in the analysis. For $n \geq 10$, a Kolmogorov-Smirnov normality test was used to test for normality. For $n < 10$, a Saphiro-Wilk normality test was adopted. In case of normal distribution, Student's *t*-test was used to calculate statistical significance when comparing two populations of data. For non-normal distributions, the non-parametric Mann-Whitney or Wilcoxon signed-rank (for unpaired and paired comparison, respectively) tests were used. When multiple (> 2) populations of data were compared, one-way ANOVA with Bonferroni *post hoc* test was used in case of Gaussian distribution. For non-normal distribution and multiple comparisons, the non-parametric Friedman test or Kruskall-Wallis test with Dunn *post hoc* correction were used for paired and unpaired comparison, respectively. All tests were two-sided. Statistical analysis was performed using Prism (GraphPad Software, La Jolla, CA) and OriginPro 9.1 (OriginLab).

4. Results

4.1 Cellular resolution 2P holographic stimulation in vivo

To stimulate neurons with cellular resolution *in vivo*, we used a liquid crystal spatial light modulator (SLM) -based holographic module which was integrated in a commercial laser scanning 2P microscope [180], [227] (Figure 20A) and we programmed the SLM (see Methods) to project extended elliptic illumination profiles that were centered on the cell body of target neurons (Figure 20B).

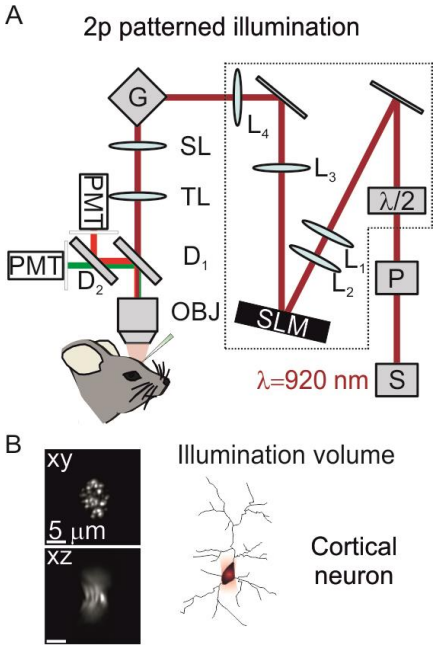

Figure 20. 2P holographic illumination with extended shapes. A. Optical set-up for 2P holographic illumination. S, laser source; P, Pockels cell; λ/2, half-wave plate; $L_{1\text{-}4}$ lenses; SLM, spatial light modulator; G, galvanometric mirrors; SL, TL, scan and tube lenses; D_1, D_2, dichroic mirrors; PMT, photomultiplier tube; OBJ, objective. **B.** Left: intensity profiles in the focal plane (xy, top) and along the axial direction (xz, bottom) of an extended shape illuminating a thin (thickness: ~ 150 nm) fluorescent layer and generated with holographic illumination system displayed in (A). λ_{exc} = 920 nm. Right: schematic of the single cell holographic stimulation paradigm. An elliptical shape was drawn on the soma of opsin-expressing neurons resulting in an extended 2P illumination volume covering the cell body of the target cell.

To validate our approach we performed simultaneous 2P targeted juxtasomal recordings and photostimulation experiments in anesthetized mice in layer 2/3 principal neurons co-expressing ChR2 and the red fluorescent protein tdTomato, which facilitated targeting neurons under the microscope (Figure 21A). Once a stable electrophysiological recording was achieved from an opsin-positive neuron

(see Methods for definition), a high resolution image was acquired in the scanning configuration and an elliptical shape (ellipse axis: 7 - 16 µm) was projected on the cell body of the recorded neuron. Significant increase in AP firing frequency was observed upon 2P holographic illumination with extended shapes (stimulus duration: 500 ms; stimulus power: 42 - 92 mW *per* cell; λ_{exc} = 920 nm, Figure 21B).

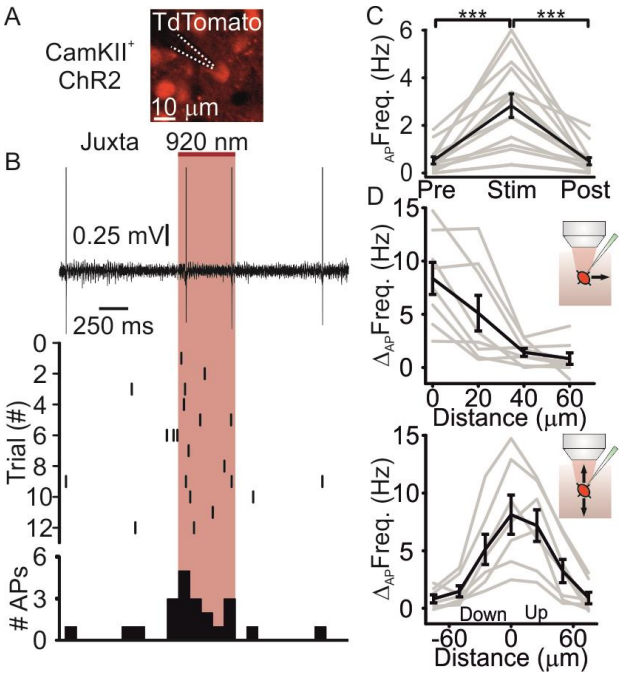

Figure 21. 2P holographic stimulation of ChR2-expressing cells *in vivo*. A. 2P image of a ChR2-mCherry (red) expressing layer 2/3 neuron in the sensory cortex. The neuron was targeted for simultaneous holographic stimulation and juxtasomal electrophysiological recording by monitoring the cytosolic fluorescence of the red reporter tdTomato which was co-expressed with ChR2. The dotted line indicates the recording pipette. **B.** Top: representative electrophysiological trace recorded before, during, and after single cell holographic stimulation (red bar, laser power: 80 mW). Middle: raster plot showing cell response over consecutive trials for the same neuron displayed on the top. Bottom: AP distribution for the trials shown in the middle panel (time bin: 100 ms). **C.** Average firing frequency before (Pre), during (Stim) and after (Post) holographic stimulation of ChR2-expressing layer 2/3 neurons. p = 2.3E-5, Friedmann test with Dunn's correction, N = 14 cells from 4 mice. Average laser power: 79 mW; range: 42 - 92 mW. **D.** Firing frequency increase *vs* displacement of the excitation volume in the radial (top) and axial (bottom) direction during holographic illumination of layer 2/3 neurons expressing ChR2 and C1V1. Top: N = 8 cells from 3 mice. Bottom: N = 7 cells from 3 mice. In this as well as in other figures, the black line represents the average of all single experiments which are depicted with gray lines. *, p < 0.05; **, p < 0.01; ***, p < 0.001.

To verify that the observed effect depended on opsin activation and not on membrane depolarization due to direct 2P stimulation [228], we performed similar experiments in opsin-negative cells (Figure

22). We found that holographic illumination with extended shapes of the same spatial profile and light intensity did not significantly modify the membrane potential nor the AP firing rate of recorded opsin-negative neurons *in vivo* (Figures 22A, C). To evaluate the spatial resolution of our stimulation method, we measured the spiking response to holographic photostimulation of opsin-positive neurons while incrementally shifting the stimulation shape in the radial and axial direction (Figure 21F). We found spatial constants (see Methods for definition) of ~ 20 µm, ~ 35 µm and ~ 25 µm in the radial, $axial_{up}$, and $axial_{down}$ directions, respectively.

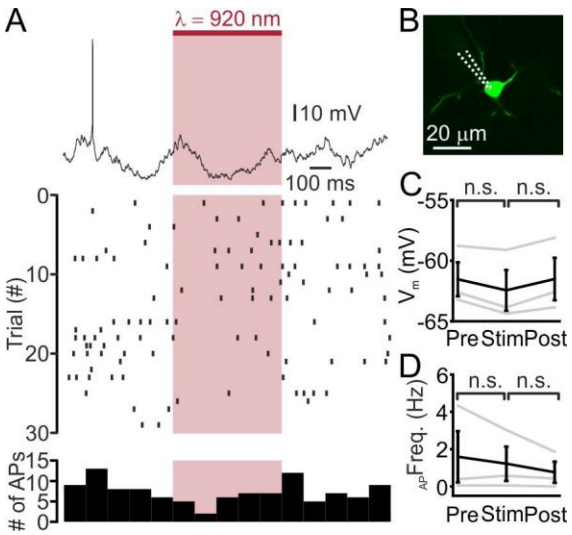

Figure 22. No effect of 2P holographic illumination on opsin-negative neurons *in vivo*. A. Top: representative whole-cell current-clamp trace recorded before, during, and after single cell holographic stimulation (red bar, laser power: 80 mW; λ_{exc} = 920 nm) in an opsin negative layer 2/3 cortical neuron. Middle: raster plot showing cell response over consecutive trials for the same cell displayed on the top. Bottom: AP distribution for the trials shown in the middle panel (time bin: 100 ms). **B.** 2P image of one opsin-negative layer 2/3 neuron which was recorded in whole-cell configuration and filled with Alexa Fluor 488 (green). Dotted lines indicate the glass pipette. **C.** Average membrane potential before (Pre), during (Stim) and after (Post) holographic illumination of opsin-negative neurons in layer 2/3. p = 0.19, Friedmann test with Dunn's correction, N = 3 cells from 2 mice. Laser power, 80 mW; λ_{exc} = 920 nm. n.s. indicates p > 0.05. **D.** Average firing frequency before (Pre), during (Stim) and after (Post) holographic illumination of opsin-negative neurons in L2/3. p = 0.53, Friedmann test with Dunn's correction, N = 3 cells from 2 mice.

Targeting ChR2 to the soma (Figure 23) significantly decreased the average power needed to promote spiking responses in the illuminated neuron (ChR2: average laser power *per* cell, 79 mW; Δ_{AP}Freq =

2.3 ± 0.4 Hz, N = 14 from 4 mice. Soma-targeted ChR2: average laser power *per* cell, 30 mW; Δ_{AP}Freq = 5.3 ± 1.1 Hz, N = 21 from 6 mice, p = 2.3E-3, Wilcoxon signed rank test for paired comparison).

Co-expressing ChR2 with another excitatory opsin (e.g., C1V1) had similar effect (Figure 24). Importantly, somatic targeting of ChR2 significantly improved the spatial resolution of holographic stimulation compared to non soma-targeted opsins, decreasing the radial (10 µm *vs* 20 µm for soma-targeted and non soma-targeted opsins respectively, p = 2.7E-2, unpaired Student's *t*-test) and $axial_{up}$ (13 µm *vs* 35 µm for soma-targeted and non soma-targeted opsins respectively, p = 6.8E-5; unpaired Student's *t*-test) spatial constants (Table 1).

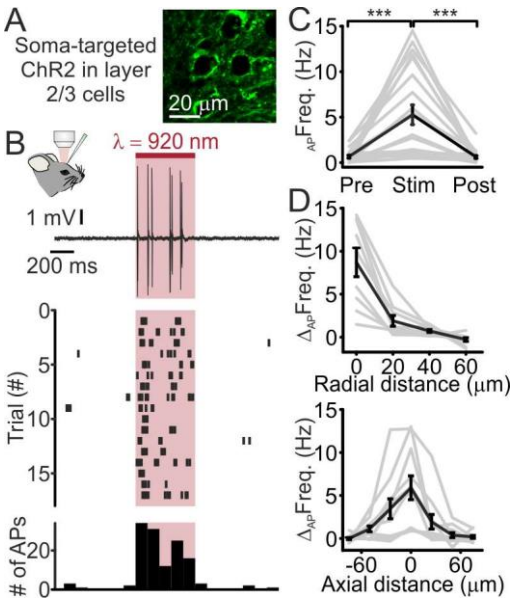

Figure 23. Somatic targeting of opsins increases the spatial resolution of holographic stimulation *in vivo*. **A.** Confocal image of layer 2/3 neurons expressing soma-targeted ChR2-eYFP (green). **B.** Top: representative juxtasomal electrophysiological trace recorded before, during, and after single cell holographic stimulation (red bar, laser power: 30 mW; λ_{exc} = 920 nm) of a cortical layer 2/3 neuron expressing a soma-targeted ChR2. Middle: raster plot showing cell response over consecutive trials for the same cell displayed on the top. Bottom: AP distribution for the trials shown in the middle panel (time bin: 100 ms). **C.** Average firing frequency before (Pre), during (Stim) and after (Post) holographic stimulation of layer 2/3 neurons expressing the soma-targeted ChR2. p = 1.3E-7, Friedmann test with Dunn's correction, N = 21 cells from 6 mice. Laser power, 30 mW. **D.** Firing frequency increase *vs* displacement of the excitation volume in the radial (top) and axial (bottom) direction during holographic illumination. Top: N = 9 cells from 3 mice. Bottom: N = 11 cells from 3 mice.

Taken together these initial data demonstrate that 2P holographic illumination allows efficient perturbation of the spiking activity of opsin-expressing layer 2/3 principal neurons with cellular resolution *in vivo*.

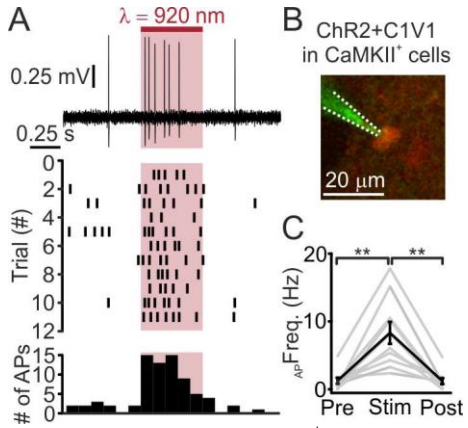

Figure 24. 2P holographic stimulation of layer 2/3 CaMKII$^+$ cortical neurons *in vivo*. A. Top: representative electrophysiological trace recorded before, during, and after single cell holographic stimulation (red bar, laser power: 31 mW) in a neuron co-expressing ChR2 and C1V1. Middle: raster plot showing cell response over consecutive trials for the same cell displayed on the top. Bottom: AP distribution for the trials shown in the middle panel (time bin: 100 ms). **B.** 2P image of a layer 2/3 CaMKII$^+$ neuron co-expressing ChR2, C1V1, and tdTomato (red). **c.** Average firing frequency before (Pre), during (Stim) and after (Post) holographic stimulation of ChR2+C1V1-expressing layer 2/3 neurons. p = 1E-4, Friedmann test with Dunn's correction, N = 10 cells from 3 mice. Laser power: 31 mW.

4.2 Two-photon holographic stimulation across cortical cell types and layers

We investigated whether holographic stimulation could be efficiently applied to cortical cell types other than layer 2/3 excitatory neurons. To this end, we first expressed ChR2 in two major subpopulations of cortical interneurons in layer 2/3, the somatostatin-positive (SST$^+$) and the parvalbumin-positive (PV$^+$) interneurons. Using simultaneous photostimulation and 2P targeted juxtasomal recordings *in vivo*, we found that illumination with an extended 2P shape covering the cell body of recorded neurons (stimulus power: 30 mW *per* cell) significantly increased their firing rate (Figures 25A-C, leftmost and middle panels). We then expressed ChR2 selectively in sodium channel, non voltage-gated 1 alpha-positive (Scnn$^+$) excitatory neurons of layer 4, the main thalamorecipient cortical population of the sensory cortex.

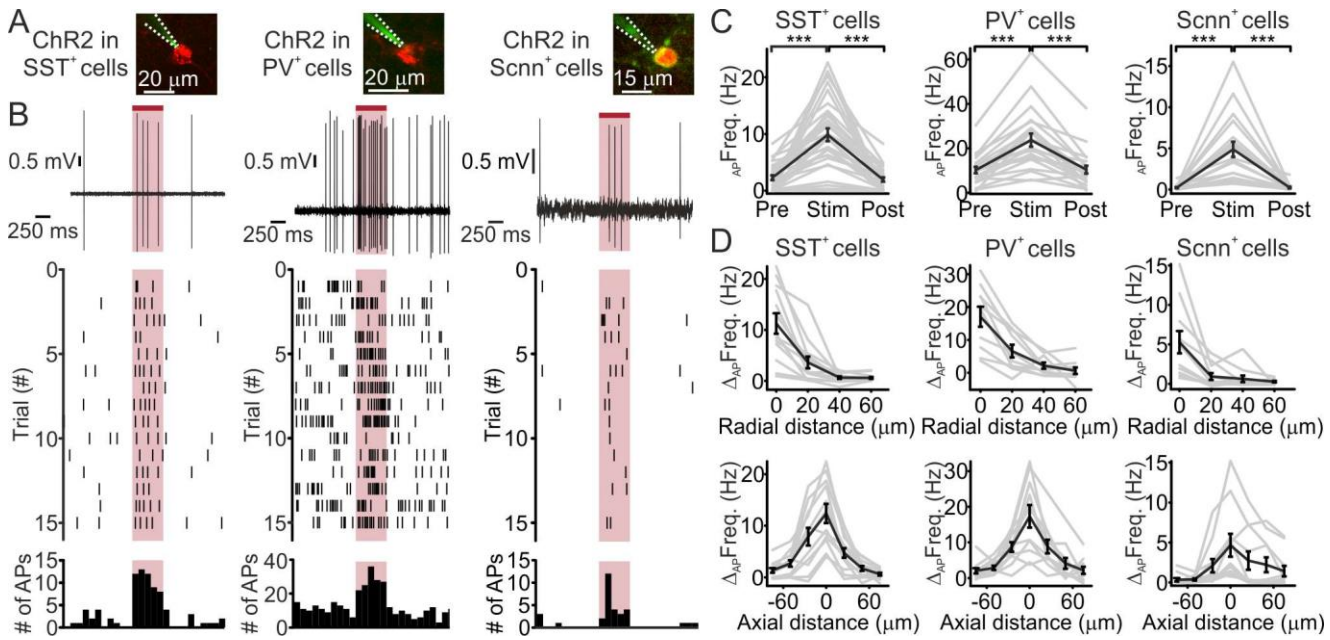

Figure 25. 2P holographic stimulation across cell types and layers *in vivo*. A. 2P image of one layer 2/3 SST^+ (left) and one layer 2/3 PV^+ (middle) interneurons expressing mCherry (red). One layer 4 $Scnn^+$ neuron expressing ChR2-eYFP (green) together with tdTomato (red) is shown on the right. Neurons were recorded in the juxtasomal electrophysiological configuration with a glass pipette (dotted white line) filled with Alexa Fluor 488 (green). **B.** Top: representative electrophysiological traces recorded before, during, and after single cell holographic stimulation (red bar) for one SST^+ (left), one PV^+ (middle) and one $Scnn^+$ (right) cell. λ_{exc} = 920 nm. Laser power: 30 mW for SST- and PV^+ cells, 50 mW for $Scnn^+$ neurons. Middle: raster plot showing cell response over several consecutive trials for the same neurons displayed on the top. Bottom: AP distribution for the trials shown in the middle panel (time bin: 100 ms) for all cell types (SST, left; PV, middle; Scnn, right). **C.** Average firing frequency before (Pre), during (Stim) and after (Post) holographic stimulation of ChR2-expressing layer 2/3 SST^+ (left), layer 2/3 PV^+ (middle), and layer 4 $Scnn^+$ (right) neurons. SST^+ cells: p = 1.3E-9, Friedmann test with Dunn's correction, N = 31 cells from 7 mice. Laser power: 30 mW. PV^+ cells: p = 1.2E-7, ANOVA test with Bonferroni's correction, N = 22 cells from 7 mice. Laser power: 30 mW. $Scnn^+$ cells p =5.2E-7, Friedmann test with Dunn's correction, N = 19 cells from 8 mice. Laser power: 50 mW. **D.** Firing frequency increase *vs* displacement of the excitation volume in the radial (top) and axial (bottom) direction during holographic illumination for layer 2/3 SST^+ (left), layer 2/3 PV^+ (middle), and layer 4 $Scnn^+$ (right) neurons. SST^+ cells: top, N = 13 cells from 3 mice; bottom, N = 12 cells from 3 mice. PV^+ cells: top, N = 10 cells from 4 mice; bottom, N = 11 cells from 4 mice. $Scnn^+$ cells: top and bottom, N = 11 cells from 5 mice.

As for more superficial cells, we found that holographic illumination (stimulus power: 50 mW *per* cell) significantly increased the spike rate of layer 4 $Scnn^+$ neurons (Figures 25A-C rightmost panels). The spatial resolution of our optical manipulation was cell-type specific (Figure 25D and Table 1). SST^+ and $Scnn^+$ cells had smaller radial spatial constant with respect to layer 2/3 principal neurons (SST^+, p = 2.5E-2, unpaired Student's *t*-test; $Scnn^+$, p = 5E-3, Mann-Whitney test). SST^+ cells also had smaller $axial_{up}$ spatial constant with respect to layer 2/3 principal neurons (p = 7.8E-3, Mann-Whitney test)

while the $axial_{down}$ spatial constant was similar for all types of neurons tested (Table 1). Only layer 2/3 pyramidal neurons showed a significant difference between the spatial constants in the axial up and axial down directions (axial up spatial constant larger than the axial down spatial constant, p = 0.011, N = 7 from 3 mice, paired Student's *t*-test), probably as a consequence of the markedly polarized morphology of these cells with the large apical dendrite directed towards layer 1. All cell types displayed a direct proportionality between the response to photostimulation and illumination power (Figure 26). Moreover, while the probability of discharging one or more APs during 2P stimulation was already significantly greater than the spontaneous probability of firing within the first 10 ms for SST^+ and PV^+ interneurons (p = 9.1E-3 Wilcoxon signed rank test and p = 4.3E-3 paired Student's *t*-test for SST^+ and PV^+ interneurons respectively, Figure 26 rightmost panels), the probability of firing increased as a function of time during the stimulation for all cell types and conditions tested.

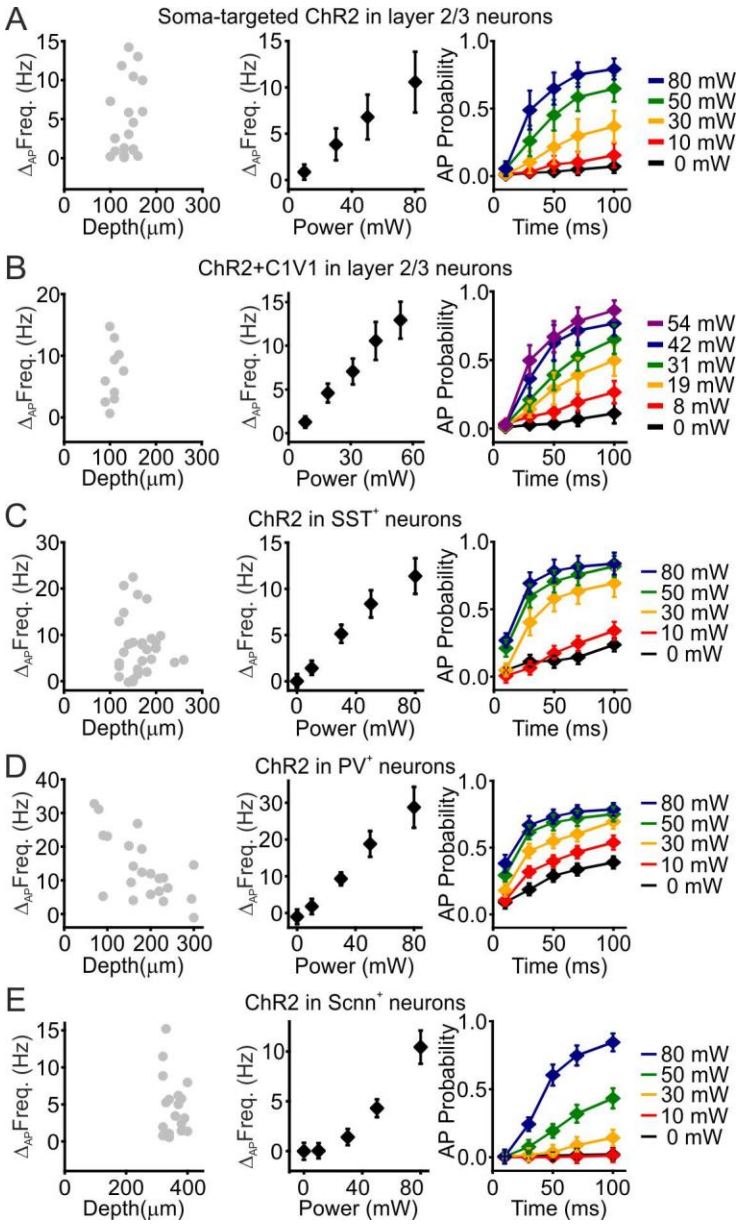

Figure 26. Firing probability during holographic illumination increases with stimulation power. A. Left panel: average AP frequency increase during holographic illumination (λ_{exc} = 920 nm) as a function of the depth of the recorded cells for layer 2/3 neurons expressing the soma-targeted ChR2. N = 21 neurons from 6 mice; laser power, 30 mW. Middle panel: average AP frequency increase during holographic illumination as a function of laser power. N = 8 cells from 4 mice. Right panel: average probability of firing during holographic illumination as a function of time after the beginning of the stimulation at different power levels. N = 8 cells from 4 mice. **B.** Same as in (A) for layer 2/3 cells expressing ChR2 and C1V1. Left panel: N = 10 cells from 3 mice; laser power, 31 mW. Middle panel: N = 10 cells from 3 mice. Right panel: N = 10 cells from 3 mice. **C.** Same as in (A) for layer 2/3 SST^+ cells expressing ChR2. Left panel: N = 31 cells from 7 mice; laser power, 30 mW. Middle panel: N = 12 cells from 3 mice. Right panel: N = 12 cells from 3 mice. **D.** Same as in (A), but for layer 2/3 PV^+ interneurons expressing ChR2. Left panel: N = 22 cells from 7 mice, laser power: 30 mW. Middle panel: N = 13 cells from 5 mice. Right panel: N = 13 cells from 5 mice. **E.** Same as in (A), but for layer 4 $Scnn^+$ neurons expressing ChR2. Left panel: N = 19 cells from 8 mice, laser power: 50 mW. Middle panel: N = 14 cells from 7 mice. Right panel: N = 14 cells from 7 mice.

4.3 Cellular resolution 2P holographic inhibition *in vivo*

Our previous data demonstrate that holographic stimulation with extended shapes can be used for activation of neurons with high spatial resolution *in vivo*. We determined whether holographic illumination could also be used for efficient 2P optogenetic inhibition with cellular resolution. To address this question, we focused on GtACR2, a chloride-permeable channelrhodopsin [109]. Although the 2P excitability of GtACR2 has not yet been reported, we reasoned that its large photocurrent, its high light-sensitivity, and its blue light-sensitive single-photon absorption spectrum made it a good candidate for 2P holographic stimulation at $\lambda < 1000$ nm. In addition, expression of GtACR2 has been reported to be well tolerated by neurons [109]. We first expressed this inhibitory opsin in the cortex and recorded GtACR2-mediated photocurrents in patch-clamp voltage-clamp configuration from opsin-positive cells (see Methods for definition) in acute brain slices (Figure 27A). We found that holographic illumination of GtACR2-expressing neurons with an elliptical shape targeted to the cell body of the recorded cell (λ_{exc} = 920 nm; average power, 30 mW; stimulus duration, 500 ms) triggered clear outward currents (range, 6 - 112 pA; holding potential, -50 mV; chloride equilibrium potential, -68 mV). Peak amplitude of photocurrents increased with power (Figure 27B) and showed a nearly power-squared dependence for low power values (inset in Figure 27B). Moreover, while keeping light power density constant we performed holographic 2P illumination at different light wavelengths (range: 740 - 1040 nm). We found that GtACR2 photocurrents had large peak amplitude at 920 nm and decreased for longer and shorter wavelengths (Figure 27C). We thus concluded that GtACR2 can be efficiently stimulated through a 2P absorption process, that holographic illumination triggers clear photocurrents in opsin-expressing neurons, and that the 2P absorption spectrum of GtACR2 shows a clear peak at ~ 920 nm.

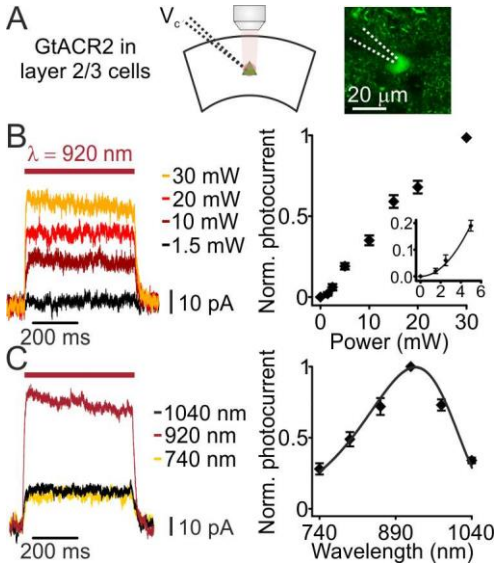

Figure 27. 2P holographic activation of the inhibitory opsin GtACR2 with extended shapes. A. Left: schematic of the experimental configuration for slice recordings. Neurons expressing GtACR2 were recorded in voltage-clamp (V_c) and held at -50 mV while 2P holographic illumination with an elliptical shape covering the cell soma was performed. Chloride equilibrium potential: -68 mV. Right: 2P image of a layer 2/3 neuron expressing GtACR2-eGFP that was recorded in voltage-clamp configuration. The glass pipette (dotted lines) was filled with Alexa Fluor 488. **B.** Left: representative traces showing GtACR2-mediated photocurrents evoked by 2P holographic illumination at different illumination powers. Traces are averages over 3 stimulation trials. Right: average peak photocurrent evoked by 2P holographic illumination at various laser powers. λ_{exc} = 920 nm. In each cell, photocurrent values were normalized to the maximal photocurrent recorded at 30 mW light power. The inset displays the nonlinear dependence of photocurrents on the laser power at low power values. N = 7-11 cells from 2-3 mice. **C.** Left: representative traces showing photocurrents mediated by GtACR2 and evoked by 2P holographic illumination at different wavelengths. Traces are averages of 4 stimulation trials. Average laser power: 25 mW. Right: average GtACR2 peak photocurrent evoked by 2P holographic illumination as a function of the wavelength of the stimulation beam. Photocurrent values were normalized to the peak photocurrent at 920 nm. Values were fitted with a three parameter Weibull function. N = 9 cells from 4 mice; laser power: 20-30 mW.

Given the results described above, we then asked whether holographic stimulation of GtACR2 could be used to efficiently decrease neural excitability with cellular resolution *in vivo*. To this end, we performed whole-cell current-clamp recordings from layer 2/3 cortical neurons expressing GtACR2 in anesthetized mice (Figure 28). We found that illumination with an extended shape covering the cell body of the recorded neuron (stimulus power: 10 - 80 mW *per* cell) while a small depolarizing current was injected (average current amplitude: 74 pA) lead to a significant hyperpolarization of the cell (average membrane potential Pre: -46.2 ± 1.1 mV, Stim: -50.1 ± 1.1 mV , Post: -44.4 ± 1.3 mV, p =

2E-15, ANOVA test with Bonferroni's correction, N = 14 from 7 mice). Moreover, we found that holographic illumination significantly decreased cellular firing induced by a small current injection (Figures 28A-B). We measured the spiking response of GtACR2-positive neurons to holographic illumination while incrementally shifting the stimulation shape in the radial and axial direction (Figure 28C). We found spatial constants of ~ 11 µm, ~ 33 µm and ~ 29 µm in the radial, $axial_{up}$, and $axial_{down}$ directions respectively (Table 1), not dissimilar from those observed for holographic stimulation of excitatory opsins (Table 1).

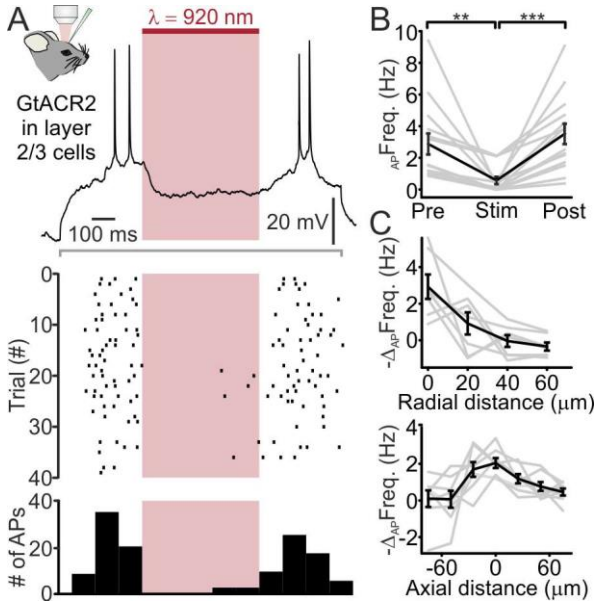

Figure 28. 2P holographic inhibition of GtACR2-expressing neurons with cellular resolution *in vivo*. A. Top: representative trace showing the membrane potential of one layer 2/3 GtACR2-expressing neuron recorded in whole-cell configuration during simultaneous current injection (grey line below the trace; current amplitude, 70 pA) and 2P holographic illumination (red bar). Laser power: 80 mW. Inset: schematic of the experiment for simultaneous 2P holographic illumination and patch-clamp whole-cell recordings from GtACR2-positive neurons *in vivo*. Middle: raster plot showing cell response over several consecutive trials for the same cell displayed on the top. Bottom: AP distribution for the trials shown in the middle panel (time bin: 100 ms). **B.** Average firing frequency before (Pre), during (Stim) and after (Post) holographic inhibition of GtACR2-expressing layer 2/3 neurons. Holographic stimulation was performed while injecting a small depolarizing current (average current amplitude, 74 pA; range, 50-100 pA). p =1.8E-5, Friedmann test with Dunn's correction, N = 14 cells from 7 mice. Average laser power, 50 mW; range, 10-80 mW. **C.** Firing frequency decrease *vs* displacement of the excitation volume in the radial (top) and axial (bottom) direction during holographic illumination. Top: N = 7 cells from 4 mice. Bottom: N = 8 cells from 5 mice.

4.4 Simultaneous two-photon imaging of red-shifted indicator and holographic stimulation of blue light-sensitive opsin

Red-shifted channelrhodopsins have been used for 2P stimulation of single neurons simultaneously with GECI-based calcium imaging [147], [165], [203]. One potential drawback of this approach is the remaining absorption by all red-shifted channelrhodopsins in the blue range of their action spectrum [92]. As shown above, our data demonstrate that holographic illumination of blue light-sensitive opsins (ChR2 and GtACR2) at λ = 920 nm can be used to bidirectionally control the excitability of cortical neurons with cellular resolution. We therefore asked whether this stimulation approach could be coupled with imaging of red-shifted functional indicators (e.g., jRCaMP), which are typically best excited in the 2P regime at longer wavelength ($\lambda \sim$ 1100 nm) [63], [229], [230], a wavelength at which blue light-sensitive channelrhodopsins show no detectable activity [159]. To test this possibility, we first evaluated whether raster scanning at these long wavelengths causes opsin activation leading to significant alteration of neuronal spiking activity *in vivo*. We expressed the soma-targeted ChR2 in layer 2/3 cortical neurons and performed juxtasomal electrophysiological recordings from $ChR2^+$ neurons while raster scanning the field of view containing the recorded cell at λ = 1100 nm and scan rate of 11 Hz (scan resolution, 0.58 µm/pixel; dwell time, 4 µs; Figure 29). We found that raster scanning did not significantly affect the firing activity of layer 2/3 soma-targeted $ChR2^+$ neurons at both 30 mW and 50 mW imaging power (Figure 29B-C). As an important control, we found that raster scanning the same field of view at shorter wavelength (λ = 920 nm) and moderate power (laser power: 30 mW) did significantly increase the spiking activity of soma-targeted ChR2-expressing neurons. Moreover, whole-cell current-clamp recordings performed on layer 2/3 neurons expressing the inhibitory opsin GtACR2 showed that raster scanning at λ = 1100 nm did not significantly modify the average membrane potential of opsin-positive neurons (average membrane potential: -62.1 ± 3.3 mV *vs* -62.1 ± 3.3 mV in the absence and presence of raster scanning (laser power, 30 mW), respectively; -

63.7 ± 3.2 mV *vs* -63.9 ± 3.6 mV in the absence and presence of raster scanning (laser power, 50 mW), respectively; p = 1 Wilcoxon signed rank test , N = 4 from 2 mice), as expected from the 2P absorption spectrum of GtACR2 (Figure 27).

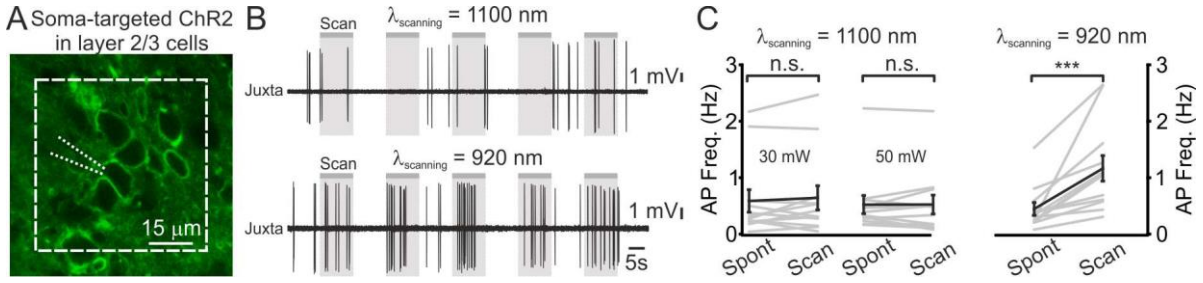

Figure 29. Scanning with infrared-shifted wavelengths does not modify the activity of cells expressing blue light-sensitive opsins. A. 2P image of layer 2/3 neurons expressing the soma-targeted ChR2-eYFP (green) in an anesthetized mouse. One ChR2$^+$ neuron was recorded with a glass pipette (dotted white lines) while 2P raster scanning inside the indicated area (dashed white line) was performed at 11 Hz. **B.** Representative traces recorded in the juxtasomal electrophysiological configuration from one soma-targeted ChR2-expressing neuron during epochs (grey bars) of 2P raster scanning at wavelength 1100 nm (top) and wavelength 920 nm (bottom). Laser power, 30 mW in both conditions. **C.** Average AP frequency during epochs of spontaneous activity (Spont) and during raster scanning (Scan). The left panel shows the comparison when scanning was performed at λ = 1100 nm (laser power, 30 mW and 50 mW). The right panel displays the comparison when scanning was done at λ = 920 nm (laser power, 30 mW). The frame rate was 11 Hz and the scanned area was ~ 60 x 60 µm^2 for all experimental conditions. p = 0.47 for λ = 1100 nm and 30 mW, p = 0.85 for λ = 1100 nm and 50 mW, p = 5E-4 for λ = 920 nm and 30 mW, Wilcoxon signed rank test for paired comparison, N = 12 fields of view from 3 mice.

We finally combined holographic stimulation with raster scanning imaging to perform simultaneous 2P imaging of jRCaMP1a and 2P activation of ChR2 *in vivo*. Using two laser sources (Figure 30A), tuned at 1100 nm (for imaging) and at 920 nm (for holographic stimulation), we performed concurrent imaging and holographic photostimulation experiments in mice that co-expressed jRCaMP1a and soma-targeted ChR2 in layer 2/3 cortical neurons (Figure 30B) or jRCaMP1a and ChR2 in SST$^+$ interneurons (Figure 31). We found that successive holographic stimulation of the cell body of ChR2-expressing neurons (stimulus power: 50 mW *per* cell) reliably evoked fluorescent transients in the stimulated cell (Figure 31B). We then combined this all-optical approach with the photostimulation of multiple specified neurons.

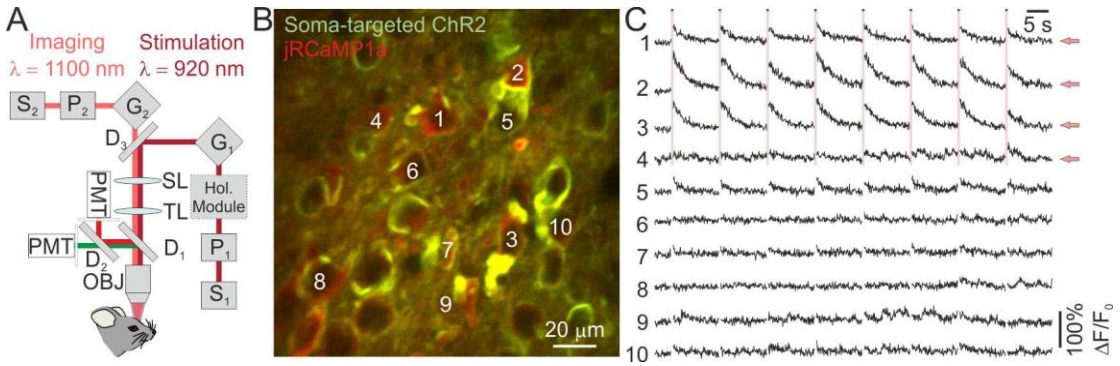

Figure 30. Simultaneous 2P imaging of red-shifted indicator and 2P holographic stimulation of blue-shifted opsin *in vivo*. A. Schematic of the optical set-up for simultaneous 2P imaging (λ_{exc} = 1100 nm) and 2P holographic illumination (λ_{exc} = 920 nm). S_1, stimulation laser source; S_2, imaging laser source; $P_{1\text{-}2}$, Pockels cells; $G_{1\text{-}2}$, galvanometric mirrors; SL, TL, scan and tube lenses; $D_{1\text{-}3}$, dichroic mirrors; PMT, photomultiplier tube; OBJ, objective; Hol. Module, holographic module (comprising the SLM, the $\lambda_{1/2}$, and $L_{1\text{-}4}$ displayed in Figure 1). **B.** 2P image showing layer 2/3 neurons expressing soma-targeted ChR2-eYFP (green) and jRCaMP1a (red) in an anesthetized mouse. **C.** Calcium transients recorded from jRCaMP1a-positive cells (imaging power, 30 mW; frame rate, 11 Hz). The numbers on the left refer to the neurons indicated in panel B. Neurons 1-4 (red arrows) were simultaneously stimulated with four elliptical shapes covering the cell somata. Each stimulation episode is indicated by a red bar (stimulation power *per* cell: ~ 50 mW). Periods of stimulation are removed from the jRCaMP1a fluorescence traces (see Methods section).

We controlled the SLM to generate extended shapes covering the cell bodies of a group of four neurons (Figures 30B-C). We photostimulated the selected neurons (stimulus power, 56 mW *per* cell), while simultaneously imaging these and the surrounding neurons at 11 Hz. Targeted neurons that displayed clear ChR2-expression (neuron 1-3 in Figures 30B-C) showed strong and reliable responses to photostimulation. Neighboring neurons responded weakly to holographic stimulation of target neurons, as expected from previous work [203].

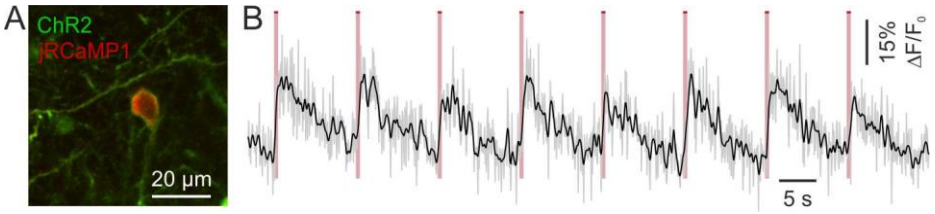

Figure 31. Simultaneous 2P imaging of red-shifted indicator and 2P holographic stimulation of blue light-sensitive opsin in SST$^+$ cells *in vivo*. A. 2P image of one layer 2/3 SST$^+$ interneuron co-expressing ChR2-eYFP and JRCaMP1a. **B.** Calcium transients obtained from the neuron shown in (A) during simultaneous 2P imaging ($\lambda_{scanning}$ = 1100 nm; laser power, 25 mW; frame rate, 11 Hz; scanned area, ~ 90 x 90 µm^2) and holographic stimulation ($\lambda_{stimulation}$ = 920 nm; laser power, 50 mW). $\Delta F/F_0$ (grey trace) was smoothed with a moving average filter (black trace).

Promoter	Construct	$l_{1/2}$ radial (µm)	N radial	$l_{1/2}$ axial$_{up}$ (µm)	$l_{1/2}$ axial$_{down}$ (µm)	N axial
CaMKII$^+$	ChR2+C1V1	20 ± 4	8	35 ± 3	25 ± 2	7
SOM$^+$	ChR2	11 ± 2	13	19 ± 3	24 ± 3	12
PV$^+$	ChR2	12 ± 2	10	26 ± 4	28 ± 4	11
Scnn$^+$	ChR2	6 ± 2	11	30 ± 9	19 ± 3	11
hSyn	ChR2_st	10 ± 2	9	13 ± 3	21 ± 3	11
hSyn	GtACR2	11 ± 4	7	33 ± 4	29 ± 7	8

Table 1. Radial and axial spatial resolution of holographic 2P stimulation across experimental conditions. Average ± s.e.m. values of length of half response ($l_{1/2}$) in the radial and axial (up and down) directions for all conditions tested in this study. N indicates the number of experiments. ChR2_st, soma-targeted ChR2.

5. Discussion

Cellular resolution simultaneous 2P imaging and manipulation is increasingly recognized as a crucial tool for the causal investigation of brain networks (for reviews see [9], [18], [153], [231]). With such a technique, it is possible to perturb the activity of functionally-identified ensembles of neurons, allowing causal testing of the role of specific patterns of activity in regulating network dynamics and behavior [18], [83], [196]. In this paper, we developed and validated an all-optical approach for simultaneous 2P imaging of a red-shifted functional indicator and bidirectional perturbation of neural activity using blue light-sensitive optogenetic actuators *in vivo*. To manipulate the activity of neurons with cellular resolution, we used holographic stimulation with extended shapes and validated our approach across different cell types and layers of the mouse neocortex in anesthetized animals.

The combined use of red-shifted indicators and blue light-sensitive opsins reduces crosstalk between imaging and phostostimulation

Our method greatly expands the potential of simultaneous imaging and perturbation for the functional dissection of brain circuits. Previous published work in the mammalian brain *in vivo* [147], [165], [203] demonstrated that the genetically encoded blue light-sensitive calcium indicator GCaMP [55], [232] can be coupled to the red-shifted excitatory opsin C1V1 [160] for simultaneous 2P imaging and perturbation. However, red-shifted opsins generally display a blue-shifted tail in their absorption spectrum that may complicate spectral separation and lead to crosstalk between GCaMP imaging and opsin activation under certain experimental conditions [203]. This is especially true for red-shifted excitatory opsins with long off kinetics that are often the preferred choice for 2P activation using scanning approaches [159]. We here showed (Figure 29-31) that the use of jRCaMP1a, a red-shifted functional indicator that is excited using 2P stimulation between 1050 nm and 1150 nm, in combination with blue light-sensitive opsins (e.g., ChR2) that display maximal 2P excitability around 920 nm

minimizes this form of crosstalk. Using combined imaging and electrophysiological recordings (Figure 29), we found that the activity of ChR2-expressing cells was not modified by raster scanning ($\lambda_{imaging}$ = 1100 nm; laser intensity, 30 - 50 mW; frame rate, 11 Hz; scan resolution, 0.58 μm/pixel; field of view dimension, 58 x 58 μm^2). The absence of crosstalk likely stems from the spectral separation of the two light-sensitive molecules that we have used (i.e., jRCaMP1a and ChR2), but also from the fast closing kinetics of ChR2 [105] and the low power required for imaging. The experimental configuration that we presented in this study also provides other advantages. For example, the use of red-shifted functional indicators may facilitate deep imaging by using longer wavelengths for fluorescence excitation and emission, which are less sensitive to tissue scattering [68]. Additionally, thanks to their stability for long term expression [63], they can be efficiently used for chronic experiments. Moreover, the stimulation of blue light-sensitive opsins at 920 nm may decrease tissue heating which is higher at the longer wavelengths (λ = 1040 nm) [233] that have been used for stimulation of red-shifted opsins (e.g., C1V1) [147], [158], [159], [165], [203].

2P holographic stimulation of inhibitory opsins

Previous work *in vivo* demonstrated cellular resolution 2P activation of excitatory opsins [147], [165], [203]. Here we show for the first time that holographic 2P illumination can be used for efficient suppression of neural activity with high spatial resolution *in vivo*. Although previous evidence *in vitro* showed that some light-sensitive proton pumps are excitable with a 2P process [159], we here focused on the use of chloride-permeable anion channelrhodopsins. We reasoned that the increased flow of ions per photocycle that characterizes light-sensitive channels would allow generating larger photocurrents and more efficient hyperpolarization of neurons *in vivo* compared to the use of light-sensitive pumps, which only transport a single ion during a photocycle. Among the various chloride-permeable opsins [95], [96], we focused on GtACR2 because of its higher single-channel conductance and its blue light-

sensitive single-photon absorption spectrum [109]. We first demonstrated that GtACR2 was efficiently stimulated through an absorption process that is compatible with 2P excitation. Significant photocurrents were generated through holographic illumination of the cell body of GtACR2-expressing neurons in the acute brain slice preparation (Figure 27). The photocurrent had maximal peak amplitude for λ = 920 nm, similarly to ChR2 [155], [156]. Moreover, holographic stimulation of GtACR2 significantly hyperpolarized principal neurons *in vivo* and efficiently reduced their firing rate while maintaining cellular resolution of the optogenetic perturbation (Figure 28). These results demonstrate that holographic 2P optogenetics can be applied for cellular resolution optical inhibition of brain networks *in vivo*, making it possible to alter endogenous patterns of activity in response to sensory stimuli with unprecedented cellular specificity. Further applications of this new method, which combines digital holography with 2P activation of inhibitory chloride-permeable channels, may include targeted inhibition of specific portion of neural dendrites to study the impact of local inhibitory inputs on dendritic integration *in vivo*.

Holographic stimulation with extended shapes compared to other methods

Cellular resolution 2P excitation of multiple neurons simultaneously using opsins can be obtained with various methods. In one approach commonly named "spiral scan" configuration, a SLM is used to multiplex the laser beam and divide it into several different beamlets each addressing one of the neurons of interest. All beamlets are then scanned using a spiral trajectory across the cell bodies of the target neurons [158], [203]. Alternatively, an extended circular shape approximately the size of a cell body can be obtained by underfilling the back-aperture of the objective, effectively reducing its numerical aperture. This shape can then be sequentially projected to the target neurons [165]. The perturbation methods involving an extended shape that is projected to the cell body of the target neuron is appealing because it allows simultaneous activation of the light-sensitive opsins that are somatically

expressed and may lead to larger instantaneous photocurrents and more efficient perturbation of neuronal excitability compared to sequential approaches. Digital holography has been efficiently used to dynamically generate extended shapes of illumination [191], [192], [209], [211], [212]. One advantage of this approach is that it allows the generation of multiple extended regions of interest within a field of view, enabling simultaneous (and not sequential) stimulation of ensembles of neurons. Previous studies demonstrated that this approach can be efficiently applied to modulate cellular excitability *in vitro* [191], [192], [211], [212]. In this study, we demonstrate the applicability of holographic illumination for cellular resolution bidirectional perturbation of neurons in the mouse neocortex *in vivo* (but see also [209]). We found that holographic stimulation of $ChR2^{+}$ cells efficiently drives neurons to spike (Figures 21 and 25), while holographic illumination of GtACR2-expressing neurons reliably decreases their firing rate (Figure 28). Importantly, we demonstrate that this approach is generalizable and can be applied to cell types that differ in biophysical properties, morphological structure and anatomical location (Figure 25). This is necessary to allow for the application of our method to investigate the role of precise spatiotemporal patterns of neural activity in driving higher cortical functions, as activity patterns are distributed in space and time across several cellular subtypes [18]. Moreover, while previous work [147], [165], [203], [234] demonstrated 2P manipulation of neurons in superficial (i.e., layer 2/3) cortical layers *in vivo*, we showed that this approach can also access deeper layers (i.e., layer 4) in the intact brain. This will allow manipulating activity patterns with cellular resolution in the main thalamorecipient cortical lamina and study how these patterns are processed as they flow through the complex circuitry of the cortical column.

Limitations of our current approach

Although our method efficiently decreased crosstalk between the imaging laser and opsin activation, stimulation with extended shapes induced artefacts in the fluorescence detection, as observed also by

previous investigators [164]. Under our experimental configuration, this artefactual signal may be due to unwanted stimulation by holographic illumination of the fluorescence protein that is tagged to the opsin (e.g., eGFP), the fluorescence of which may leak into the red fluorescence detection channel despite the appropriate barrier filter positioned in front of the photomultiplier (PMT). Or, because the absorption spectrum of jRCaMP1a is low but not negligible at 920 nm (i.e., the wavelength used for stimulation), the artefactual fluorescence signal may also originate from direct activation of jRCaMP1a by holographic stimulation. If jRCaMP1a is expressed at high levels and the area covered by stimulated neuronal somata represents a significant portion of the field of view, the integrated emission of dim jRCaMP1a fluorescence generated by holographic stimulation at 920 nm may generate significant artefacts in the red PMT signal. Under our experimental conditions, this artefactual signal could be removed using background subtraction (Figure 31) or required a blanking period (Figure 30). A solution to this problem could be to synchronize photostimulation with imaging, so that stimulation is performed when the portions of the field of view that are of no interest are being scanned [164]. The use of holographic stimulation with low repetition rate lasers may also facilitate the implementation of such a solution, because of the briefer stimulation pulses that are required under these experimental conditions [154], [209]–[212].

Future developments

Utilizing of low repetition rate lasers for holographic stimulation may also decrease the average stimulation power *per* cell, the latency of neural spiking response, and the jitter of evoked spikes beyond what has been achieved in the current study [209], [211]. The use of low repetition rate lasers might thus be important for optogenetic stimulation when the experimental question necessitates the precise temporal control over patterns of spiking activity in brain circuits. This is the case for instance for a “virtual sensation” experiment, in which the aim is to reproduce a sensory perception in the

absence of the sensory input by driving activity patterns with high temporal (and spatial) precision [83]. To obtain high temporal precision in stimulating cells with complex AP patterns high refresh rate SLMs are also needed. Current technologies allow changing the stimulation pattern with delays that range from few ms to tens of ms [235]. However, there are other scenarios where this temporal precision might not be needed. For example, when natural network dynamics induced by a sensory stimulus need only to be "biased" by slightly increasing or decreasing the probability of firing of specific ensembles of neurons [83]. Our system represents an efficient technical solution to be applied to this stochastic perturbation approach.

The spatial resolution and efficiency of stimulation may be further improved by implementing temporal focusing and by reducing inhomogeneities within the extended shape (i.e., speckles). For example, temporal focusing may be used to improve the axial resolution of excitation [161], [191], [192]. However in this regard, it is important to note that our data show that the spatial resolution in the axial and radial direction was found to depend on the cell type being stimulated (Figure 25), suggesting that the morphology of the cell may be the main limiting factor when the opsin is expressed throughout the cell. In support of this hypothesis, we found that restricting opsin expression to the cell soma improved the spatial resolution of holographic illumination *in vivo*, confirming previous findings in acute brain slice preparation [164].

6. Bibliography

[1] J. G. White, E. Southgate, J. N. Thomson, and S. Brenner, “The Structure of the Nervous System of the Nematode Caenorhabditis elegans,” *Philos. Trans. R. Soc. B Biol. Sci.*, vol. 314, no. 1165, pp. 1–340, Nov. 1986.

[2] E. R. Kandel, J. H. Schwartz, T. M. Jessell, S. A. Siegelbaum, and A. J. Hudspeth, *Principles of Neural Science, Fifth Edition*, vol. 3. 2014.

[3] M. F. Bear, B. W. Connors, and M. A. Paradiso, *Neuroscience*. 2007.

[4] D. Purves, G. Augustine, D. Fitzpatrick, W. Hall, A. LaMantia, and L. White, *Neuroscience*. 2012.

[5] Z. F. Mainen and T. J. Sejnowski, “Reliability of spike timing in neocortical neurons.,” *Science*, vol. 268, no. 5216, pp. 1503–6, Jun. 1995.

[6] M. R. Cohen and J. H. R. Maunsell, “Attention improves performance primarily by reducing interneuronal correlations,” *Nat. Neurosci.*, vol. 12, no. 12, pp. 1594–1600, Dec. 2009.

[7] G. Buzsáki, *Rhythms of the brain*. Oxford University Press, 2006.

[8] D. H. O’Connor, D. Huber, and K. Svoboda, “Reverse engineering the mouse brain,” *Nature*, vol. 461, no. 7266, pp. 923–929, Oct. 2009.

[9] S. Bovetti and T. Fellin, “Optical dissection of brain circuits with patterned illumination through the phase modulation of light,” *J. Neurosci. Methods*, vol. 241, pp. 66–77, 2015.

[10] C. Stosiek, O. Garaschuk, K. Holthoff, and A. Konnerth, “In vivo two-photon calcium imaging of neuronal networks,” *Proc. Natl. Acad. Sci. U. S. A.*, vol. 100, no. 12, pp. 7319–24, Jul. 2003.

[11] K. Ohki, S. Chung, Y. H. Ch’ng, P. Kara, and R. C. Reid, “Functional imaging with cellular resolution reveals precise micro-architecture in visual cortex.,” *Nature*, vol. 433, no. 7026, pp. 597–603, Feb. 2005.

[12] J. N. D. Kerr, C. P. J. de Kock, D. S. Greenberg, R. M. Bruno, B. Sakmann, and F. Helmchen, “Spatial Organization of Neuronal Population Responses in Layer 2/3 of Rat Barrel Cortex,” *J. Neurosci.*, vol. 27, no. 48, pp. 13316–13328, 2007.

[13] R. V Rikhye and M. Sur, “Spatial Correlations in Natural Scenes Modulate Response Reliability in Mouse Visual Cortex.,” *J. Neurosci.*, vol. 35, no. 43, pp. 14661–14680, 2015.

[14] A. J. Peters, S. X. Chen, and T. Komiyama, “Emergence of reproducible spatiotemporal activity during motor learning.,” *Nature*, vol. 510, no. 7504, pp. 263–7, 2014.

[15] R. H. R. Hahnloser, A. a Kozhevnikov, and M. S. Fee, “An ultra-sparse code underlies the

generation of neural sequences in a songbird.," *Nature*, vol. 419, no. 6902, pp. 65–70, 2002.

[16] Y. Ziv, L. D. Burns, E. D. Cocker, E. O. Hamel, K. K. Ghosh, L. J. Kitch, A. El Gamal, and M. J. Schnitzer, "Long-term dynamics of CA1 hippocampal place codes," vol. 2013, no. January, 2013.

[17] R. Yuste, "From the neuron doctrine to neural networks," *Nat. Rev. Neurosci.*, vol. 16, no. 8, pp. 487–497, Jul. 2015.

[18] L. Carrillo-reid, W. Yang, J. K. Miller, and D. S. Peterka, "Imaging and Optically Manipulating Neuronal Ensembles," no. March, pp. 271–293, 2017.

[19] A. Schüz and G. Palm, "Density of neurons and synapses in the cerebral cortex of the mouse," *J. Comp. Neurol.*, vol. 286, no. 4, pp. 442–455, 1989.

[20] A. Schüz, D. Chaimow, D. Liewald, and M. Dortenman, "Quantitative Aspects of Corticocortical Connections: A Tracer Study in the Mouse," *Cereb. Cortex*, vol. 16, no. 10, pp. 1474–1486, Oct. 2006.

[21] S. M. Gaglani, L. Lu, R. W. Williams, and G. D. Rosen, "The genetic control of neocortex volume and covariation with neocortical gene expression in mice," *BMC Neurosci.*, vol. 10, no. 1, p. 44, May 2009.

[22] D. Feldmeyer, M. Brecht, F. Helmchen, C. C. H. Petersen, J. F. A. Poulet, J. F. Staiger, H. J. Luhmann, and C. Schwarz, "Progress in Neurobiology Barrel cortex function," *Prog. Neurobiol.*, vol. 103, pp. 3–27, 2013.

[23] G. Buzsáki, C. a Anastassiou, and C. Koch, "The origin of extracellular fields and currents--EEG, ECoG, LFP and spikes.," *Nat. Rev. Neurosci.*, vol. 13, no. 6, pp. 407–20, Jun. 2012.

[24] T. W. Margrie, A. H. Meyer, A. Caputi, H. Monyer, M. T. Hasan, A. T. Schaefer, W. Denk, and M. Brecht, "Targeted whole-cell recordings in the mammalian brain in vivo.," *Neuron*, vol. 39, no. 6, pp. 911–8, Sep. 2003.

[25] D. H. HUBEL and T. N. WIESEL, "Receptive fields of single neurones in the cat's striate cortex.," *J. Physiol.*, vol. 148, pp. 574–91, Oct. 1959.

[26] L. Bareket-Keren and Y. Hanein, "Carbon nanotube-based multi electrode arrays for neuronal interfacing: progress and prospects.," *Front. Neural Circuits*, vol. 6, p. 122, 2012.

[27] M. E. Spira and A. Hai, "Multi-electrode array technologies for neuroscience and cardiology," *Nat. Nanotechnol.*, vol. 8, no. 2, pp. 83–94, Feb. 2013.

[28] J. Viventi and J. A. Blanco, "Development of high resolution, multiplexed electrode arrays: Opportunities and challenges," in *2012 Annual International Conference of the IEEE*

Engineering in Medicine and Biology Society, 2012, pp. 1394–1396.

[29] J. J. Jun, N. A. Steinmetz, J. H. Siegle, D. J. Denman, M. Bauza, B. Barbarits, A. K. Lee, C. A. Anastassiou, A. Andrei, Ç. Aydın, M. Barbic, T. J. Blanche, V. Bonin, J. Couto, B. Dutta, S. L. Gratiy, D. A. Gutnisky, M. Häusser, B. Karsh, P. Ledochowitsch, C. M. Lopez, C. Mitelut, S. Musa, M. Okun, M. Pachitariu, J. Putzeys, P. D. Rich, C. Rossant, W. Sun, K. Svoboda, M. Carandini, K. D. Harris, C. Koch, J. O'Keefe, and T. D. Harris, "Fully integrated silicon probes for high-density recording of neural activity," *Nature*, vol. 551, no. 7679, pp. 232–236, Nov. 2017.

[30] G. Agarwal, I. H. Stevenson, A. Berényi, K. Mizuseki, G. Buzsáki, and F. T. Sommer, "Spatially distributed local fields in the hippocampus encode rat position.," *Science*, vol. 344, no. 6184, pp. 626–30, May 2014.

[31] M. Shein-Idelson, L. Pammer, M. Hemberger, and G. Laurent, "Large-scale mapping of cortical synaptic projections with extracellular electrode arrays," *Nat. Methods*, vol. 14, no. 9, pp. 882–890, Aug. 2017.

[32] T. Kim, J. G. McCall, Y. H. Jung, X. Huang, E. R. Siuda, Y. Li, J. Song, Y. M. Song, H. A. Pao, R.-H. Kim, C. Lu, S. D. Lee, I.-S. Song, G. Shin, R. Al-Hasani, S. Kim, M. P. Tan, Y. Huang, F. G. Omenetto, J. A. Rogers, and M. R. Bruchas, "Injectable, cellular-scale optoelectronics with applications for wireless optogenetics.," *Science*, vol. 340, no. 6129, pp. 211–6, Apr. 2013.

[33] D. A. Dombeck, C. D. Harvey, L. Tian, L. L. Looger, and D. W. Tank, "Functional imaging of hippocampal place cells at cellular resolution during virtual navigation.," *Nat. Neurosci.*, vol. 13, no. 11, pp. 1433–40, Nov. 2010.

[34] R. C. Craddock, S. Jbabdi, C.-G. Yan, J. T. Vogelstein, F. X. Castellanos, A. Di Martino, C. Kelly, K. Heberlein, S. Colcombe, and M. P. Milham, "Imaging human connectomes at the macroscale," *Nat. Methods*, vol. 10, no. 6, pp. 524–539, May 2013.

[35] K. Uğurbil, J. Xu, E. J. Auerbach, S. Moeller, A. T. Vu, J. M. Duarte-Carvajalino, C. Lenglet, X. Wu, S. Schmitter, P. F. Van de Moortele, J. Strupp, G. Sapiro, F. De Martino, D. Wang, N. Harel, M. Garwood, L. Chen, D. A. Feinberg, S. M. Smith, K. L. Miller, S. N. Sotiropoulos, S. Jbabdi, J. L. R. Andersson, T. E. J. Behrens, M. F. Glasser, D. C. Van Essen, E. Yacoub, and WU-Minn HCP Consortium, "Pushing spatial and temporal resolution for functional and diffusion MRI in the Human Connectome Project," *Neuroimage*, vol. 80, pp. 80–104, Oct. 2013.

[36] D. C. Van Essen, S. M. Smith, D. M. Barch, T. E. J. Behrens, E. Yacoub, K. Ugurbil, and WU-Minn HCP Consortium, "The WU-Minn Human Connectome Project: An overview,"

Neuroimage, vol. 80, pp. 62–79, Oct. 2013.

[37] D. Shoham, D. E. Glaser, A. Arieli, T. Kenet, C. Wijnbergen, Y. Toledo, R. Hildesheim, and A. Grinvald, "Imaging cortical dynamics at high spatial and temporal resolution with novel blue voltage-sensitive dyes.," *Neuron*, vol. 24, no. 4, pp. 791–802, Dec. 1999.

[38] C. Grienberger and A. Konnerth, "Imaging Calcium in Neurons," *Neuron*, vol. 73, no. 5, pp. 862–885, Mar. 2012.

[39] S. Bovetti, C. Moretti, and T. Fellin, "Mapping brain circuit function in vivo using two-photon fluorescence microscopy," *Microsc. Res. Tech.*, vol. 77, no. 7, pp. 492–501, Jul. 2014.

[40] W. Yang and R. Yuste, "In vivo imaging of neural activity," vol. 14, no. 4, 2017.

[41] K. Svoboda and R. Yasuda, "Principles of Two-Photon Excitation Microscopy and Its Applications to Neuroscience," *Neuron*, vol. 50, no. 6, pp. 823–839, Jun. 2006.

[42] R. Y. Tsien, "A non-disruptive technique for loading calcium buffers and indicators into cells," *Nature*, vol. 290, no. 5806, pp. 527–528, Apr. 1981.

[43] R. Yuste and L. C. Katz, "Control of postsynaptic Ca2+ influx in developing neocortex by excitatory and inhibitory neurotransmitters.," *Neuron*, vol. 6, no. 3, pp. 333–44, Mar. 1991.

[44] P. G. Haydon, "GLIA: listening and talking to the synapse.," *Nat. Rev. Neurosci.*, vol. 2, no. 3, pp. 185–193, Mar. 2001.

[45] A. Volterra and J. Meldolesi, "Astrocytes, from brain glue to communication elements: the revolution continues," *Nat. Rev. Neurosci.*, vol. 6, no. 8, pp. 626–640, Aug. 2005.

[46] T. Fellin, "Communication between neurons and astrocytes: relevance to the modulation of synaptic and network activity," *J. Neurochem.*, vol. 108, no. 3, pp. 533–544, Feb. 2009.

[47] R. Y. Tsien, "New calcium indicators and buffers with high selectivity against magnesium and protons: design, synthesis, and properties of prototype structures.," *Biochemistry*, vol. 19, no. 11, pp. 2396–404, May 1980.

[48] T. Terai and T. Nagano, "Small-molecule fluorophores and fluorescent probes for bioimaging," *Pflügers Arch. - Eur. J. Physiol.*, vol. 465, no. 3, pp. 347–359, Mar. 2013.

[49] T. Knöpfel, J. Díez-García, and W. Akemann, "Optical probing of neuronal circuit dynamics: genetically encoded versus classical fluorescent sensors," *Trends Neurosci.*, vol. 29, no. 3, pp. 160–166, Mar. 2006.

[50] G. Y. Wiederschain, "The Molecular Probes handbook. A guide to fluorescent probes and labeling technologies," *Biochem.*, vol. 76, no. 11, pp. 1276–1276, Nov. 2011.

[51] F. Helmchen and J. Waters, "Ca2+ imaging in the mammalian brain in vivo.," *Eur. J.*

Pharmacol., vol. 447, no. 2–3, pp. 119–29, Jul. 2002.

[52] A. Miyawaki, J. Llopis, R. Heim, J. M. McCaffery, J. A. Adams, M. Ikura, and R. Y. Tsien, "Fluorescent indicators for Ca2+based on green fluorescent proteins and calmodulin," *Nature*, vol. 388, no. 6645, pp. 882–887, Aug. 1997.

[53] L. L. Looger and O. Griesbeck, "Genetically encoded neural activity indicators," *Curr. Opin. Neurobiol.*, vol. 22, no. 1, pp. 18–23, Feb. 2012.

[54] V. Pérez Koldenkova and T. Nagai, "Genetically encoded Ca2+ indicators: Properties and evaluation," *Biochim. Biophys. Acta - Mol. Cell Res.*, vol. 1833, no. 7, pp. 1787–1797, Jul. 2013.

[55] T.-W. Chen, T. J. Wardill, Y. Sun, S. R. Pulver, S. L. Renninger, A. Baohan, E. R. Schreiter, R. a Kerr, M. B. Orger, V. Jayaraman, L. L. Looger, K. Svoboda, and D. S. Kim, "Ultrasensitive fluorescent proteins for imaging neuronal activity.," *Nature*, vol. 499, no. 7458, pp. 295–300, Jul. 2013.

[56] M. Ohkura, M. Matsuzaki, H. Kasai, K. Imoto, and J. Nakai, "Genetically Encoded Bright Ca^{2+} Probe Applicable for Dynamic Ca^{2+} Imaging of Dendritic Spines," *Anal. Chem.*, vol. 77, no. 18, pp. 5861–5869, Sep. 2005.

[57] Y. N. Tallini, M. Ohkura, B.-R. Choi, G. Ji, K. Imoto, R. Doran, J. Lee, P. Plan, J. Wilson, H.-B. Xin, A. Sanbe, J. Gulick, J. Mathai, J. Robbins, G. Salama, J. Nakai, and M. I. Kotlikoff, "Imaging cellular signals in the heart in vivo: Cardiac expression of the high-signal Ca2+ indicator GCaMP2," *Proc. Natl. Acad. Sci.*, vol. 103, no. 12, pp. 4753–4758, Mar. 2006.

[58] L. Tian, S. A. Hires, T. Mao, D. Huber, M. E. Chiappe, S. H. Chalasani, L. Petreanu, J. Akerboom, S. A. McKinney, E. R. Schreiter, C. I. Bargmann, V. Jayaraman, K. Svoboda, and L. L. Looger, "Imaging neural activity in worms, flies and mice with improved GCaMP calcium indicators," *Nat. Methods*, vol. 6, no. 12, pp. 875–881, 2009.

[59] K. Horikawa, Y. Yamada, T. Matsuda, K. Kobayashi, M. Hashimoto, T. Matsu-ura, A. Miyawaki, T. Michikawa, K. Mikoshiba, and T. Nagai, "Spontaneous network activity visualized by ultrasensitive Ca2+ indicators, yellow Cameleon-Nano," *Nat. Methods*, vol. 7, no. 9, pp. 729–732, Sep. 2010.

[60] A. E. Palmer, Y. Qin, J. G. Park, and J. E. McCombs, "Design and application of genetically encoded biosensors.," *Trends Biotechnol.*, vol. 29, no. 3, pp. 144–52, Mar. 2011.

[61] J. Akerboom, T.-W. Chen, T. J. Wardill, L. Tian, J. S. Marvin, S. Mutlu, N. Carreras Caldéron, F. Esposti, B. G. Borghuis, X. R. Sun, A. Gordus, M. B. Orger, R. Portugues, F. Engert, J. J. Macklin, A. Filosa, A. Aggarwal, R. A. Kerr, R. Takagi, S. Kracun, E. Shigetomi, B. S. Khakh,

H. Baier, L. Lagnado, S. S.-H. Wang, C. I. Bargmann, B. E. Kimmel, V. Jayaraman, K. Svoboda, D. S. Kim, E. R. Schreiter, and L. L. Looger, "Optimization of a GCaMP Calcium Indicator for Neural Activity Imaging," *J. Neurosci.*, vol. 32, no. 40, pp. 13819–13840, 2012.

[62] J. Akerboom, N. Carreras Calderón, L. Tian, S. Wabnig, M. Prigge, J. Tolö, A. Gordus, M. B. Orger, K. E. Severi, J. J. Macklin, R. Patel, S. R. Pulver, T. J. Wardill, E. Fischer, C. Schüler, T.-W. Chen, K. S. Sarkisyan, J. S. Marvin, C. I. Bargmann, D. S. Kim, S. Kügler, L. Lagnado, P. Hegemann, A. Gottschalk, E. R. Schreiter, and L. L. Looger, "Genetically encoded calcium indicators for multi-color neural activity imaging and combination with optogenetics.," *Front. Mol. Neurosci.*, vol. 6, no. March, p. 2, 2013.

[63] H. Dana, B. Mohar, Y. Sun, S. Narayan, A. Gordus, J. P. Hasseman, G. Tsegaye, G. T. Holt, A. Hu, D. Walpita, R. Patel, J. J. Macklin, C. I. Bargmann, M. B. Ahrens, E. R. Schreiter, V. Jayaraman, L. L. Looger, K. Svoboda, and D. S. Kim, "Sensitive red protein calcium indicators for imaging neural activity," *Elife*, vol. 5, no. MARCH2016, pp. 2738–50, 2016.

[64] M. Ohkura, T. Sasaki, C. Kobayashi, Y. Ikegaya, and J. Nakai, "An Improved Genetically Encoded Red Fluorescent Ca2+ Indicator for Detecting Optically Evoked Action Potentials," *PLoS One*, vol. 7, no. 7, p. e39933, Jul. 2012.

[65] W. Denk and K. Svoboda, "Photon upmanship: why multiphoton imaging is more than a gimmick.," *Neuron*, vol. 18, no. 3, pp. 351–7, Mar. 1997.

[66] J. B. Pawley, Ed., *Handbook Of Biological Confocal Microscopy*. Boston, MA: Springer US, 2006.

[67] W. Denk, K. R. Delaney, A. Gelperin, D. Kleinfeld, B. W. Strowbridge, D. W. Tank, and R. Yuste, "Anatomical and functional imaging of neurons using 2-photon laser scanning microscopy.," *J. Neurosci. Methods*, vol. 54, no. 2, pp. 151–62, Oct. 1994.

[68] F. Helmchen and W. Denk, "Deep tissue two-photon microscopy," *Nat. Methods*, vol. 2, no. 12, pp. 932–940, Dec. 2005.

[69] W. R. Zipfel, R. M. Williams, and W. W. Webb, "Nonlinear magic: multiphoton microscopy in the biosciences.," *Nat. Biotechnol.*, vol. 21, no. 11, pp. 1369–77, Nov. 2003.

[70] M. Göppert-Mayer, "Über Elementarakte mit zwei Quantensprüngen," *Ann. Phys.*, vol. 401, no. 3, pp. 273–294, Jan. 1931.

[71] D. G. Ouzounov, T. Wang, M. Wang, D. D. Feng, N. G. Horton, J. C. Cruz-hernández, Y. Cheng, J. Reimer, A. S. Tolias, N. Nishimura, and C. Xu, "In vivo three-photon imaging of activity of GCaMP6-labeled neurons deep in intact mouse brain," no. February, pp. 20–24, 2017.

[72] C. R. Stoltzfus and A. Rebane, “Optimizing ultrafast illumination for multiphoton-excited fluorescence imaging,” *Biomed. Opt. Express*, vol. 7, no. 5, p. 1768, 2016.

[73] W. Kaiser and C. G. B. Garrett, “Two-Photon Excitation in Ca F 2 : Eu 2 +,” *Phys. Rev. Lett.*, vol. 7, no. 6, pp. 229–231, Sep. 1961.

[74] I. D. Abella, “Optical Double-Photon Absorption in Cesium Vapor,” *Phys. Rev. Lett.*, vol. 9, no. 11, pp. 453–455, Dec. 1962.

[75] W. Denk, J. H. Strickler, and W. W. Webb, “Two-photon laser scanning fluorescence microscopy.,” *Science*, vol. 248, no. 4951, pp. 73–6, Apr. 1990.

[76] G. Y. Fan, H. Fujisaki, A. Miyawaki, R. K. Tsay, R. Y. Tsien, and M. H. Ellisman, “Video-rate scanning two-photon excitation fluorescence microscopy and ratio imaging with cameleons.,” *Biophys. J.*, vol. 76, no. 5, pp. 2412–20, May 1999.

[77] A. Negrean and H. D. Mansvelder, “Optimal lens design and use in laser-scanning microscopy.,” *Biomed. Opt. Express*, vol. 5, no. 5, pp. 1588–609, 2014.

[78] A. Nagy, J. Wu, and K. M. Berland, “Observation volumes and {gamma}-factors in two-photon fluorescence fluctuation spectroscopy.,” *Biophys. J.*, vol. 89, no. 3, pp. 2077–2090, 2005.

[79] K. Ohki, S. Chung, P. Kara, M. Hübener, T. Bonhoeffer, and R. C. Reid, “Highly ordered arrangement of single neurons in orientation pinwheels,” *Nature*, vol. 442, no. 7105, pp. 925–928, Aug. 2006.

[80] H. Ko, L. Cossell, C. Baragli, J. Antolik, C. Clopath, S. B. Hofer, and T. D. Mrsic-Flogel, “The emergence of functional microcircuits in visual cortex.,” *Nature*, vol. 496, no. 7443, pp. 96–100, 2013.

[81] B. F. Grewe, D. Langer, H. Kasper, B. M. Kampa, and F. Helmchen, “High-speed in vivo calcium imaging reveals neuronal network activity with near-millisecond precision.,” *Nat. Methods*, vol. 7, no. 5, pp. 399–405, May 2010.

[82] X. Chen, N. L. Rochefort, B. Sakmann, and A. Konnerth, “Reactivation of the Same Synapses during Spontaneous Up States and Sensory Stimuli,” *Cell Rep.*, vol. 4, no. 1, pp. 31–39, 2013.

[83] S. Panzeri, C. D. Harvey, E. Piasini, P. E. Latham, and T. Fellin, “Cracking the Neural Code for Sensory Perception by Combining Statistics, Intervention, and Behavior.,” *Neuron*, vol. 93, no. 3, pp. 491–507, Feb. 2017.

[84] W. T. Newsome, K. H. Britten, and J. A. Movshon, “Neuronal correlates of a perceptual decision,” *Nature*, vol. 341, no. 6237, pp. 52–54, Sep. 1989.

[85] R. Romo and E. Salinas, “Cognitive neuroscience: Flutter Discrimination: neural codes,

perception, memory and decision making," *Nat. Rev. Neurosci.*, vol. 4, no. 3, pp. 203–218, Mar. 2003.

[86] K. Deisseroth, "Optogenetics," *Nat. Methods*, vol. 8, no. 1, pp. 26–29, Jan. 2011.

[87] E. S. Boyden, F. Zhang, E. Bamberg, G. Nagel, and K. Deisseroth, "Millisecond-timescale, genetically targeted optical control of neural activity.," *Nat. Neurosci.*, vol. 8, no. 9, pp. 1263–8, Sep. 2005.

[88] K. Deisseroth, "Optogenetics: 10 years of microbial opsins in neuroscience.," *Nat. Neurosci.*, vol. 18, no. 9, pp. 1213–1225, 2015.

[89] F. Zhang, M. Prigge, F. Beyrière, S. P. Tsunoda, J. Mattis, O. Yizhar, P. Hegemann, and K. Deisseroth, "Red-shifted optogenetic excitation: a tool for fast neural control derived from Volvox carteri," *Nat. Neurosci.*, vol. 11, no. 6, pp. 631–633, Jun. 2008.

[90] V. Gradinaru, K. R. Thompson, and K. Deisseroth, "eNpHR: a Natronomonas halorhodopsin enhanced for optogenetic applications," *Brain Cell Biol.*, vol. 36, no. 1–4, pp. 129–139, Aug. 2008.

[91] X. Han, B. Y. Chow, H. Zhou, N. C. Klapoetke, A. Chuong, R. Rajimehr, A. Yang, M. V. Baratta, J. Winkle, R. Desimone, and E. S. Boyden, "A High-Light Sensitivity Optical Neural Silencer: Development and Application to Optogenetic Control of Non-Human Primate Cortex," *Front. Syst. Neurosci.*, vol. 5, p. 18, 2011.

[92] J. Mattis, K. M. Tye, E. a Ferenczi, C. Ramakrishnan, D. J. O'Shea, R. Prakash, L. a Gunaydin, M. Hyun, L. E. Fenno, V. Gradinaru, O. Yizhar, and K. Deisseroth, "Principles for applying optogenetic tools derived from direct comparative analysis of microbial opsins," *Nat. Methods*, vol. 9, no. 2, pp. 159–172, 2011.

[93] J. Y. Lin, P. M. Knutsen, A. Muller, D. Kleinfeld, and R. Y. Tsien, "ReaChR: a red-shifted variant of channelrhodopsin enables deep transcranial optogenetic excitation.," *Nat. Neurosci.*, vol. 16, no. 10, pp. 1499–508, 2013.

[94] L. Madisen, T. Mao, H. Koch, J. Zhuo, A. Berenyi, S. Fujisawa, Y.-W. A. Hsu, A. J. Garcia, X. Gu, S. Zanella, J. Kidney, H. Gu, Y. Mao, B. M. Hooks, E. S. Boyden, G. Buzsáki, J. M. Ramirez, A. R. Jones, K. Svoboda, X. Han, E. E. Turner, and H. Zeng, "A toolbox of Cre-dependent optogenetic transgenic mice for light-induced activation and silencing," *Nat. Neurosci.*, vol. 15, no. 5, pp. 793–802, Mar. 2012.

[95] A. Berndt, S. Y. Lee, C. Ramakrishnan, and K. Deisseroth, "Structure-guided transformation of channelrhodopsin into a light-activated chloride channel.," *Science*, vol. 344, no. 6182, pp. 420–

4, 2014.

[96] J. Wietek, J. S. Wiegert, N. Adeishvili, F. Schneider, H. Watanabe, S. P. Tsunoda, A. Vogt, M. Elstner, T. G. Oertner, and P. Hegemann, “Conversion of channelrhodopsin into a light-gated chloride channel.,” *Science*, vol. 344, no. 6182, pp. 409–412, 2014.

[97] C. Cosentino, L. Alberio, S. Gazzarrini, M. Aquila, E. Romano, S. Cermenati, P. Zuccolini, J. Petersen, M. Beltrame, J. L. Van Etten, J. M. Christie, G. Thiel, and A. Moroni, “Engineering of a light-gated potassium channel,” *Science (80-.).*, vol. 348, no. 6235, pp. 707–710, May 2015.

[98] N. C. Klapoetke, Y. Murata, S. S. Kim, S. R. Pulver, A. Birdsey-Benson, Y. K. Cho, T. K. Morimoto, A. S. Chuong, E. J. Carpenter, Z. Tian, J. Wang, Y. Xie, Z. Yan, Y. Zhang, B. Y. Chow, B. Surek, M. Melkonian, V. Jayaraman, M. Constantine-paton, G. K. Wong, and E. S. Boyden, “Independent optical excitation of distinct neural populations.,” *Nat. Methods*, vol. 11, no. 3, pp. 338–46, 2014.

[99] E. G. Govorunova, O. A. Sineshchekov, E. M. Rodarte, R. Janz, O. Morelle, M. Melkonian, G. K.-S. Wong, and J. L. Spudich, “The Expanding Family of Natural Anion Channelrhodopsins Reveals Large Variations in Kinetics, Conductance, and Spectral Sensitivity,” *Sci. Rep.*, vol. 7, no. March, p. 43358, 2017.

[100] F. Schneider, C. Grimm, and P. Hegemann, “Biophysics of Channelrhodopsin.,” *Annu. Rev. Biophys.*, vol. 44, pp. 167–186, 2015.

[101] E. G. Govorunova and L. A. Koppel, “The road to optogenetics: Microbial rhodopsins,” *Biochem.*, vol. 81, no. 9, pp. 928–940, 2016.

[102] G. Nagel, T. Szellas, W. Huhn, S. Kateriya, N. Adeishvili, P. Berthold, D. Ollig, P. Hegemann, and E. Bamberg, “Channelrhodopsin-2, a directly light-gated cation-selective membrane channel.,” *Proc. Natl. Acad. Sci. U. S. A.*, vol. 100, no. 24, pp. 13940–5, Nov. 2003.

[103] V. Gradinaru, K. R. Thompson, F. Zhang, M. Mogri, K. Kay, M. B. Schneider, and K. Deisseroth, “Targeting and readout strategies for fast optical neural control in vitro and in vivo.,” *J. Neurosci.*, vol. 27, no. 52, pp. 14231–8, Dec. 2007.

[104] F. Zhang, L.-P. Wang, E. S. Boyden, and K. Deisseroth, “Channelrhodopsin-2 and optical control of excitable cells,” *Nat. Methods*, vol. 3, no. 10, pp. 785–792, Oct. 2006.

[105] J. Y. Lin, M. Z. Lin, P. Steinbach, and R. Y. Tsien, “Characterization of engineered channelrhodopsin variants with improved properties and kinetics.,” *Biophys. J.*, vol. 96, no. 5, pp. 1803–14, Mar. 2009.

[106] F. Zhang, J. Vierock, O. Yizhar, L. E. Fenno, S. Tsunoda, A. Kianianmomeni, M. Prigge, A.

Berndt, J. Cushman, J. Polle, J. Magnuson, P. Hegemann, and K. Deisseroth, “The microbial opsin family of optogenetic tools,” *Cell*, vol. 147, no. 7, pp. 1446–1457, Dec. 2011.

[107] J. Y. Lin, “A user’s guide to channelrhodopsin variants: features, limitations and future developments.,” *Exp. Physiol.*, vol. 96, no. 1, pp. 19–25, Jan. 2011.

[108] A. Berndt, “Structure-Guided Transformation,” *Science*, vol. 344, no. April, pp. 420–424, 2014.

[109] E. G. Govorunova, O. A. Sineshchekov, R. Janz, X. Liu, and J. L. Spudich, “NEUROSCIENCE. Natural light-gated anion channels: A family of microbial rhodopsins for advanced optogenetics,” *Science (80-.).*, vol. 349, no. 6248, pp. 647–650, 2015.

[110] F. Zhang, L.-P. Wang, M. Brauner, J. F. Liewald, K. Kay, N. Watzke, P. G. Wood, E. Bamberg, G. Nagel, A. Gottschalk, and K. Deisseroth, “Multimodal fast optical interrogation of neural circuitry.,” *Nature*, vol. 446, no. 7136, pp. 633–9, Apr. 2007.

[111] J. K. Lanyi, A. Duschl, G. W. Hatfield, K. May, and D. Oesterhelt, “The primary structure of a halorhodopsin from Natronobacterium pharaonis. Structural, functional and evolutionary implications for bacterial rhodopsins and halorhodopsins.,” *J. Biol. Chem.*, vol. 265, no. 3, pp. 1253–60, Jan. 1990.

[112] V. Gradinaru, F. Zhang, C. Ramakrishnan, J. Mattis, R. Prakash, I. Diester, I. Goshen, K. R. Thompson, and K. Deisseroth, “Molecular and Cellular Approaches for Diversifying and Extending Optogenetics,” *Cell*, vol. 141, no. 1, pp. 154–165, 2010.

[113] E. S. Boyden, “A history of optogenetics: the development of tools for controlling brain circuits with light.,” *F1000 Biol. Rep.*, vol. 3, no. 11, p. 11, 2011.

[114] D. Oesterhelt and W. Stoeckenius, “Functions of a new photoreceptor membrane.,” *Proc. Natl. Acad. Sci. U. S. A.*, vol. 70, no. 10, pp. 2853–7, Oct. 1973.

[115] B. Y. Chow, X. Han, A. S. Dobry, X. Qian, A. S. Chuong, M. Li, M. A. Henninger, G. M. Belfort, Y. Lin, P. E. Monahan, and E. S. Boyden, “High-performance genetically targetable optical neural silencing by light-driven proton pumps.,” *Nature*, vol. 463, no. 7277, pp. 98–102, 2010.

[116] D. Lin, M. P. Boyle, P. Dollar, H. Lee, E. S. Lein, P. Perona, and D. J. Anderson, “Functional identification of an aggression locus in the mouse hypothalamus,” *Nature*, vol. 470, no. 7333, pp. 221–226, Feb. 2011.

[117] A. R. Adamantidis, F. Zhang, A. M. Aravanis, K. Deisseroth, and L. de Lecea, “Neural substrates of awakening probed with optogenetic control of hypocretin neurons,” *Nature*, vol. 450, no. 7168, pp. 420–424, Nov. 2007.

[118] C. K. Kim, A. Adhikari, and K. Deisseroth, “Integration of optogenetics with complementary methodologies in systems neuroscience,” *Nat. Publ. Gr.*, vol. 18, 2017.

[119] S. M. Tyree ID and L. de Lecea, “Optogenetic Investigation of Arousal Circuits.”

[120] P. Capelli, C. Pivetta, M. Soledad Esposito, and S. Arber, “Locomotor speed control circuits in the caudal brainstem,” *Nature*, vol. 551, no. 7680, p. 373, Oct. 2017.

[121] W. Han, L. A. Tellez, M. J. Rangel, S. C. Motta, X. Zhang, I. O. Perez, N. S. Canteras, S. J. Shammah-Lagnado, A. N. van den Pol, and I. E. de Araujo, “Integrated Control of Predatory Hunting by the Central Nucleus of the Amygdala.,” *Cell*, vol. 168, no. 1–2, p. 311–324.e18, Jan. 2017.

[122] F. Zhang, V. Gradinaru, A. R. Adamantidis, R. Durand, R. D. Airan, L. de Lecea, and K. Deisseroth, “Optogenetic interrogation of neural circuits: technology for probing mammalian brain structures,” *Nat. Protoc.*, vol. 5, no. 3, pp. 439–456, Mar. 2010.

[123] Y. El-Shamayleh, A. M. Ni, and G. D. Horwitz, “Strategies for targeting primate neural circuits with viral vectors.,” *J. Neurophysiol.*, vol. 116, no. 1, pp. 122–34, Jul. 2016.

[124] B. R. Arenkiel, J. Peca, I. G. Davison, C. Feliciano, K. Deisseroth, G. J. Augustine, M. D. Ehlers, and G. Feng, “In Vivo Light-Induced Activation of Neural Circuitry in Transgenic Mice Expressing Channelrhodopsin-2,” *Neuron*, vol. 54, no. 2, pp. 205–218, Apr. 2007.

[125] D. Grimm, J. S. Lee, L. Wang, T. Desai, B. Akache, T. A. Storm, and M. A. Kay, “In Vitro and In Vivo Gene Therapy Vector Evolution via Multispecies Interbreeding and Retargeting of Adeno-Associated Viruses,” *J. Virol.*, vol. 82, no. 12, pp. 5887–5911, Jun. 2008.

[126] D. Atasoy, Y. Aponte, H. H. Su, and S. M. Sternson, “A FLEX switch targets Channelrhodopsin-2 to multiple cell types for imaging and long-range circuit mapping.,” *J. Neurosci.*, vol. 28, no. 28, pp. 7025–30, Jul. 2008.

[127] S. Gong, M. Doughty, C. R. Harbaugh, A. Cummins, M. E. Hatten, N. Heintz, and C. R. Gerfen, “Targeting Cre Recombinase to Specific Neuron Populations with Bacterial Artificial Chromosome Constructs,” *J. Neurosci.*, vol. 27, no. 37, pp. 9817–9823, Sep. 2007.

[128] C. R. Gerfen, R. Paletzki, and N. Heintz, “GENSAT BAC cre-recombinase driver lines to study the functional organization of cerebral cortical and basal ganglia circuits,” *Neuron*, vol. 80, no. 6, pp. 1368–1383, Dec. 2013.

[129] H. Taniguchi, M. He, P. Wu, S. Kim, R. Paik, K. Sugino, D. Kvitsani, Y. Fu, J. Lu, Y. Lin, G. Miyoshi, Y. Shima, G. Fishell, S. B. Nelson, Z. J. Huang, and Z. J. Huang, “A Resource of Cre Driver Lines for Genetic Targeting of GABAergic Neurons in Cerebral Cortex,” *Neuron*, vol.

71, no. 6, pp. 995–1013, Sep. 2011.

[130] L. Madisen, A. R. Garner, D. Shimaoka, A. S. Chuong, N. C. Klapoetke, L. Li, A. van der Bourg, Y. Niino, L. Egolf, C. Monetti, H. Gu, M. Mills, A. Cheng, B. Tasic, T. N. Nguyen, S. M. Sunkin, A. Benucci, A. Nagy, A. Miyawaki, F. Helmchen, R. M. Empson, T. Knöpfel, E. S. Boyden, R. C. Reid, M. Carandini, and H. Zeng, "Transgenic mice for intersectional targeting of neural sensors and effectors with high specificity and performance," *Neuron*, vol. 85, no. 5, pp. 942–958, 2015.

[131] L. Petreanu, D. Huber, A. Sobczyk, and K. Svoboda, "Channelrhodopsin-2–assisted circuit mapping of long-range callosal projections," *Nat. Neurosci.*, vol. 10, no. 5, pp. 663–668, May 2007.

[132] L. Petreanu, T. Mao, S. M. Sternson, and K. Svoboda, "The subcellular organization of neocortical excitatory connections," *Nature*, vol. 457, no. 7233, pp. 1142–1145, Feb. 2009.

[133] H. Adesnik, W. Bruns, H. Taniguchi, Z. J. Huang, and M. Scanziani, "A neural circuit for spatial summation in visual cortex," *Nature*, vol. 490, no. 7419, pp. 226–231, Oct. 2012.

[134] R. Beltramo, G. D'Urso, M. D. Maschio, P. Farisello, S. Bovetti, Y. Clovis, G. Lassi, V. Tucci, D. De Pietri Tonelli, and T. Fellin, "Layer-specific excitatory circuits differentially control recurrent network dynamics in the neocortex," *Nat. Med.*, vol. 16, no. 2, pp. 1–10, Feb. 2013.

[135] M. dal Maschio, D. Ghezzi, G. Bony, A. Alabastri, G. Deidda, M. Brondi, S. S. Sato, R. P. Zaccaria, E. Di Fabrizio, G. M. Ratto, and L. Cancedda, "High-performance and site-directed in utero electroporation by a triple-electrode probe," *Nat. Commun.*, vol. 3, p. 960, Jul. 2012.

[136] J. Szczurkowska, A. W. Cwetsch, M. dal Maschio, D. Ghezzi, G. M. Ratto, and L. Cancedda, "Targeted in vivo genetic manipulation of the mouse or rat brain by in utero electroporation with a triple-electrode probe," *Nat. Protoc.*, vol. 11, no. 3, pp. 399–412, Feb. 2016.

[137] S. Q. Lima and G. Miesenböck, "Remote Control of Behavior through Genetically Targeted Photostimulation of Neurons," *Cell*, vol. 121, no. 1, pp. 141–152, Apr. 2005.

[138] G. Nagel, M. Brauner, J. F. Liewald, N. Adeishvili, E. Bamberg, and A. Gottschalk, "Light Activation of Channelrhodopsin-2 in Excitable Cells of Caenorhabditis elegans Triggers Rapid Behavioral Responses," *Curr. Biol.*, vol. 15, no. 24, pp. 2279–2284, Dec. 2005.

[139] F. Zhang, A. M. Aravanis, A. Adamantidis, L. de Lecea, and K. Deisseroth, "Circuit-breakers: optical technologies for probing neural signals and systems," *Nat. Rev. Neurosci.*, vol. 8, no. 8, pp. 577–581, Aug. 2007.

[140] A. D. Douglass, S. Kraves, K. Deisseroth, A. F. Schier, and F. Engert, "Escape behavior elicited

by single, channelrhodopsin-2-evoked spikes in zebrafish somatosensory neurons.," *Curr. Biol.*, vol. 18, no. 15, pp. 1133–7, Aug. 2008.

[141] A. M. Aravanis, L.-P. Wang, F. Zhang, L. A. Meltzer, M. Z. Mogri, M. B. Schneider, and K. Deisseroth, "An optical neural interface: *in vivo* control of rodent motor cortex with integrated fiberoptic and optogenetic technology," *J. Neural Eng.*, vol. 4, no. 3, pp. S143–S156, Sep. 2007.

[142] Y. Iwai, S. Honda, H. Ozeki, M. Hashimoto, and H. Hirase, "A simple head-mountable LED device for chronic stimulation of optogenetic molecules in freely moving mice," *Neurosci. Res.*, vol. 70, no. 1, pp. 124–127, May 2011.

[143] D. Huber, L. Petreanu, N. Ghitani, S. Ranade, T. Hromádka, Z. Mainen, and K. Svoboda, "Sparse optical microstimulation in barrel cortex drives learned behaviour in freely moving mice.," *Nature*, vol. 451, no. 7174, pp. 61–4, Jan. 2008.

[144] O. Yizhar, L. E. Fenno, T. J. Davidson, M. Mogri, and K. Deisseroth, "Optogenetics in Neural Systems," *Neuron*, vol. 71, no. 1, pp. 9–34, Jul. 2011.

[145] J. J. Mancuso, J. Kim, S. Lee, S. Tsuda, N. B. H. Chow, and G. J. Augustine, "Optogenetic probing of functional brain circuitry," *Exp. Physiol.*, vol. 96, no. 1, pp. 26–33, Jan. 2011.

[146] K. B. Clancy, P. Schnepel, A. T. Rao, and D. E. Feldman, "Structure of a single whisker representation in layer 2 of mouse somatosensory cortex.," *J. Neurosci.*, vol. 35, no. 9, pp. 3946–3958, 2015.

[147] L. Carrillo-reid, W. Yang, Y. Bando, D. S. Peterka, and R. Yuste, "Imprinting and recalling cortical ensembles," *Science (80-.).*, vol. 353, no. 6300, pp. 691–694, 2016.

[148] E. Ronzitti, C. Ventalon, M. Canepari, and B. C. Forget, "Recent advances in patterned photostimulation for optogenetics," 2017.

[149] M. Mahn, M. Prigge, S. Ron, R. Levy, and O. Yizhar, "Biophysical constraints of optogenetic inhibition at presynaptic terminals.," *Nat. Neurosci.*, vol. 19, no. 4, pp. 554–6, 2016.

[150] C. Wu, E. Ivanova, Y. Zhang, and Z. H. Pan, "rAAV-Mediated Subcellular Targeting of Optogenetic Tools in Retinal Ganglion Cells In Vivo," *PLoS One*, vol. 8, no. 6, pp. 1–10, 2013.

[151] P. Zhu, O. Fajardo, J. Shum, Y.-P. Zhang Schärer, and R. W. Friedrich, "High-resolution optical control of spatiotemporal neuronal activity patterns in zebrafish using a digital micromirror device," *Nat. Protoc.*, vol. 7, no. 7, pp. 1410–1425, Jul. 2012.

[152] A. W. Lohmann and D. P. Paris, "Binary fraunhofer holograms, generated by computer.," *Appl. Opt.*, vol. 6, no. 10, pp. 1739–48, Oct. 1967.

[153] V. Emiliani, A. E. Cohen, K. Deisseroth, and M. Häusser, "All-Optical Interrogation of Neural

Circuits.," *J. Neurosci.*, vol. 35, no. 41, pp. 13917–26, 2015.

[154] N. C. Pégard, A. R. Mardinly, I. A. Oldenburg, S. Sridharan, L. Waller, and H. Adesnik, "Three-dimensional scanless holographic optogenetics with temporal focusing (3D-SHOT).," *Nat. Commun.*, vol. 8, no. 1, p. 1228, Oct. 2017.

[155] S. K. Mohanty, R. K. Reinscheid, X. Liu, N. Okamura, T. B. Krasieva, and M. W. Berns, "In-depth activation of channelrhodopsin 2-sensitized excitable cells with high spatial resolution using two-photon excitation with a near-infrared laser microbeam.," *Biophys. J.*, vol. 95, no. 8, pp. 3916–26, 2008.

[156] J. P. Rickgauer and D. W. Tank, "Two-photon excitation of channelrhodopsin-2 at saturation.," *Proc. Natl. Acad. Sci. U. S. A.*, vol. 106, no. 35, pp. 15025–30, Sep. 2009.

[157] K. Feldbauer, D. Zimmermann, V. Pintschovius, J. Spitz, C. Bamann, and E. Bamberg, "Channelrhodopsin-2 is a leaky proton pump.," *Proc. Natl. Acad. Sci. U. S. A.*, vol. 106, no. 30, pp. 12317–22, Jul. 2009.

[158] A. M. Packer, D. S. Peterka, J. J. Hirtz, R. Prakash, K. Deisseroth, and R. Yuste, "Two-photon optogenetics of dendritic spines and neural circuits," *Nat. Methods*, vol. 9, no. 12, pp. 1202–1205, 2012.

[159] R. Prakash, O. Yizhar, B. Grewe, C. Ramakrishnan, N. Wang, I. Goshen, A. M. Packer, D. S. Peterka, R. Yuste, M. J. Schnitzer, and K. Deisseroth, "Two-photon optogenetic toolbox for fast inhibition, excitation and bistable modulation.," *Nat. Methods*, vol. 9, no. 12, pp. 1171–9, Dec. 2012.

[160] O. Yizhar, L. E. Fenno, M. Prigge, F. Schneider, T. J. Davidson, D. J. O'Shea, V. S. Sohal, I. Goshen, J. Finkelstein, J. T. Paz, K. Stehfest, R. Fudim, C. Ramakrishnan, J. R. Huguenard, P. Hegemann, and K. Deisseroth, "Neocortical excitation/inhibition balance in information processing and social dysfunction.," *Nature*, vol. 477, no. 7363, pp. 171–178, 2011.

[161] D. Oron, E. Tal, and Y. Silberberg, "Scanningless depth-resolved microscopy.," *Opt. Express*, vol. 13, no. 5, pp. 1468–1476, Mar. 2005.

[162] G. Zhu, J. van Howe, M. Durst, W. Zipfel, and C. Xu, "Simultaneous spatial and temporal focusing of femtosecond pulses.," *Opt. Express*, vol. 13, no. 6, pp. 2153–2159, Mar. 2005.

[163] B. K. Andrasfalvy, B. V Zemelman, J. Tang, and A. Vaziri, "Two-photon single-cell optogenetic control of neuronal activity by sculpted light.," *Proc. Natl. Acad. Sci. U. S. A.*, vol. 107, no. 26, pp. 11981–6, Jun. 2010.

[164] C. A. Baker, Y. M. Elyada, A. Parra, and M. M. L. Bolton, "Cellular resolution circuit mapping

with temporal-focused excitation of soma-targeted channelrhodopsin," *Elife*, vol. 5, no. AUGUST, pp. 1–15, 2016.

[165] J. P. Rickgauer, K. Deisseroth, and D. W. Tank, "Simultaneous cellular-resolution optical perturbation and imaging of place cell firing fields," *Nat. Neurosci.*, vol. 17, no. 12, pp. 1816–24, 2014.

[166] A. M. Packer, B. Roska, and M. Häusser, "Targeting neurons and photons for optogenetics.," *Nat. Neurosci.*, vol. 16, no. 7, pp. 805–15, Jul. 2013.

[167] V. Szabo, C. Ventalon, V. DeSars, J. Bradley, and V. Emiliani, "Spatially selective holographic photoactivation and functional fluorescence imaging in freely behaving mice with a fiberscope," *Neuron*, vol. 84, no. 6, pp. 1157–1169, 2014.

[168] S. Zucca, G. D. Urso, V. Pasquale, D. Vecchia, G. Pica, S. Bovetti, C. Moretti, S. Varani, M. Chiappalone, S. Panzeri, and M. Molano-mazo, "An inhibitory gate for state transition in cortex," pp. 1–31, 2017.

[169] J. W. Goodman and J. W., *Introduction to Fourier optics*. McGraw-Hill, 1996.

[170] V. A. (Viktor A. Soĭfer, *Methods for computer design of diffractive optical elements*. Wiley, 2002.

[171] D. G. G. Jennifer E.Curtis, Brian A.Koss, "Dynamic holographic optical tweezers," *Opt. Commun.*, vol. 207, no. 1–6, pp. 169–175, Jun. 2002.

[172] R. Di Leonardo, F. Ianni, and G. Ruocco, "Computer generation of optimal holograms for optical trap arrays," *Opt. Express*, vol. 15, no. 4, pp. 1913–1922, 2007.

[173] A. Bañas and J. Glückstad, "Light Shaping with Holography, GPC and Holo-GPC," *Opt. Data Process. Storage*, vol. 3, no. 1, pp. 20–40, Jan. 2017.

[174] R. K. Tyson, *Principles of adaptive optics*. .

[175] J. W. Hardy, *Adaptive optics for astronomical telescopes*. Oxford University Press, 1998.

[176] R. Lynge Eriksen, V. Ricardo Daria, and J. Glückstad, "Fully dynamic multiple-beam optical tweezers," *Opt. Express*, vol. 10, no. 14, p. 597, Jul. 2002.

[177] H. Melville, G. Milne, G. Spalding, W. Sibbett, K. Dholakia, and D. McGloin, "Optical trapping of three-dimensional structures using dynamic holograms," *Opt. Express*, vol. 11, no. 26, p. 3562, Dec. 2003.

[178] C. Lutz, T. S. Otis, V. DeSars, S. Charpak, D. A. DiGregorio, and V. Emiliani, "Holographic photolysis of caged neurotransmitters," *Nat. Methods*, vol. 5, no. 9, pp. 821–827, Sep. 2008.

[179] V. Nikolenko, "SLM microscopy: scanless two-photon imaging and photostimulation using

spatial light modulators," *Front. Neural Circuits*, vol. 2, no. December, pp. 1–14, 2008.

[180] M. Dal Maschio, F. Difato, R. Beltramo, A. Blau, F. Benfenati, and T. Fellin, "Simultaneous two-photon imaging and photo-stimulation with structured light illumination," *Opt. Express*, vol. 18, no. 18, pp. 18720–18731, Aug. 2010.

[181] B. O. Watson, V. Nikolenko, R. Araya, D. S. Peterka, A. Woodruff, and R. Yuste, "Two-photon microscopy with diffractive optical elements and spatial light modulators," *Front. Neurosci.*, vol. 4, Sep. 2010.

[182] E. Papagiakoumou, F. Anselmi, A. Bègue, V. de Sars, J. Glückstad, E. Y. Isacoff, and V. Emiliani, "Scanless two-photon excitation of channelrhodopsin-2.," *Nat. Methods*, vol. 7, no. 10, pp. 848–54, Oct. 2010.

[183] S. Bovetti, C. Moretti, S. Zucca, M. Dal Maschio, P. Bonifazi, and T. Fellin, "Simultaneous high-speed imaging and optogenetic inhibition in the intact mouse brain," *Sci. Rep.*, vol. 7, no. July 2016, p. 40041, 2017.

[184] C. Moretti, A. Antonini, S. Bovetti, C. Liberale, and T. Fellin, "Scanless functional imaging of hippocampal networks using patterned two-photon illumination through GRIN lenses.," *Biomed. Opt. Express*, vol. 7, no. 10, pp. 3958–3967, Oct. 2016.

[185] W. Yang, J. eun K. Miller, L. Carrillo-Reid, E. Pnevmatikakis, L. Paninski, R. Yuste, and D. S. Peterka, "Simultaneous Multi-plane Imaging of Neural Circuits," *Neuron*, vol. 89, no. 2, p. 284, 2016.

[186] M. Dal Maschio, F. Difato, R. Beltramo, A. M. De Stasi, A. Blau, and T. Fellin, *Optical Investigation of Brain Networks Using Structured Illumination*, First Edit. Elsevier Inc., 2012.

[187] V. Nikolenko, D. S. Peterka, R. Araya, A. Woodruff, and R. Yuste, "Spatial Light Modulator Microscopy," *Cold Spring Harb. Protoc.*, vol. 2013, no. 12, p. pdb.top079517-top079517, Dec. 2013.

[188] D. Palima and J. Glückstad, "Comparison of generalized phase contrast and computer generated holography for laser image projection," *Opt. Express*, vol. 16, no. 8, pp. 5338–5349, 2008.

[189] F. ZERNIKE, "How I discovered phase contrast.," *Science*, vol. 121, no. 3141, pp. 345–9, Mar. 1955.

[190] B. Sun, P. S. Salter, and M. J. Booth, "Effects of aberrations in spatiotemporal focusing of ultrashort laser pulses," *J. Opt. Soc. Am. A*, vol. 31, no. 4, p. 765, Apr. 2014.

[191] A. Bègue, E. Papagiakoumou, B. Leshem, R. Conti, L. Enke, D. Oron, and V. Emiliani, "Two-photon excitation in scattering media by spatiotemporally shaped beams and their application in

optogenetic stimulation.," *Biomed. Opt. Express*, vol. 4, no. 12, pp. 2869–79, Jan. 2013.

[192] E. Papagiakoumou, A. Bègue, B. Leshem, O. Schwartz, B. M. Stell, J. Bradley, D. Oron, and V. Emiliani, "Functional patterned multiphoton excitation deep inside scattering tissue," *Nat. Photonics*, vol. 7, no. 4, pp. 274–278, 2013.

[193] H. Dana, N. Kruger, A. Ellman, and S. Shoham, "Line temporal focusing characteristics in transparent and scattering media," *Opt. Express*, vol. 21, no. 5, p. 5677, Mar. 2013.

[194] O. Hernandez, E. Papagiakoumou, D. Tanesee, K. Felin, C. Wyart, and V. Emiliani, "Three-dimensional spatiotemporal focusing of holographic patterns," *Nat. Commun.*, vol. 7, no. June, p. 11928, 2016.

[195] G. Sinclair, J. Leach, P. Jordan, G. Gibson, E. Yao, Z. Laczik, M. Padgett, and J. Courtial, "Interactive application in holographic optical tweezers of a multi-plane Gerchberg-Saxton algorithm for three-dimensional light shaping.," *Opt. Express*, vol. 12, no. 8, pp. 1665–1670, 2004.

[196] M. dal Maschio, J. C. Donovan, T. O. Helmbrecht, and H. Baier, "Linking Neurons to Network Function and Behavior by Two-Photon Holographic Optogenetics and Volumetric Imaging," *Neuron*, vol. 94, no. 4, p. 774–789.e5, 2017.

[197] S. Quirin, J. Jackson, D. S. Peterka, and R. Yuste, "Simultaneous imaging of neural activity in three dimensions.," *Front. Neural Circuits*, vol. 8, no. April, p. 29, 2014.

[198] O. Fajardo, P. Zhu, and R. W. Friedrich, "Control of a specific motor program by a small brain area in zebrafish," *Front. Neural Circuits*, vol. 7, p. 67, 2013.

[199] N. R. Wilson, C. a Runyan, F. L. Wang, and M. Sur, "Division and subtraction by distinct cortical inhibitory networks in vivo.," *Nature*, vol. 488, no. 7411, pp. 343–8, Aug. 2012.

[200] Y.-P. Zhang and T. G. Oertner, "Optical induction of synaptic plasticity using a light-sensitive channel," *Nat. Methods*, vol. 4, no. 2, pp. 139–141, Feb. 2007.

[201] V. Nikolenko, B. O. Watson, R. Araya, A. Woodruff, D. S. Peterka, and R. Yuste, "SLM Microscopy: Scanless Two-Photon Imaging and Photostimulation with Spatial Light Modulators.," *Front. Neural Circuits*, vol. 2, p. 5, 2008.

[202] F. Anselmi, C. Ventalon, A. Begue, D. Ogden, and V. Emiliani, "Three-dimensional imaging and photostimulation by remote-focusing and holographic light patterning," *Proc. Natl. Acad. Sci.*, vol. 108, no. 49, pp. 19504–19509, Dec. 2011.

[203] A. M. Packer, L. E. Russell, H. W. P. Dalgleish, and M. Häusser, "Simultaneous all-optical manipulation and recording of neural circuit activity with cellular resolution in vivo.," *Nat.*

Methods, vol. 12, no. 2, pp. 140–6, 2015.

[204] D. Förster, M. Dal Maschio, E. Laurell, and H. Baier, "An optogenetic toolbox for unbiased discovery of functionally connected cells in neural circuits," *Nat. Commun.*, vol. 8, no. 1, p. 116, Dec. 2017.

[205] A. Berndt, S. Y. Lee, J. Wietek, C. Ramakrishnan, E. E. Steinberg, A. J. Rashid, H. Kim, S. Park, A. Santoro, P. W. Frankland, S. M. Iyer, S. Pak, S. Ährlund-Richter, S. L. Delp, R. C. Malenka, S. A. Josselyn, M. Carlén, P. Hegemann, and K. Deisseroth, "Structural foundations of optogenetics: Determinants of channelrhodopsin ion selectivity," *Proc. Natl. Acad. Sci.*, vol. 113, no. 4, pp. 822–829, Jan. 2016.

[206] J. Wietek, R. Beltramo, M. Scanziani, P. Hegemann, T. G. Oertner, and J. Simon Wiegert, "An improved chloride-conducting channelrhodopsin for light-induced inhibition of neuronal activity in vivo," *Sci. Rep.*, vol. 5, no. April, p. 14807, 2015.

[207] O. A. Sineshchekov, E. G. Govorunova, H. Li, and J. L. Spudich, "Gating mechanisms of a natural anion channelrhodopsin," *Proc. Natl. Acad. Sci.*, vol. 112, no. 46, pp. 14236–14241, Nov. 2015.

[208] G. A. Mohamed, R.-K. Cheng, J. Ho, S. Krishnan, F. Mohammad, A. Claridge-Chang, and S. Jesuthasan, "Optical inhibition of larval zebrafish behaviour with anion channelrhodopsins," *BMC Biol.*, vol. 15, no. 1, p. 103, Dec. 2017.

[209] O. A. Shemesh, D. Tanese, V. Zampini, C. Linghu, K. Piatkevich, E. Ronzitti, E. Papagiakoumou, E. S. Boyden, and V. Emiliani, "Temporally precise single-cell-resolution optogenetics," *Nat. Neurosci.*, pp. 1–16, 2017.

[210] S. Paluch-Siegler, T. Mayblum, H. Dana, I. Brosh, I. Gefen, and S. Shoham, "All-optical bidirectional neural interfacing using hybrid multiphoton holographic optogenetic stimulation.," *Neurophotonics*, vol. 2, no. 3, p. 31208, 2015.

[211] E. Chaigneau, E. Ronzitti, A. M. Gajowa, J. G. Soler-Llavina, D. Tanese, Y. B. A. Brureau, E. Papagiakoumou, H. Zeng, and V. Emiliani, "Two-photon holographic stimulation of ReaChR," *Front. Cell. Neurosci.*, vol. 10, no. October, p. 234, 2016.

[212] E. Ronzitti, R. Conti, V. Zampini, D. Tanese, A. Foust, and N. Klapoetke, "Sub-millisecond optogenetic control of neuronal firing with two-photon holographic photoactivation of Chronos Short Title (50ch): Sub-ms Two-Photon Holographic Control of Neuronal Firing," 2017.

[213] W. Mittmann, D. J. Wallace, U. Czubayko, J. T. Herb, A. T. Schaefer, L. L. Looger, W. Denk, and J. N. D. Kerr, "Two-photon calcium imaging of evoked activity from L5 somatosensory

neurons in vivo.," *Nat. Neurosci.*, vol. 14, no. 8, pp. 1089–1093, 2011.

[214] P. Theer, M. T. Hasan, and W. Denk, "Two-photon imaging to a depth of 1000 μm in living brains by use of a Ti:Al_2O_3 regenerative amplifier," *Opt. Lett.*, vol. 28, no. 12, p. 1022, Jun. 2003.

[215] A. Hopt and E. Neher, "Highly Nonlinear Photodamage in Two-Photon Fluorescence Microscopy," vol. 80, no. April, pp. 2029–2036, 2001.

[216] A. L. Allegra Mascaro, L. Sacconi, and F. S. Pavone, "Multi-photon nanosurgery in live brain," *Front. Neuroenergetics*, vol. 2, no. 1, pp. 1–8, 2010.

[217] A. A. Davis, M. J. Farrar, N. Nishimura, M. M. Jin, and C. B. Schaffer, "Optoporation and Genetic Manipulation of Cells Using Femtosecond Laser Pulses," *Biophysj*, vol. 105, no. 4, pp. 862–871, 2013.

[218] S. N. Arkhipov, I. Saytashev, and M. Dantus, "Intravital Imaging Study on Photodamage Produced by Femtosecond Near-infrared Laser Pulses In Vivo," no. 1, pp. 308–313, 2016.

[219] J. Sawinski, D. J. Wallace, D. S. Greenberg, S. Grossmann, W. Denk, and J. N. D. Kerr, "Visually evoked activity in cortical cells imaged in freely moving animals.," *Proc. Natl. Acad. Sci. U. S. A.*, vol. 106, no. 46, pp. 19557–62, 2009.

[220] B. M. Kampa, M. M. Roth, W. Göbel, and F. Helmchen, "Representation of visual scenes by local neuronal populations in layer 2/3 of mouse visual cortex.," *Front. Neural Circuits*, vol. 5, no. December, p. 18, 2011.

[221] K. Hamaguchi, M. Tanaka, and R. Mooney, "A Distributed Recurrent Network Contributes to Temporally Precise Vocalizations," *Neuron*, vol. 91, no. 3, pp. 680–693, 2016.

[222] V. Venkatachalam and A. E. Cohen, "Imaging GFP-based reporters in neurons with multiwavelength optogenetic control," *Biophys. J.*, vol. 107, no. 7, pp. 1554–1563, 2014.

[223] A. Antonini, C. Liberale, and T. Fellin, "Fluorescent layers for characterization of sectioning microscopy with coverslip-uncorrected and water immersion objectives," *Opt. Express*, vol. 22, no. 12, p. 14293, Jun. 2014.

[224] J. Schindelin, I. Arganda-Carreras, E. Frise, V. Kaynig, M. Longair, T. Pietzsch, S. Preibisch, C. Rueden, S. Saalfeld, B. Schmid, J.-Y. Tinevez, D. J. White, V. Hartenstein, K. Eliceiri, P. Tomancak, and A. Cardona, "Fiji: an open-source platform for biological-image analysis," *Nat. Methods*, vol. 9, no. 7, pp. 676–682, 2012.

[225] A. M. De Stasi, P. Farisello, I. Marcon, S. Cavallari, A. Forli, D. Vecchia, G. Losi, M. Mantegazza, S. Panzeri, G. Carmignoto, A. Bacci, and T. Fellin, "Unaltered Network Activity

and Interneuronal Firing during Spontaneous Cortical Dynamics in Vivo in a Mouse Model of Severe Myoclonic Epilepsy of Infancy," *Cereb. Cortex*, vol. 26, no. 4, pp. 1778–1794, 2016.

[226] K. Kitamura, B. Judkewitz, M. Kano, W. Denk, and M. Hausser, "Targeted patch-clamp recordings and single-cell electroporation of unlabeled neurons in vivo," *Nat Methods*, vol. 5, no. 1, pp. 61–67, 2008.

[227] M. Dal Maschio, A. M. De Stasi, F. Benfenati, and T. Fellin, "Three-dimensional *in vivo* scanning microscopy with inertia-free focus control.," *Opt. Lett.*, vol. 36, no. 17, pp. 3503–3505, Sep. 2011.

[228] H. Hirase, V. Nikolenko, J. H. Goldberg, and R. Yuste, "Multiphoton stimulation of neurons.," *J. Neurobiol.*, vol. 51, no. 3, pp. 237–47, Jun. 2002.

[229] T. W. Dunn, Y. Mu, S. Narayan, O. Randlett, E. A. Naumann, C. T. Yang, A. F. Schier, J. Freeman, F. Engert, and M. B. Ahrens, "Brain-wide mapping of neural activity controlling zebrafish exploratory locomotion," *Elife*, vol. 5, no. MARCH2016, pp. 1–89, 2016.

[230] M. Kondo, K. Kobayashi, M. Ohkura, J. Nakai, and M. Matsuzaki, "Two-photon calcium imaging of the medial prefrontal cortex and hippocampus without cortical invasion," *Elife*, vol. 6, p. e26839, Sep. 2017.

[231] L. Grosenick, J. H. Marshel, and K. Deisseroth, "Closed-loop and activity-guided optogenetic control," *Neuron*, vol. 86, no. 1, pp. 106–139, 2015.

[232] L. Tian, S. A. Hires, T. Mao, D. Huber, M. E. Chiappe, S. H. Chalasani, L. Petreanu, J. Akerboom, S. A. McKinney, E. R. Schreiter, C. I. Bargmann, V. Jayaraman, K. Svoboda, and L. L. Looger, "Imaging neural activity in worms, flies and mice with improved GCaMP calcium indicators," *Nat. Methods*, vol. 6, no. 12, pp. 875–881, Dec. 2009.

[233] K. Podgorski and G. Ranganathan, "Brain heating induced by near-infrared lasers during multiphoton microscopy.," *J. Neurophysiol.*, vol. 116, no. 3, pp. 1012–23, Sep. 2016.

[234] M. M. Karnani, J. Jackson, I. Ayzenshtat, A. Hamzehei Sichani, K. Manoocheri, S. Kim, and R. Yuste, "Opening Holes in the Blanket of Inhibition: Localized Lateral Disinhibition by VIP Interneurons," *J. Neurosci.*, vol. 36, no. 12, pp. 3471–3480, 2016.

[235] G. Thalhammer, R. W. Bowman, G. D. Love, M. J. Padgett, and M. Ritsch-Marte, "Speeding up liquid crystal SLMs using overdrive with phase change reduction.," *Opt. Express*, vol. 21, no. 2, pp. 1779–97, Jan. 2013.

8. Acknowledgements

I would like to thank my supervisor Tommaso Fellin, for giving me the opportunity of doing a PhD in a highly cooperative and interdisciplinary laboratory and for being a guide for my personal and scientific growth. Many thanks to past and present laboratory members, for their teachings and for fruitful discussions, which slowly shaped my attitude toward science and life (Dania Vecchia, Stefano Zucca, Noemi Binini, Claudio Moretti, Serena Bovetti, Andrea Sattin, Francesca Succol, Federico Pecoraro, Marco Brondi, Sebastiano Curreli, Valentina Pasquale, Pedro Lagomarsino, Stefano Varani, Francesco Nespoli, Andrea Antonini, Luca Sità, Angela De Stasi and Giulia D'Urso). Special thanks to my family, for sowing the seeds of my passion for science and always supporting me. Finally, I should like to thank UNIGE and IIT, for providing the framework of my educational program and scientific work.